Pi-Stack Engineering of Semiconducting Perylene Tetracarboxylic Derivatives

by

Chenming Xue

A dissertation submitted to the Graduate Faculty in Chemistry in partial fulfillment of the requirements for the degree of Doctor of Philosophy The City University of New York.

2011

This manuscript have been read and accepted for the Graduate Faculty in Chemistry in satisfaction of the dissertation requirement for the degree of Doctor of Philosophy.

	Shi Jin
_____	_____
Date	Chair of Examining Committee
	Mahesh K. Lakshman
_____	_____
Date	Executive Officer

Zhonghua Yu

Shuiqin Zhou

Supervisory Committee

THE CITY UNIVERSITY OF NEW YORK

Abstract

Pi-Stack Engineering of Semiconducting Perylene Tetracarboxylic Derivatives

By

Chenming Xue

Advisor: Professor Shi Jin

In the past decades, there has been intensive research in generating novel perylene tetracarboxylic derivatives because of a vast number of applications based on their semiconducting characteristics. The properties of the new materials rely heavily on not only the single molecular structure, but also the way of molecular packing in condensed states. The formation of effective π-stacking structures is the key issue. In this thesis, I focused in synthesizing novel perylene tetracarboxylic derivatives by attaching various substituents at the imide nitrogens. Consequently different phases appeared and exhibited different way of molecular packing. In Chapter 1, it is the general background of perylene tetracarboxylic derivatives including (a) synthesis routes, (b) optical and electronic properties, (c) the molecular packing in condensed phases or assembling in solutions; and also the introduction of condensed state phases including amorphous, crystalline and liquid crystalline (LC) phases. In Chapter 2, a series of solution processible amorphous glassy perylene tetracarboxylic diimides (PDIs) has been designed, synthesized and characterized. The π-stacking order in the amorphous glass phase was successfully tailored by the steric means and qualitatively evaluated. In

Chapter 3, the *n*-alkyl chain length dependence of a series of two-dimensional (2D) smectic LC PDIs has been explored. When the *n*-alkyl chain is no shorter than decyl group, the PDI could exhibit a novel 2D crystalline smectic LC phase. In this phase, the PDI cores microphase separate from flexible *n*-alkyl chains forming 2D crystalline layers. Thermoanalysis data quantitatively reveal that the *n*-alkyl chains in this phase have the essentially the same order as that in the isotropic liquid state. Such truly disordered *n*-alkyl chains effectively decouple the inter-layer molecular correlation and make the phase genuine LC. The PDI π-stacking order in this LC phase is crystalline because it is a part of the 2D crystalline intra-layer order. Chapter 4, PDI π-stacking order has been engineered in the crystalline phase. By introducing two structuring factors, a series of crystalline PDIs with finely tunable PDI π-stacking order was obtained. The crystalline PDIs with exceptionally red-shifted λ_{max} were obtained. Several PDIs possess λ_{max} values greater than any literature-reported ones. These materials can be excellent candidates in solar cell devices. In Chapter 5, new chiral main-chain PDI containing polymers were synthesized. These polymers can form intramolecular helical π-stacks in diluted solutions. In Chapter 6, a novel synthetic route leading to unsymmetrical perylene tetracarboxylic derivatives has been developed. Based on this synthetic method, more perylene tetracarboxylic derivatives can be generated.

In my research in this thesis, not only synthesis is an important part because it provides novel materials, but the characterization is critical as well. Infrared spectroscopy, Ultra-violet, fluorescence, differential scanning calorimetry, circular

dichroism, polarized light microscopy, gel permeation chromatography, X-ray diffraction including both small angle and wide angle have been used. Additionally, molecular simulation is also very useful in design and obtaining details in molecular packing.

Overall, the achievements in this research contribute a considerable advance in the field of generating semiconducting perylene tetracarboxylic derivatives which have versatile potential applications such as in solar cell devices, organic field effect transistors and light emitting diodes.

This is
dedicated to
My beloved family

Acknowledgements

It is under the guidance of my advisor Professor Shi Jin that I have been able to achieve such a step towards the summit of science. I would like to have the pleasure to express my deep gratitude to my dear professor for his guidance and devotion in this challenging Ph.D journey. To work in this group is such an honor that I will appreciate it for all my life.

I would like to thank my research committee members, Professor Shuiqin Zhou from College of Staten Island, Professor Zhonghua Yu from City College and my advisor for their time, advices and support. Thank you very much for the annual reviews and helpful advisements.

I also want to thank my colleagues in Professor Jin's group, Runkun Sun, Bin Wang, Hao Zhang, Guolin Lu, and MinZhi Chen from Nanjing University (China).

I am grateful to professors from CSI/CUNY for the advisements. Also I would like to give thank to Dr. Nan-Loh Yang for letting me get into this great chemistry PhD program in College of Staten Island and the financial support through these years.

I own special thanks to my dear family and friends. I would like to thank my parents Mr. Rong Xue and Ms. Xuewen Tu, my girlfriend Yuanyuan Zhao for their love and support.

Table of Contents

List of Figures

List of tables

List of Schemes

CHAPTER 1. INTRODUCTION

1.1 Synthesis…….3

1.2 Properties…….....6

1.2.1 Optical……....6

1.2.2 Redox properties…….....8

1.2.3 Structural properties……...9

1.3 Packing and assembling…….....11

1.3.1 Packing behavior in crystalline phase……..……...…..…11

1.3.2 Self-assembly behavior of PDIs in solution……..…...…14

1.3.3 Perylene diimide aggregates in the liquid-crystalline state……..……15

1.4 Solid state morphology…….…….....17

1.4.1 Glassy amorphous phase……..…18

1.4.2 Crystalline phase……..20

1.4.3 Liquid crystalline phases……..21

CHAPTER 2. A SERIES OF SOLUTION-PROCESSABLE AMORPHOUS GLASSY CORE-UNSUBSTITUTED PERYLENE TETRACARBOXYLIC DIIMIDES

2.1 Introduction……...25

2.2 Molecular design…….…..27

2.3 Results……..….29

2.3.1 Structural and morphological characterization of molecular glassy PDI films……..…...29

2.3.2 Spectroscopic characterization of molecular glassy PDI films……...….33

2.3.3 Phase transition behavors of molecular glassy PDI films…….…...37

2.3.4 Stability and formation tendency of amorphous glassy PDIs……..41

2.4 Discussion…….....44

2.4.1 Thermal behavior……..……...44

2.4.2 Exhibition of π-π interactions……...…….…47

2.4.3 The variation of amorphous PDIs……..…….....50

2.5 Conclusion……52

2.6 Experimental section…….53

CHAPTER 3. THE 2D CRYSTALLINE SMECTIC LIQUID CRYSTALLINE PHASE AND TRANSITION BEHAVIORS OF A SERIES OF PERYLENE TETRA-CARBOXYLIC DIIMIDES: THE *n*-ALKYL CHAIN LENGTH DEPENDENCE

3.1 Introduction……..…….66

3.2 Results……..…….68

3.2.1 Differential scanning calorimetry……..…….…….68

3.2.2 X-ray diffraction……...……...72

3.2.3 FT-IR……..……..……78

3.2.4 Solubility test…….……..……80

3.3 Discussion...……..……81

3.3.1 *n*-Alkyl chain length dependence of the 2D crystalline

smectic phase……..…….……81

3.3.2 *n*-Alkyl chain length dependence of the orange phase……...….86

3.4 Conclusions……...92

3.5 Experimental section……..…...92

CHAPTER 4.BLACK CRYSTALLINE PERYLENE TETRACARBOXYLIC DIIMIDES WITH EXCEPTIONAL RED-SHIFT ABSORPTION

4.1 Introduction……..……...103

4.2 Molecular design……..……...107

4.3 Results and discussion……..……...111

4.4 Experimental…….……..118

CHAPTER 5. SYNTHESIS AND CHARACTERIZATIONS OF THE FIRST SOLUBLE NONRACIMIC CHIRAL MAIN-CHAIN PERYLENE TETRACARBOXYLIC DIIMIDE POLYMERS

5.1 Introduction……..……...128

5.2 Results and discussion…….……...130

5.3 Conclusion…….……..……...145

5.4 Experimental section…….…..…….146

CHAPTER 6. PERYLENE MONOANHYDRIDE DIESTER: A VERSATILE INTERMEDIATE FOR THE SYNTHESIS OF UNSYMMETRICALLY SUBSTITUTED PERYLENE TETRACARBOXYLIC DERIVATIVES

6.1 Introduction……..……...153

6.2 Results and discussion…….……...155

6.3 Experimental section……..……..…….....159

BIBLIOGRAPHY

1. Chapter 1…….…….....164
2. Chapter 2…….…….…...170
3. Chapter 3…….…….…...176
4. Chapter 4…….…….…...179
5. Chapter 5…….…….…...180
6. Chapter 6…….……...185

List of Figures

Figure 1.1 HOMO (top) and LUMO (bottom) of perylene diimides in which both frontier orbital exhibit nodes at the imide nitrogens……..……..7

Figure 1.2 Absorption(solid curve) and normalized emission (dashed) spectra of diimide in diluted $CHCl_3$ solution……..…..8

Figure 1.3 Bond lengths of 6b in the crystal…….……..10

Figure 1.4 Conformation of the single molecular phenoxy substituents in bay-substituted PDI 5…….....10

Figure 1.5 Most common π–π stacking of PDIs 6 in the solid state involving longitudinal and transverse offsets…….....12

Figure 1.6 Transverse and longitudinal displacements of the stacked π-systems in the crystals of red, maroon and black perylene diimide pigments…….....13

Figure 1.7 Two dimensional schematic drawing of three types of orders: (a) Short-range bond orientational and positional order, long range molecular orientational order, (b) Long-range bond orientational and molecular orientational order, (c) Long range positional, bond orientational and molecular orientational order…….....22

Figure 1.8 Classification scheme for small molecule liquid crystals……..23

Figure 1.9 Structure of the nematic phase……..23

Figure 1.10 Structure of the smectic phase……..….....23

Figure 2.1 Molecular structure and model of amorphous molecules……..29

Figure 2.2 DBlleu (left) and DB2bu (right) drop-cast films at room temperature…….30

Figure 2.3 WAXD curves of PDIs: (a) drop-cast, (b) fast cooled from melt to RT…....31

Figure 2.4 AFM height image and the corresponding section analysis of a spin-coated DBala film…….....33

Figure 2.5 UV absorption spectra of amorphous PDIs from spin coating (a) and fast cooled from the melting (b)……......36

Figure 2.6 Fluorescence spectra of spin-coated (a) and fast-cooled PDI films (b) (Peaks were normalized to the same intensity, excited at 490 nm.)…….36

Figure 2.7 DSC data of amorphous materials ……38

Figure 2.8 PLM graphes displaying crystals appeared during the 1st heating ……...…40

Figure 2.9 DSC traces of glassy PDIs after being annealed at 5 °C below T_gs for 12 hours ……43

Figure 2.10 AFM analysis of DBala films of fast dry casted solution……..…...44

Figure 2.11 DSC curves of the precipitated samples prepared by exposing 1 mg/ml $CHCl_3$ solutions in methanol vapor at RT for a week at RT……..…45

Figure 3.1 The first heating curves of orange solids (C9 – C14Alas)…….....70

Figure 3.2 The second heating scan of C10 - C16Alas……...71

Figure 3.3 After cooled from melt, C12Ala samples were annealed at RT for different periods of time……72

Figure 3.4 1D WAXD of C4-C9Alas in the second heating……..…….74

Figure 3.5 1D-WAXD patterns of C10-C16Alas at 140 °C……..…..74

Figure 3.6 SAXD of C10-C16 Ala at 70°C (a); d-spacing of the small-angle

diffraction plotted versus n……...…….74

Figure 3.7 VTSAXD of C16Ala (a); plot of d-spacing versus n (b)……..75

Figure 3.8 PLM micrographs of a mechanically sheared C10Ala at RT with different alignment with respect to the polarizer……..……...……76

Figure 3.9 1D WAXD of (a) C14Ala and (b) C16Ala…….…...77

Figure 3.10 WAXD of orange solid of C9-C13Alas……...…….78

Figure 3.11 IR of *n*-alkyl chain stretching band shift of C16Alas during 2nd heating from RT to melt……..…..79

Figure 3.12 FT-IR of *n*-alkyl chain stretching bands of C12Ala during phase transition from crystalline state to disordered state…….……..…80

Figure 3.13 Relative solubility of CnAlas in heptane, C12Ala was set to 1 and the real solubility of C12Ala is 1.87×10^{-7} mol/L……..……..81

Figure 3.14 The phase boundary diagram of CnAlas……...……83

Figure 3.15 *n*-dependent transition enthalpy and entropy……..……..85

Figure 3.16 2D WAXD pattern of C16Ala on silica waver after annealed for 24h at 150 ^{o}C…….…..86

Figure 3.17 Orange crystalline structure of C12Ala. (a)model (b) simulation results……...……92

Figure 4.1 Absorption of G4 in dilute chloroform solution……..111

Figure 4.2 Absorption of dispersion of G4-16 in chloroform solution after adding methanol (MeOH:$CHCl_3$=2:1) for 30min……...…111

Figure 4.3 Powders WAXD of G4-G16……..……..114

Figure 4.4 d-Spacing values of G4-G16…….....……..115

Figure 4.5 The ester $\nu_{C=O}$ region of Gms……...……117

Figure 5.1 ^{1}H NMR spectra of ML-Ala11 (A1) and PL-Ala11 (A2); ML-Leu11 (B1) and PL-Leu 11 (B2)……..…133

Figure 5.2 FT-IR spectra of ML-Ala11 (A1) and PL-Ala11 (A2); ML-Leu11 (B1) and PL-Leu 11 (B2)……..134

Figure 5.3 SEC curves of PL-Ala11 (A), PL-Leu11 (B) and PL-Leu11A(C)……..137

Figure 5.4 The photograph of a PL-Leu11 film cast from chloroform solution……...137

Figure 5.5 UV-vis spectra of PL-Ala11 (solid) and ML-Ala11 (dash) (A); PL-Leu11 (solid) and ML-Leu11 (dash) (B)…….....141

Figure 5.6 CD spectra of PL-Ala11 (solid line) and ML-Ala11 (dash line) (A); PL-Leu11 (solid line) and ML-Leu 11 (dash line) (B)……144

Figure 5.7 Differential pulse voltammetry traces of ML-Ala11 (1); ML-Leu11 (2); PL-Ala11 (3) and PL-Leu11 (4)…….……..145

List of Tables

Table 2.1 Thermal analysis of amorphous materials based on DSC experiments……..32

Table 3.1 Phase transition temperatures (onset, ^{o}C), enthalpy changes (ΔH, kJ/mol) and entropy changes (ΔS) of CnAlas……...69

Table 3.2 Indices of C10-C16Alas……..78

Table 3.3 Enthalpy and entropy change of n-alkyl chain melting……..…...90

Table 4.1 Absorption peaks (λ_{max}) of dispersion of G4-16 in chloroform solution after adding methanol (MeOH:$CHCl_3$=2:1) for 30min……..113

Table 4.2 Absorption of solution casted films……..113

Table 4.3 The frequency values of ester $\nu_{C=O}$ Gms…….……..117

Table 5.1 Condensation of 1 with amines…….……..…...138

Table 5.2 The first reduction potentials of perylene tetracarboxylic derivatives vs. Fc/Fc^{+}……..…….145

Table 6.1 Molecular Weights and Polydispersity of PDI Polymers……..157

Table 6.2 Reduction Potentials of PDIs vs. Fc/Fc^{+}……...159

List of Schemes

Scheme 1.1 Different perylene tetracarboxylic derivatives based on the substitution Pattern……4

Scheme 3.1 Synthesis of CnAlas (*n* = 4 – 14, 16)……95

Scheme 5.1 ADMET synthesis of main-chain PDI polymers…..…….132

Scheme 6.1……..…….155

Scheme 6.2……..…….158

CHAPTER 1. INTRODUCTION

In the recent decades, organic materials have captured many researchers' attention because they exhibit all sorts of interesting properties in the solid state such as optical, electronic, photoelectric and magnetic properties. Among them, photo- and electro-active organic materials are especially important subjects, because they have wide applications such as organic semiconductors, photoactive materials, photoconductors and others. In addition, organic semiconducting materials have a number of potential applications in electronic and optoelectronic devices such as sensors, plastic batteries, solar cells, field-effect transistors, optical data storage, organic electroluminescent devices and switching devices. In contrast to inorganic materials, organic materials have advantages as light weight, potentially low cost, capability of forming large-area thin-films and flexible device fabrication.[1-3]

In order to improve the properties of the organic semiconducting materials, researchers have devoted considerably in molecular design. Mostly, organic semiconducting materials are based on conjugated π-electron systems. Among them there are two types of organic semiconducting materials: *p*-type, in which holes in the valence band are the majority charge carriers. (Most organic conducting materials are of this type); and *n*-type, in which the major charge carriers are electrons in the conduction band. Most of *n*-type materials are on the basis of electron-deficient molecules that may be used as the electron-acceptor in an organic photovoltaic solar cell. In comparison with *p*-type materials, *n*-type organic materials are much less common. Thus, developing new *n*-type semiconducting materials have captured much attention.

Perylene tetracarboxylic acid derivatives including perylene tetracarboxylic tetraesters, perylene tetracarboxylic diester monoimides and perylene tetracarboxylic diimides (PDIs) are excellent candidates as *n*-type molecules.

Among them, PDIs have attracted a great deal of interest in the field of organic electronics and optoelectronics. They have been widely utilized in organic photovoltaic solar cells,[4] field-effect transistors,[5] light-emitting diodes[7] , as *n*-type semiconductors[6] and liquid crystals,[8] because of the high electron affinity and the strong ability to form π-stacks as well as thermal and chemical stability of the diimide structure. Originally, PDIs were applied as industrial dyes and pigments.[9]

PDI molecules with covalent multichromophoric architectures are thermal- and photo- stable and the single molecules feature high fluorescence quantum yields, leading to wide applications. For example, they were applied in light-induced energy and electron transfer processes[10] as well as in the field of laser dyes and fluorescent light collectors.[11] Actually, PDIs are the best fluorophores available for single molecule spectroscopy.[12] At single molecule level, if desirable receptor units are attached to the PDI fluorophore, these dyes are suitable for sensors.[13]

Another topic, namely, the supramolecular organization of PDIs is a subject that draws considerable attention and has been studied widely nowadays. Since the optical and electronic properties are directly and greatly affected by different π-stacking arrangements,[14] to achieve desirable organization through the control of the spatial arrangement of PDIs by molecular recognition-directed self-assembly is the key point. The organization of PDIs is directed by the favorable intermolecular π-π interactions and other elements such as hydrogen bonding,[15] metal ion coordination[16] and global

morphology (various packing ways).[17] As the results, various self-organizations of functional dyes are useful to create defined multichromophoric objects or solid state materials with novel desirable optical and electronic functionalities. The fundamentals for all of the above characteristics of PDIs are based on PDI molecules. Thus, the progress of synthesis of representative PDIs will be discussed.

1.1. Synthesis.

For perylene tetracarboxylic derivatives, they can be classified into different groups based on the substitution pattern. For all the groups of perylene derivatives mentioned below, there will be (a) perylene core substituted, like **2**, **3**, **4**, **5;** (b) perylene core unsubstituted, like **6** and (c) perylene diester monoimides which means one cyclic imide group is opened and there are three substituent sites in a single molecule, like **8**, and (d) perylene tetraester, like **7**. The different sorts of perylene tetracarboxylic derivatives have been depicted in **Scheme 1.1**.

The simplest and most common PDIs are **6,** which have been obtained by the reaction of perylene dianhydride (PDA) with a multitude of aromatic and aliphatic amines. Among them the simplest **6a** and **6b** are insoluble and have high melting points, limiting their potential applications. Therefore, developing new soluble perylene dyes has become a significant topic. There are two different successful strategies: the first one was developed by Langhals' group, who made PDIs soluble by connecting solubilizing substituents to the imide nitrogen atoms (**6c**, **6d**).[18] The PDIs obtained by this approach in the single molecular state exhibit indistinguishable absorption and emission properties because nodes in the HOMO and LUMO at the imide nitrogen decouple the PDI core and the imide substituents.[19]

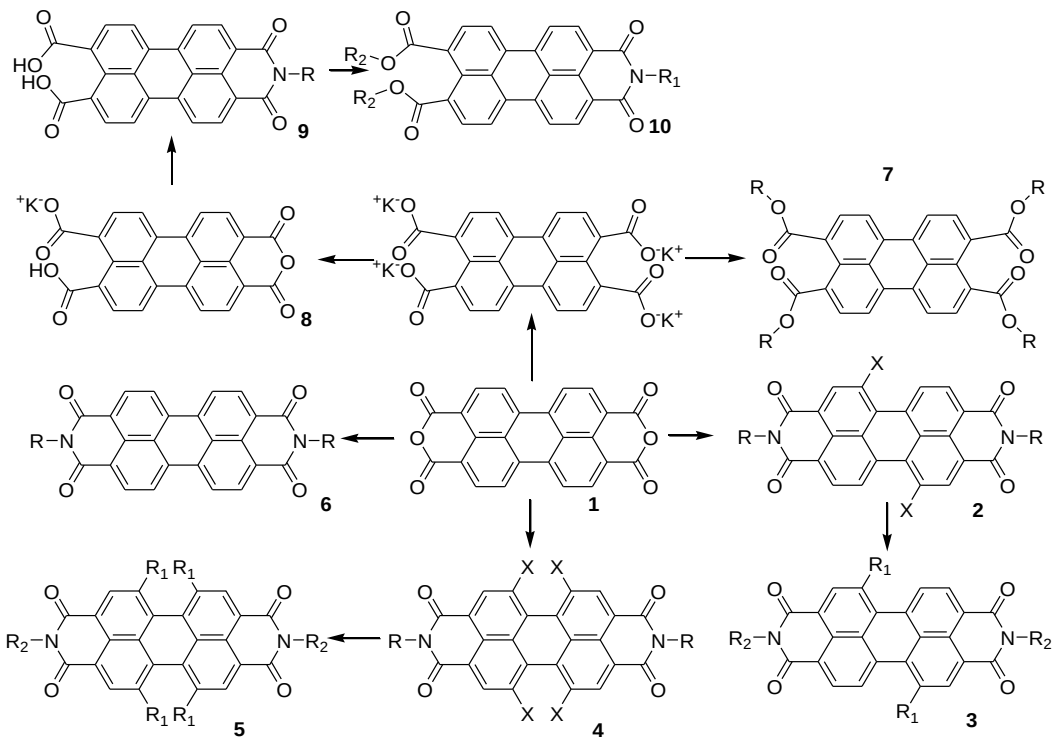

3a: R_1 = 

3b: R_1 = **-CN**

3c: R_1 = 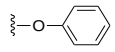 , R_2 = **cyclohexyl**

4: **R** = 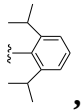 , **x = Cl**

5: R_1 = 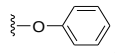 , R_2 = 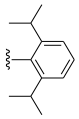

6a: **R = H**

6b: **R = CH_3**

6c: **R** = 

6d: **R** = 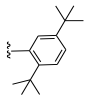

Scheme 1.1. Different perylene tetracarboxylic derivatives based on the substitution pattern

The second elaborate but synthetically more complicated strategy was to introduce substituents at the carbocyclic scaffold in the bay-area of the perylene core. Researchers of Seybold's group have incorporated four phenoxy (**5**) groups in high yields by nucleophilic displacement of chlorine substituents (**4**).[20] It is difficult to introduce other nucleophiles and the reaction are of low yields.[21] Fourfold chlorination of PDI **4** is a known procedure (despite of the contamination with three- and five- fold chlorination products),[22,23] and recently it was discovered that the bromination affords di-substituted derivatives **2**,[24] even though the purification of the product is a big challenge. Gratifyingly, due to the fact that exchange of the bromine substituents of **2** is straightforward, novel perylene diimide **3** could be extended by introducing more substituents like carbon,[24] cyano,[25] oxygen[24] and nitrogen[26] to the perylene core leading to interesting optical and redox properties.

Since the synthesis is critical in developing PDIs, the details of the synthesis are introduced below. First of all, the synthesis of symmetrically substituted PDIs **6** from the PDA **1** is straightforward. The PDA is an excellent starting material because it is inexpensive and can be easily obtained analytically pure, and it is stable under common storage conditions. For the simplest **6** compounds, the condensation of PDA **1** with reactive primary aliphatic amines can be carried out straightforwardly. The reactions media can be water,[27] benzene,[28] quinoline,[29,30] or molten imidazole.[31,32] (The use of quinoline or moleten imidazole as a solvent is necessary for the less reactive amines.) In many such reactions, zinc salts like zinc acetate or zinc chloride[27-30] are important catalysts while the separation of these metal salts from the reaction products could be problematic. It is believed that the addition of zinc salt can increase the solubility of **1**

considerably.

Synthesis of un-symmetrically substituted PDIs is a challenge. A stepwise condensation of PDA **1** with two primary amines cannot afford unsymmetrically substituted PDI **6**, in which R groups on the two sides are different. This is because a reaction of the excess amount of PDA with one primary amine will not produce one side substituted PDIs as might be expected, instead the amines are completely converted to symmetrically substituted **6** and the excess of PDA remains unreacted.[33] However, Troster has discovered a smart synthesis route.[34] First, the insoluble PDA is converted to the soluble tetra potassium salt in aqueous solution by adding extra amount of KOH. Second, the monoanhydride monopotassium salt **8** is precipitated by a moderate acidification with appropriate amount of acid (phosphoric acid, HCl and acetic acid have been used) with heating as **8** is absolutely insoluble in any solvent even at high temperatures. Third, **8** can be further condensed to **9** with some primary amines. Finally, after ring closure and condensed with another amine, the unsymmetrical **6** can be prepared. Furthermore, the novel perylene derivatives **10** with three substituents can be obtained by esterification reaction of potassium dicarboxylate salt of **9**.

1.2. General properties of PDIs

1.2.1. Optical

It is well known of PDIs **6** illustrating intense yellow-green photoluminescence in the single molecule state and in the past decades various PDIs have been synthesized for the applications as fluorescent standards, fluorescent light collectors, or laser dyes.[35] For such applications, the fact that the imide substituent has a negligible influence on the absorption and emission properties of PDIs because of the nodes of the HOMO and

LUMO orbital at the two imide nitrogen has been proven to be very advantageous, guaranteeing the spectra stability of the materials. (**Figure 1.1**)

Since their optical properties are determined by the π-electron system, it is not strange that PDIs **6** exhibit identical absorption and emission spectra with scarce variations and the fluorescence quantum yield is quantitative. Since the fluorescence quantum yield and lifetime of **6c** was not affected by circumstance changes in solution, it was suggested as a convenient standard to determine fluorescence quantum yields.[39]

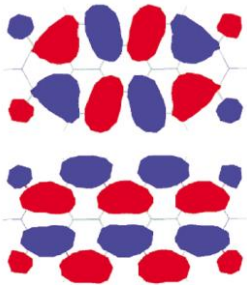

Figure 1.1. HOMO (top) and LUMO (bottom) of perylene diimides in which both frontier orbital exhibit nodes at the imide nitrogens. [12]-Reproduced by permission of the Royal Society of Chemistry

The absorption and fluorescence emission spectra of **6** in diluted $CHCl_3$ solutions are shown in **Figure 1.2**. **6** displayed identical four well-resolved absorption peaks at 432, 458, 490, and 524 nm, respectively and the emission spectra in obvious mirror image relationship to the absorption spectrum.

To avoid the change of single molecular optical properties, appropriate imide substituents are well-suited to tailor PDI dyes for the solubility requirements and preventing the possible aggregation that has a pronounced influence on the optical behaviors. For instance, PDIs with swallow tailed substituents **6c** generated by Langhals have a very high solubility,[18] and for the PDI with 1-nonyldecyl chains

solubility up to 35g in 100ml *n*-heptane has been reported.[37]

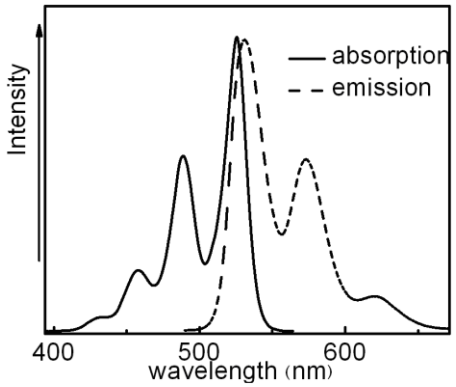

Figure 1.2. Absorption(solid curve) and normalized emission (dashed) spectra of diimide in diluted $CHCl_3$ solution

Pronounced changes in the absorption and emission bands were observed if the PDIs are substituted at the aromatic core in the bay-area, *i.e.* the positions 1, 6, 7, and 12. With two phenoxy groups attached at positions 1 and 7 the absorption maximum shifts by about 20 nm and with four phenoxy groups by almost 50 nm compared to that of the unsubstituted dyes **6**, and the color of the fluorescence changes to orange (**3c**) and red (**5**). In both cases all favorable properties of these perylene fluorophores like high fluorescence quantum yield, small solvent effects on the optical properties and high photostability are maintained. More pronounced spectral changes occur upon substitution at bay positions with two electron-donating pyrrolidino groups that affords the dye **3a** with a green color due to the bathochromic shift of 160 nm and the emission is in the infrared region. As this spectral shift is caused by charge transfer, pronounced solvatochromism is observed for these green dyes and their fluorescence quantum yield is decreased. By contrast, little spectral changes take place if electron-withdrawing substituents such as halogen atoms, are attached at the bay positions (**2**, **4**, **3b**).

1.2.2. Redox properties

The electrochemical properties of PDIs have been investigated comprehensively in the past and some representative PDIs were summarized in [18], in which all of them have been recalculated to a common reference, the ferrocene/ferrocenium (Fc/Fc^+) couple. The data demonstrate that PDIs are fairly electron-deficient dyes, easy to reduce and rather difficult to oxidize, in agreement with the molecular structural characteristic. For most PDIs **6**, two reversible reduction and one reversible oxidation waves are found in cyclic voltammetry (CV), many of which exhibit a first reduction potential already comparable to C60, a type of widely used *n*-type semiconducting materials. Similar to optical properties, substituents in the bay-area have a pronounced effect on the respective redox potentials. For example, substitution by chlorine or especially the cyano group leads to strong oxidative dyes. On the other hand, with an electron-donating substituent such as phenoxy group, the reduction is disfavored by 0.1V. Even two reversible oxidation waves were observed for pyrrolidino compound **3a**, and correspondingly the reduction requires a lower potential. Therefore, these dyes are not considered as electron-deficient as the parent PDIs. Generally, the photo-oxidation is the major destructive mechanism for dyes and the electron-deficient character of PDI dyes determines their photo stability. In contrast, when in the photoexited state the majority of these PDIs are strong reductants and this property has been widely applied by the research groups of Wasielewski[40] and Lindsey[41] in photoinduced electron transfer cascades.

1.2.3. Structural properties

The PDIs **6** with mutiaromatic cores exhibit flat π-systems which have been confirmed by X-ray diffraction of single crystals.[42,43] When we take a glance at the molecular structures in these crystals, PDIs can be regarded as a combination of two naphthalene half units (**Figure 1.3**), each of them connects to an imide group and is linked to another naphthalene unit by two sp^2 - sp^2 C-C bonds. These connecting bonds between the two half units are considered as single bonds and it is in agreement with the fact that steric strain in the bay-area could result in a twisted structure instead of the original planar one. This has been discussed for a tetrachloro-substituted PDI[44] with torsional angle of 37^o and a tetraphenoxy-substituted diazadibenzo PDI with a smaller angle of 25^o as shown in **Figure 1.4**.[45] As the result, this distortion introduces considerable constraints towards the packing of these PDIs in the solid state as well as in molecular aggregates in solution. The better solubility is the advantage afforded by this distortion. For example **5,** exhibits a solubility exceeding 100g/L in ethyl acetate at 20 ^{o}C.[46]

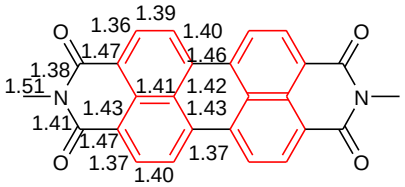

Figure 1.3. Bond lengths of **6b** in the crystal

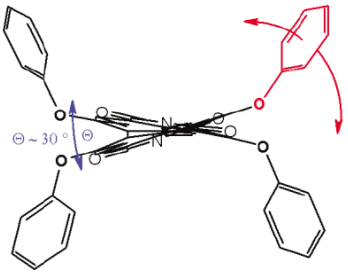

Figure 1.4. Conformation of the single molecular phenoxy substituents in bay-substituted PDI **5.** [12]-Reproduced by permission of the Royal Society of Chemistry

1.3. Packing and assembling

1.3.1. Packing behavior in crystalline phase

The color in dilute solution is mainly determined by the electronic properties of the individual molecules while in the solid state, perylene derivatives can form several polymorphs or phases having different colors because of different intermolecular electronic interactions of the nearby packed molecules. In other words, the color is an indication of different ways of crystal packing of the molecules in the solid state.[42] The PDIs **6** can be considered as D_{2h} symmetry point group and the molecular axis system usually defined as longitudinal direction (Y-direction) and transversal direction (X-direction), which have been presented in **Figure 1.5**. In the past decades, the packing of PDIs has been investigated comprehensively with a number of PDIs only distinguished by their imide substituents.[42,43] The investigated PDI molecules in the crystal structures exhibit planar geometry in which the molecules arrange in stacks having a parallel orientation at a distance of about 3.34 - 3.55Å.[42] The steric constraints of the substituents at the imide groups is the primary factor that determines the stacking distance and the offsets (both longitudinal and transverse) between neighboring PDIs. In some rare cases, rotational offsets have also be observed when ethyl and some benzyl substituents were attached to the imide nitrogen atoms. [42,43,47]

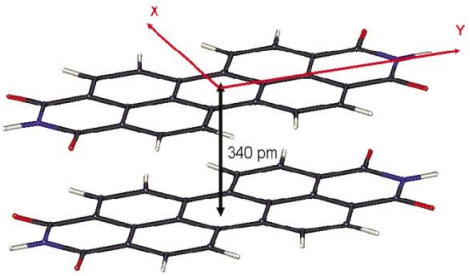

Figure 1.5. Most common π–π stacking of PDIs **6** in the solid state involving longitudinal and transverse offsets. [12]-Reproduced by permission of the Royal Society of Chemistry

The crystallochromy, i.e., the phenomenon of the color changes due to the different packing interactions in crystals, is one of the most remarkable features of these PDI crystals. Quite different from the almost identical yellow-green color of PDIs in dilute solutions, different colors are found in the solid state depending on the packing schemes. There are commercial available PDI pigments of red, maroon, red-violet and even black colors.[9b] Empirical relationship for the dependence of the crystal color upon the longitudinal and transverse offsets of the PDIs has been comprehensively studied, which reveals the bathochromic shift and the band broadening are due to the π-π overlap area between the stacked chromophores (some of the examples were displayed in **Figure 1.6**).[14]

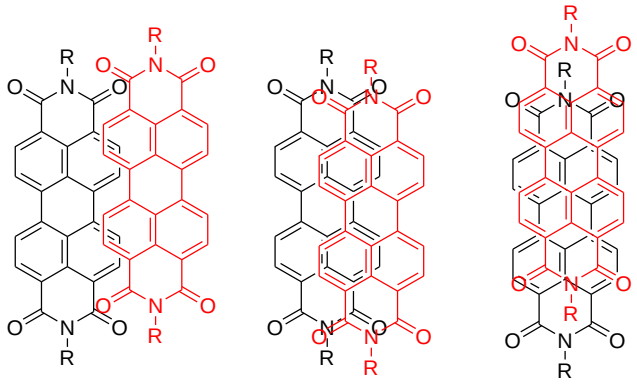

Red **maroon** **black**

Figure 1.6. Transverse and longitudinal displacements of the stacked π-systems in the crystals of red, maroon and black perylene diimide pigments

Of the longitudinal and transverse shifts, transverse offsets provide more perturbation than longitudinal offsets do to the π-π interactions which means slipping in the longitudinal direction is less effective in reducing the coupling between neighboring π-systems. As a consequence, PDIs without or with little transverse offset often illustrate black color because of the stronger π-π interaction. More detailed study and more accurate calculation towards these crystallochromy effects has been suggested by Kazmaier and Hoffmann based on extended Hückel calculations on one-dimensional infinite stacks of dyes as a function of the two offset parameters[48] and recently even more advanced work has been completed by Bernd Engels' group.[49]

The black PDIs are very useful and researchers have developed many of them.[50] In a basic study thin polycrystalline films of the black perylene bis-phenethylimide have exhibited singlet exciton transfer lengths of 2.5 μm, which is the highest value ever reported for an organic material.[60]

Some of the black pigments are considered to be of the special interest for novel high technology applications where high exciton and/or charge carrier mobilities are desired, e.g. photoconductors, field effect transistors, or photovoltaic devices.

1.3.2. Self-assembly behavior of PDIs in solution.

By attaching appropriate substituents in the molecules, a reasonable supramolecular PDI assembly of which the structural growth (or 'self-assembly') becomes possible only in one or two dimensions, while intermolecular interaction in a third dimension leading to crystalline solids is prevented.

Although the stacking of the planar π-system of PDI dyes is well documented in the crystal structures of the perylene pigments,[42,43] only recently has the aggregation of these dyes been studied in solution and the Gibbs aggregation energies could be determined.[51] Solubilizing substituents have been equipped the imide functional groups affording reasonable solubility in the least polar aliphatic solvents, in which the aggregation constants are usually very large. Due to different degrees of assemblies affected by the concentrations, significant spectral changes with colors varying from light yellow-green at very low concentrations to dark-red at high concentrations could be detected. When heated, the assemblies can reverse to monomeric forms and from temperature-dependent studies, it is confirmed that the aggregation process is an enthalpically driven process. It is expected the quite remarkable changes in the optical properties arise will lead to tunable luminescence colors for potential applications.

PDI-incorporated polymers have been investigated in solution to study the folding

behavior,[52] of which higher oligomers compose up to 11 PDI units have been incorporated. In aqueous diluted solution, all of these molecules exhibit a folded state displaying a hypsochromically shifted absorption band.

1.3.3. Perylene diimide aggregates in the liquid crystalline state

Since liquid crystalline (LC) materials have particular advantages, introducing these advantages into PDIs will bring novel properties. The LC PDIs were discovered only about ten years ago when Cormier and Gregg reported the first observation of LC PDI dyes.[53] They attached highly flexible poly(oxyethylene) substituents at the imide nitrogen atoms of the PDI core, forming **6h** and **6i**. They are low-melting point materials which are able to enter into a LC phase easily upon cooling from the melt. However, these LC phases are monotropic and not sustainable that the transformation into crystalline phases takes place only by standing.[53] More recently, LC perylene related compounds such as **6e**, **f**, **g**[47] with simple aliphatic chains, coronene diimides **11**,[54] perylene tetracarboxylic acid tetraesters **7**,[55,56] and core expended perylene diimide **12**[57] have been generated. Similar to the aggregates in solution, the π-systems pack in a resembling way but with extra packing constraints in the bulk LC phase.

6e: **R = *n*-C_7H_{15}**
6f: **R = *n*-$C_{12}H_{25}$**
6g: **R = *n*-$C_{18}H_{37}$**
6h: **R =** 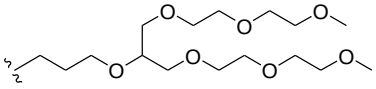
6i: **R =** 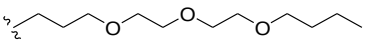

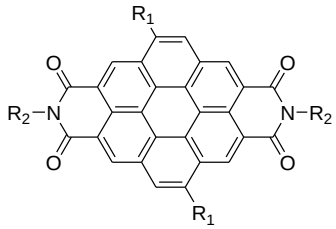

11:

11a: $R_1 = n\text{-}C_{10}H_{21}$, $R_2 = C_6H_{11}$
11b: $R_1 = n\text{-}C_{13}H_{27}$, $R_2 = C_6H_{11}$
11c: $R_1 = n\text{-}C_{10}H_{21}$, $R_2 = n\text{-}C_8H_{17}$
11d: $R_1 = n\text{-}C_{13}H_{27}$, $R_2 = n\text{-}C_8H_{17}$

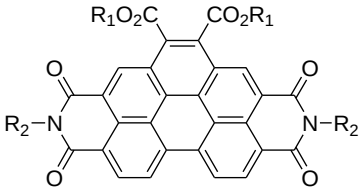

12: $R_1 = R_2$ = 2ethylhexyl

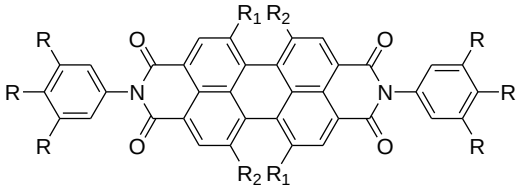

13a: $R = OC_{12}H_{25}$, $R_1 = R_2 = H$
13b: $R = OC_{12}H_{25}$, $R_1 = H$, $R_2 = p\text{-}t$BuPhO
13c: $R = OC_{12}H_{25}$, $R_1 = R_2 = p\text{-}t$BuPhO
13d: $R = OC_{12}H_{25}$, $R_1 = R_2 = Cl$
13e: $R = C_{12}H_{25}$, $R_1 = R_2 = H$

There are one important group of LC PDIs shown as **13a-e**. In the neat state, these PDIs form LC phases over a broad temperature range. With an increasing steric demand at the bay positions due to the substituents, there is an increasing distance between the π-systems as a result, which has been verified by wide angle X-ray diffraction. As expected from their molecular structure, most of these dyes form hexagonal columnar mesophases. For example, Col_{ho}(ordered) and Col_{hd}(disordered) phases of **13a-c** were found to be stable LC states from room temperature to the corresponding clearing points.[58] Tetracarboxylic acid esters **7** also displayed columnar mesophases accessible between 62 (**7g**) and 244°C (**7a**), depending on the alkyl

substituents.[56]

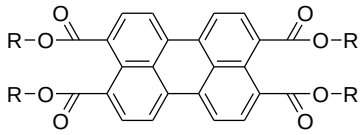

7a: **R = *n*-C_2H_5**
7b: **R = *n*-C_3H_7**
7c: **R = *n*-C_4H_9**
7d: **R = *n*-C_5H_{11}**
7e: **R = *n*-C_6H_{13}**
7f: **R = *n*-C_7H_{15}**
7g: **R = *n*-C_8H_{17}**
7h: **R = *n*-C_9H_{19}**
7i: **R = *n*-$C_{10}H_{21}$**
7k: **R = 2-ethylhexyl**

For the *n*-alkyl chain-substituted PDIs **6e-g**, the phase behavior was much complicated that several crystalline and LC phases occurred between room temperature and clearing points.[47] Interestingly, highly ordered LC layer structures with intra-layer co-facially arranged PDI cores perpendicular to the layers have been observed.

Several of these LC PDIs are promising materials for electronic applications. For example, high mobilities were measured in the LC phases, as 0.11 $cm^2V^{-1}s^{-1}$ for **6g** and 0.08 $cm^2V^{-1}s^{-1}$ for **13d**[47,14] and electroluminescent diodes which emitted yellow and orange light could be prepared from **7** and **12**.[55,59] One important attractive application of LC PDIs is in the field of photovoltaic devices, where these materials may play dual roles as light absorber and the charge transport material. It is expected that by combining these organic *n*-type semiconducting PDIs with a suitable *p*-type semiconductor forming a bulk *p*-*n* heterojunction material, a novel solar cell with high efficiency might be obtained.

1.4. Phase structures in condensed states

As PDIs are expected to be utilized in condensed states in most cases, being able

to tailor the phase structure in condensed states is a necessity. Generally speaking, knowledge about both the molecular mobility and order are needed to precisely describe a condensed state. When the order is concerned, there are two commonly encountered condensed states of matter: the liquid state and the crystalline solid state. Between the amorphous liquid state in which only short-range order can exist and the three-dimensionally (3D) long-range ordered crystalline state, there is an array of mesophases with intermediate degrees of order. However, only knowing order is not sufficient. For instance, the amorphous liquid state and the amorphous glassy state share the same type of order: only short-range order can exist. The major difference between these two states is the molecular mobility. In the liquid state, all modes of motions are fully allowed including translation, vibration and rotation. However, in the glassy state (which is a SOLID state) large-scale molecular motions are forbidden. Most of mesophases can also be found in their corresponding glassy mesophase via a vitrification process during cooling.

1.4.1. Glassy amorphous phase

In our daily life, there are familiar amorphous solids such as window glass and atactic polystyrene. Amorphous (glassy) materials are interesting because of the following aspects. First, unlike anisotropic crystals and liquid crystals, amorphous materials exhibit isotropic properties as well as homogeneous properties due to the absence of grain boundaries. Second, they are in a thermodynamically nonequilibrium state exhibiting glass transition (T_g) phenomenon which means at low temperatures, amorphous materials are glassy, hard, and brittle and when the temperature is raised, they go through the glass transition becoming soft. Usually T_g represents the onset point of

large scale molecular motion. Additionally, a concept of 'free volume' has been introduced to describe this phenomenon. The glass transition is a *second-order*-like transition, in which the volume-temperature dependence (dV/dT) undergoes a change in slope, and only its derivative expansion coefficient undergoes a discontinuity. Commonly, in a *second-order* phase transition, the first derivative of the chemical potential is continuous but its second derivative is not continuous. In a *second-order* phase transition there is no jump in the value of the enthalpy, entropy, and volume at the transition temperature. Resembling to the definition of the *first-order* transition, a *second-order* transition would have the discontinuous change in second derivative ($\partial^2\Delta G/\partial T^2$). There is no heat of transition at T_g but only a change in the heat capacity: ΔC_p, indicating the change of molecular motion.

Although nearly all substances could be obtained in the amorphous glassy form, if the cooling rate could be fast enough. This is because the formation of an ordered phase (LC or crystalline) requires a nucleation process which could be bypassed with a fast enough cooling process. However, the rate of the ordering process during cooling is strongly dependent upon the molecular structure. If one wish to obtain amorphous glassy materials with a reasonable effort, the ordering process of the molecules must be slow enough that could be bypassed by a commonly achievable cooling process. In addition, the formed amorphous glassy must be practically stable at intended applications temperatures. Thus molecular design of amorphous glass materials is important. Guidelines for the molecular design of amorphous glassy materials have been summarized as follows: 1. Nonplanar molecular structures are favored; 2. different conformers in addition to nonplanar molecular structures are required; 3. Incorporating

bulky or/and heavy substituents leads to easily formed amorphous materials as well as enhances the stability; 4. The enlargement of molecular size; 5. structurally rigid moieties such as biphenyl, naphthalene, fluorine, carbazole, and phenothiazine increase glass-transition temperatures; 6. increasing molecular size and weight also increases T_g.[3]

1.4.2. Crystalline phase

Crystals feature 3D long-range ordered structures in which the characteristic order allows us to convey a picture of an entire crystal by looking at only a small part of it. The repeating unit, also referred as the crystalline unit, is named the unit cell. Usually 3D array of points, each of which represents an identical environment in the crystal, represent the crystalline structure and such an array of points is called a crystal lattice. Through arranging the contents of the unit cell repeatedly on the crystal lattice, their whole crystal structure could be imagined. Generally unit cells are parallelepipeds (six-sided figures whose faces are parallelograms) and each unit cell can be described in terms of the lengths of the edges and the angles between these edges. The particular properties of crystals include the ability to diffract X-ray and their *first-order* transition behavior known as melting. It is well-known that during a transition, in order to stay in equilibrium the change in Gibbs energy, ΔG, must be zero. Albeit the derivatives of ΔG with respect to temperature do not have to be zero and this provides a way to characterize the thermodynamic transitions. Ehrenfest suggested in 1933 that a transition for which $(\partial \Delta G/\partial T) = -\Delta S$ is not equal to zero be called a *first-order* transition.[61] For the first-order transition, the first derivative of the chemical potential is discontinuous. A

first-order transition normally has a discontinuity in the volume-temperature dependence, as well as a heat of transition, ΔH_f, also called the enthalpy of fusion or melting.

1.4.3. Liquid crystalline phases

A more highlighted topic nowadays is about LC materials with intermediate orders between the amorphous and crystalline phase. From the phenomenological point of view, liquid crystals exhibit both crystal-like anisotropy and liquid-like mobility. Friedel made the first classification of liquid crystals with many important identified concepts including defects, layered structures in smectic phases, well-known terms of 'nematic', 'semectic', 'cholesteric' and 'mesophases'.[62] There are two classes of liquid crystals: thermotropic liquid crystals processing LC phases either on heating crystals or on cooling isotropic liquid only involve thermal effects while another class of anisotropic fluids called lytropic liquid crystals processing LC phases depend on the concentration in solvent-dispersed systems.

Depending on the molecular shapes, rod or lath-like molecules form LC phases called calamitic LC phases and flat, disc or sheet-shaped molecules form discotic LC phases. Naturally, LC phases can be classified in terms of order in three general types as illustrated in **Figure 1.7**. (This schematic drawing describes the two-dimensional projection of three types of order, assuming the preferential direction of the molecules: c-axis, perpendicular to the paper plane.)

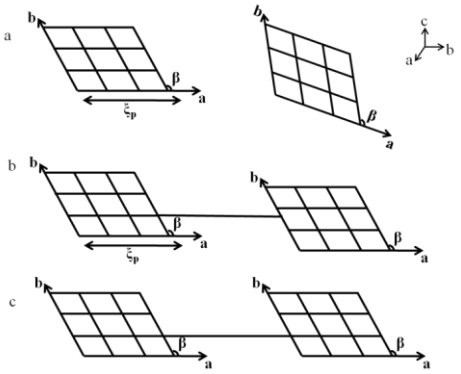

Figure 1.7 Two dimensional schematic drawing of three types of orders:

(a) Short-range bond orientational and positional order, long range molecular orientational order

(b) Long-range bond orientational and molecular orientational order

(c) Long range positional, bond orientational and molecular orientational order

The first type of order is the molecular orientational order as shown in **Figure 1.7a**, in which all the molecules have some preferential orientation with respect to the same direction. This is the only type of order that exists in all LC phases. The second type of order is the bond orientational order shown in **Figure 1.7b**, which describes the orientation along the direction of the unit vectors creating the lattice. In an LC phase, the molecules are restricted to move only along the lines of the two-dimensional grids of the layers. The positional order is the third type of order as shown in **Figure 1.7c,** in which a periodic translation of a point along any of the unit cell axes can reproduce the ordered lattice. The type of order can also be found in crystalline solids and a crystal possesses almost perfect positional, bond orientational and molecular orientational long-range order.

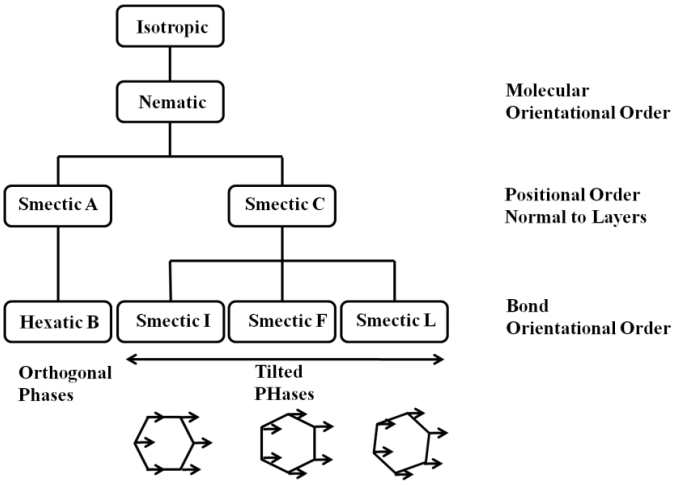

Figure 1.8. Classification scheme for small molecule liquid crystals

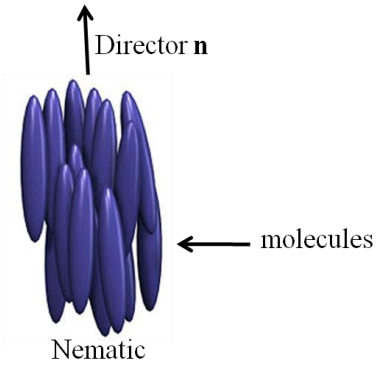

Figure 1.9. Structure of the nematic phase

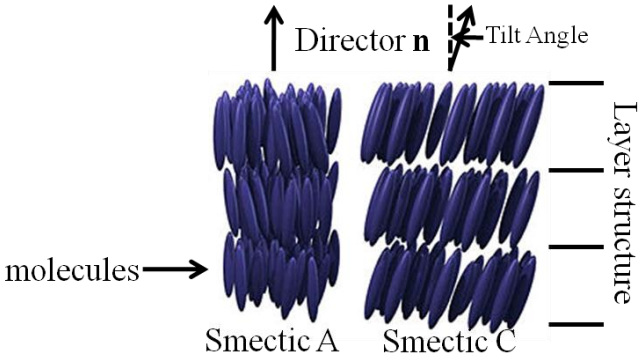

Figure 1.10. Structure of the smectic phase

Based on these three types of order in the system, various LC phases could form as shown in **Figure 1.8**.[64,65] Nematic phase is the least ordered LC phase, which may

be found just below the isotropic liquid. In the nematic phase, there is only short-range positional and bond orientational order in all three directions and molecular orientational order is the only type of long-range order. As shown in **Figure 1.9,** in this phase the rod-shaped molecules align almost parallel to each other with their long axes all pointing in the same direction roughly. Essentially, the nematic phase is a one-dimensionally ordered fluid with the preferential direction of all molecules as the director of the phase.

The lamellar structure is a common feature of the smectic phases in addition to the molecular orientational order exhibiting in all LC phases. As shown in **Figure 1.10** left, the smectic A phase (SmA) has the director perpendicular to the layer planes but there is no long-range positional order within the layers. Between successive layers there is no interlayer-correlation of the molecules. As the long axes of the molecules are normal to the layer planes on average, the SmA phase can be described as the stacking of two-dimensional liquid layers. As shown in **Figure 1.10** right, in smectic C (SmC) phase all the molecules tilt with respect to the layer normal with almost same angles. Like SmA phase, there is no long-range positional order in the layer planes. With the increasing of orders, other LC phases as shown is **Figure 1.8** may present and they are not discussed here.

CHAPTER 2. A SERIES OF SOLUTION-PROCESSABLE AMORPHOUS GLASSY CORE-UNSUBSTITUTED PERYLENE TETRACARBOXYLIC DIIMIDES

2.1. Introduction

In the past decades, small organic molecules forming stable amorphous glassy phases (molecular glasses), especially semi-conducting π-conjugated molecular glasses, have been intensively investigated because of their good processability, transparency and homogeneous properties in a variety of applications such as photochromic materials[1] which are used for surface relief grating formation,[2-10] image formation and memory,[11-13] molecular resists,[14-19] electroluminescent (EL) devices,[20-24] photovoltaic (PV) devices[25-28] and photorefractive devices.[29-32] Molecular glasses are isotropic and homogeneous without grain boundaries. In comparison to polymers that have been used to form uniform amorphous films, they are pure materials with both well-defined molecular structures and definite molecular weights eliminating any distribution.[33] Among conjugated semi-conducting amorphous molecular glassy materials, *n*-type molecular glasses have been less explored whereas they are in high demand especially in photovoltaic devices. Perylene tetracarboxylic diimides (PDIs) are among best *n*-type organic semi-conductors and have been investigated intensively for the applications as organic photovoltaic solar cells,[34-35] field-effect transistors,[36-39] *n*-type semiconductors,[40-42] light-emitting diodes,[43-45] and liquid crystals,[46-47] due to the their high electron affinity and charge-transporting capability through π-stacks.

Despite the usefulness of amorphous glassy PDIs, there are a very limited number of amorphous PDIs in literatures perhaps because of the strong ability of PDIs to form ordered π-stacks. The ordered PDI π-stacks are the basis of ordered phases such as crystalline and liquid crystalline (LC) phases. Once ordered PDI π-stacks form, the phase becomes no longer amorphous. This can explain why most of reported glassy PDIs are bay-substituted. When substituents are attached to the bay area of a perylene ring, the steric hindrance leads to a twisted instead of a planar perylene ring, which reduces π-π interaction to a sizable degree. Thus it increases the stability of the amorphous phase with respect to the corresponding ordered π-stacked phase.[48-57] On the other hand, the bay-area substituents twist the planar aromatic ring which is often considered negative for charge transport.[58,59] Additionally, the incorporation of PDI into polymers can also lead to an amorphous glassy phase,[60-64] though the polymer structures are complicated which limits the applications. In order for core-unsubstituted PDIs to form a glassy amorphous phase, usually vacuum vapor deposition is needed,[65] but in comparison with a drop-casting approach, vacuum vapor deposition is much less convenient and more expensive.

Here we present a different approach to molecular glassy PDIs. Since ordered PDI π-stacks are the basis of an ordered phase, the ability for PDI molecules to form such ordered PDI π-stacks must be reduced for a relatively easy formation of the amorphous glassy phase. On the other hand, we would like to retain the desired planar PDI rings for better charge transport performance. Thus we choose to introduce steric hindrance

toward the formation of PDI π-stacks via modifying the substituents on the imide nitrogen atoms. This approach not only could lead to an easier formation of amorphous glassy PDIs, but also could result in more soluble PDIs that can be solution-processed. Using this approach, we have synthesized a series of core-unsubstituted PDIs in which the steric hindrance toward the PDI π-stack formation has been tailored to a large degree. Most of them are soluble in common organic solvents. Amorphous glassy PDIs have been obtained by either cooling from the liquid state or directly casting from solution. For some of them, even slowly precipitating from a solution by introducing methanol results in amorphous glassy precipitates. Note that such a low precipitation procedure is usually applied to encourage crystallization. The structures, particular the existence of π-stacks, as well as phase transition behaviors have been characterized using differential scanning calorimetry (DSC), wide-angle X-ray diffraction (WAXD), ultraviolet-visible spectroscopy (UV-vis). Furthermore, the correlation between molecular structure and glass-forming properties has been elucidated.

2.2. Molecular Design

PDIs are well known for their strong ability to pack into π-stacks. Inside a stack, a PDI molecule either rotates along the stacking axis with respect to its immediate neighbor or exhibits an offset without a rotation.[66-69] Such an ordered PDI π-stack lays the foundation of an ordered phase. For instance, the discotic LC phase of a few PDIs is on the basis of PDI π-stacks that are long-range orientationally ordered but without intra-stack positional order. Long-range positional ordered PDI π-stacks either will lead

to a crystalline or a two-dimensional crystalline smectic LC phase.[70] Therefore, to design a PDI molecular glass we should engineer the molecule in such a way that makes it difficult for an ordered PDI π-stack to form. A straightforward way is to increase the steric hindrance toward the formation of an ordered PDI π-stack. To retain the desired planar perylene ring for high charge carrier mobility, such an increased steric hindrance should come from the N-substituents. Moreover, since an amorphous glassy phase is always a metastable phase which is thermodynamically less stable than its corresponding crystalline or LC phase, measures must be taken to reduce the molecular mobility so that molecules can be "frozen" in the amorphous glassy phase. In this way, the transformation from the metastable amorphous glassy phase to a more stable ordered phase will be slow enough at application temperatures. In other words, the glass transition temperature of an amorphous PDI must be substantially higher than the targeted application temperatures, typically the room temperature (RT).

The general structure is shown in **Figure 2.1**. The R group can be tailored to control the steric hindrance. Since the R group is directly attached to the first carbon atom on the imide N atom, its space demand will have a significant influence toward the formation of an ordered PDI π-stack. Because this R group has more space demand along the stacking axis, the formation of an ordered PDI π-stack becomes more difficult, it is more likely to form an amorphous phase. The purpose of using benzyl group at the two ends of the molecule is to increase T_g due to its rigid nature. A graphic representation of such a PDI molecule is also given in **Figure 2.1**.

Note that such a molecule is quite large, when measured from a energy-minimized molecular model with R = CH_3, the length (in x direction) and width (in y direction) of the molecules are 27.0 Å and 6.75 Å respectively. Such a large size will enhance the relative stability of the amorphous state with respect to its ordered counterpart.

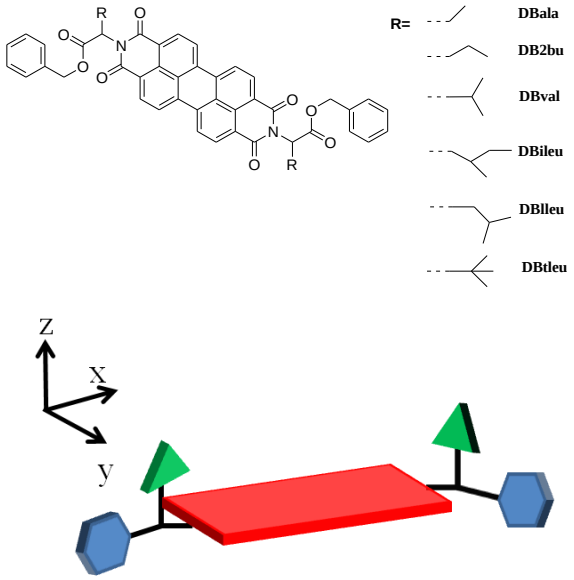

Figure 2.1. Molecular structure and model of amorphous glassy PDIs (In this model, red rectangular plates stand for PDI cores, green triangles stand for R group, and blue hexagons stand for the phenyl group)

2.3. Results

2.3.1. Structural and morphological characterization of molecular glassy PDI films

DBgly has very poor solubility in any solvent and both polarized light microscopy (PLM) and WAXD results suggest that it is a crystalline compound at RT. Since its melting point is higher than its decomposition temperature, it is not discussed in details here.

All other PDIs are highly soluble in chloroform and soluble in many common

organic solvents such as toluene, THF and dichloromethane. Among them, DBala is the least soluble one and its solubility in chloroform is greater than 100 mg/mL at RT. The 2% weight loss temperatures for all these PDIs are about 350 ^{o}C in a N_2 atmosphere as revealed by TGA.

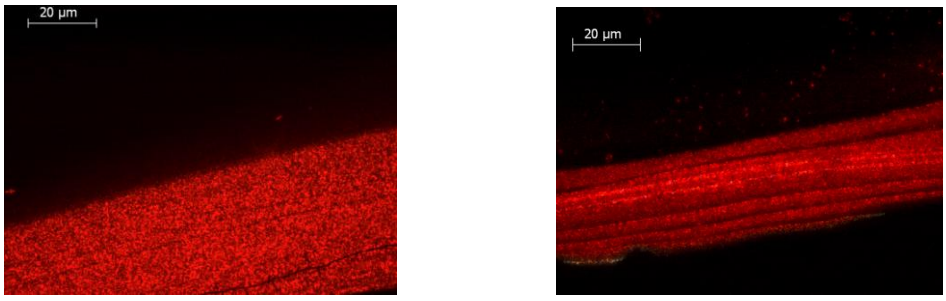

Figure 2.2. DBlleu (left) and DB2bu (right) drop-cast films at RT

Films have been prepared by both drop-casting at 45 ^{o}C on clean glass slides and spin-coating from 80 mg/ml chloroform solutions. PLM micrographs shown in **Figure 2.2** suggest that drop-cast DBlleu and DB2bu films were birefringent. This means that they are either crystalline or LC. On the other hand, all spin-coated films and the drop-cast films of other PDIs were completely dark. Since tilting a glass slide did not produce any birefringence, these films must be optically isotropic.

An optically isotropic material could be either amorphous or of cubic symmetry. To distinguish an amorphous phase from a cubic phase, WAXD experiments have been carried out and results were presented in **Figure 2.3a**.

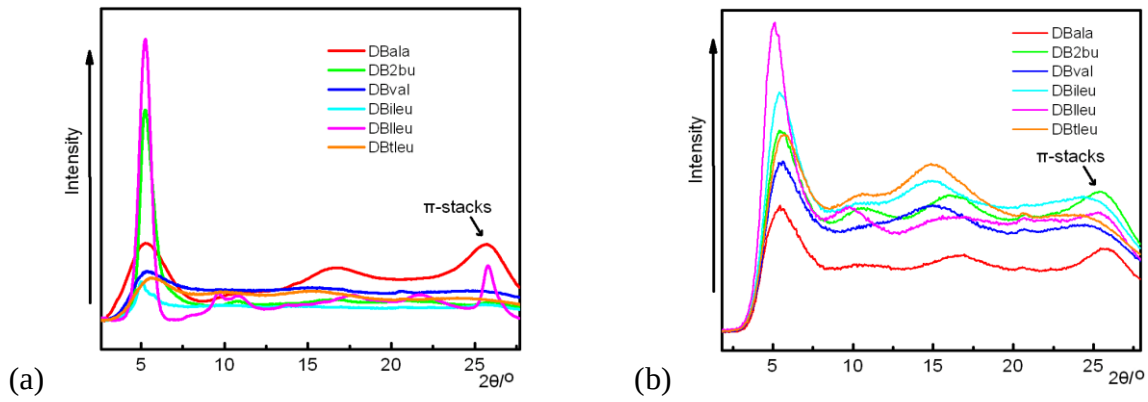

Figure 2.3. WAXD curves of PDIs: (a) drop-cast, (b) fast cooled from melt to RT

One dimensional (1D) WAXD curves shown in **Figure 2.3a** feature significantly sharper peaks at about 5^{o} 2θ angle for DB2bu and DBlleu than other PDIs, in agreement with the PLM observation, implying that drop-cast films of DB2bu and DBlleu are not genuine amorphous. The 1D WAXD curves for DBala, DBval, DBileu, DBtleu are typical for the amorphous phase. All diffraction peaks are very broad, signifying only short-rangle position exists. Combining with the fact that they appeared dark in PLM experiments, which indicates the absence of long-rangle molecular orientation order, one can conclude that drop-cast DBala, DBval, DBileu and DBtleu are amorphous. Furthermore, these films are rigid and brittle at RT, they must be amorphous glassy films. It is likely that all spin-coated PDI films are amorphous glassy because they produced dark PLM micrographs.

In contrast, the situation is slightly different when PDI films formed by cooling rapidly from the isotropic liquid state. These films were prepared by taking the samples in the molten state and directly placing them on a metallic surface at RT. PLM observations revealed that all these films were dark under crossed polarizers, hinting that

probably they are amorphous. The amorphous nature of these rapid-cooled PDI films was further confirmed by 1D WAXD curves presented in **Figure 2.3b** due to the absence of any sharp peaks.

The diffraction peak at about 5 ^{o} 2θ angle can be correlated to the length of a PDI molecule while the diffraction peak at about 25.5 ^{o} 2θ angle (d ≈3.5 Å) can be attributed to intra-stack separation of two adjacent PDI molecules. It is interesting to note that even in an amorphous phase such diffraction can still be observed. The d-spacing of this peak corresponds to the average inter-planar distance between two adjacent PDI cores in a π-stack (tightness) and the width of this peak relates to the correlation length of PDI π-stacks (order). The intra-stack inter-chromophore spacing values are listed in **Table 2.1**. Since this peak appears at different positions and exhibits different width in different amorphous specimen, it is quite clear that both the tightness and order of PDI π-stacks in an amorphous phase can be influenced by the nature of the R group.

Table 2.1. Intra-stack inter-chromophore d-spacing values of amorphous glassy PDIs

ID	d-spacing (Å)	
	fast-cooled	drop-cast
DBala	3.50	3.46
DB2bu	3.51	3.50
DBval	3.64	3.56
DBileu	3.65	3.55
Dblleu	3.51	3.46*
DBtleu	3.65	3.64

* significant crystallinity

Because an amorphous material does not have any preferred "shape", the surface of an amorphous film tends to be much smoother than that of a polycrystalline or a LC

polydomain film. The AFM micrograph and its corresponding section analysis are shown in **Figure 2.4**. With a root mean square roughness of 3.4 Å and roughness average of 2.7 Å, this is the smoothest film to the best of our knowledge if single crystalline surfaces are excluded. Such a property is highly advantageous in device fabrication.

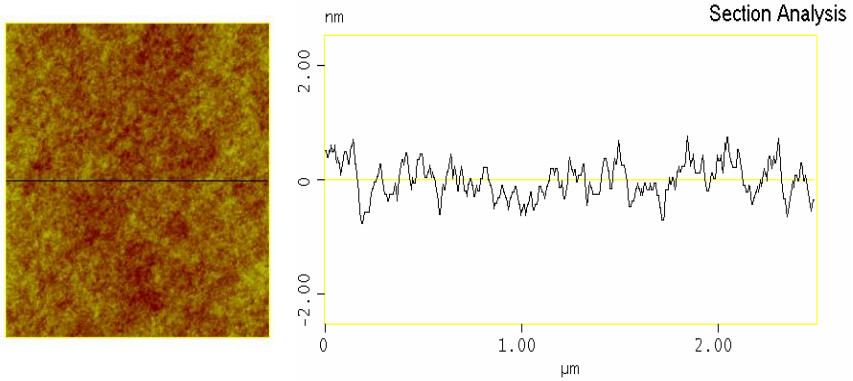

Figure 2.4. AFM height image and the corresponding section analysis of a spin-coated DBala film

2.3.2. Spectroscopic characterization of molecular glassy PDI films

It is know that π-stacking order of PDI could influence their spectroscopic responses considerably. UV-vis has been firstly employed to explore the π-stacking order of PDI chromophores in these solid films. Monomeric PDIs in diluted $CHCl_3$ solution feature absorption peaks at 526, 490, 460, and 432 nm.[55,71] All these peaks originate from the PDI π-π* transition. The fine structure appears due to the coupling between the vibrational transitions and the electronic transition. The peak at 526 nm is due to the transition from the vibrational ground state of the electronic ground state to the vibrational ground state of the first electronic excited state and it is denoted as the $0 \rightarrow 0$

transition. The peak at 490 nm is attributed to the transition from the vibrational ground state of the electronic ground state to the vibrational first excited state of the first electronic excited state and it is denoted as the $0 \rightarrow 1$ transition. In the same way, the peaks at 460 and 432 nm were denoted as the $0 \rightarrow 2$ and $0 \rightarrow 3$ transitions, respectively.

In spin-coated PDI films, the absorption at about 539, 499 and 472 nm can be observed, the later two overlap so that the 472 nm peak often appears as a shoulder, as depicted in **Figure 2.5**. The peak at 539 nm is due to the $0 \rightarrow 0$ transition, while the peaks at 499 and 472 nm can be attributed to the $0 \rightarrow 1$ and $0 \rightarrow 2$ transitions, respectively.

UV spectra of fast cooled samples are similar to spin-coated ones, except the $0 \rightarrow 0$ absorption peak of DBlleu is noticeably broader than other samples. A second order derivative analysis revealed that this peak has two components at 549 and 567 nm.

When a PDI packs into an ordered phase, strong excitonic interaction among the stacked PDIs often leads to splitting of peaks and/or appearance of absorption band at a longer wavelength.[53,74] The absence of such peaks in the UV spectra of most samples supports their amorphous nature, which is the agreement with the PLM and WAXD results. However, the fact that two components could be identified in the $0 \rightarrow 0$ transition peak of fast cooled DBlleu films favors the argument of this film being partially crystalline. This observation does not fully agree with the WAXD pattern shown in **Figure 2.3b**. This is understandable as WAXD is not sensitive enough to pick up a few percent of crystallinity. A reasonable explanation is that during the rapid

cooling, a few percent of DBlleu crystallized, which is not sufficient to cause noticeable change in the WAXD curve but detectable in UV.

Although the peak positions of these amorphous glassy PDI films remain similar to that of their free molecular state, the relative intensities change considerably. Upon on aggregation, the absorption maximum blue-shifts by 0.17 eV from the 0→0 transition to the 0→1 transition, probably due to strong electron-phonon coupling in the stacked chromophores. In the monomeric state, the $A^{0\rightarrow0}/A^{0\rightarrow1}$ (intensity ratio of the 0→0 transition to the 0→1 transition) is equal to 1.6. When PDI chromophores are incorporated into π-stacks, $A^{0\rightarrow0}/A^{0\rightarrow1}$ decreases. It has been found that the more PDI molecules are added to a stack, the smaller the $A^{0\rightarrow0}/A^{0\rightarrow1}$. Thus the $A^{0\rightarrow0}/A^{0\rightarrow1}$ may be used to estimate the degree of aggregation in the amorphous glassy PDI films.[72] The $A^{0\rightarrow0}/A^{0\rightarrow1}$ values are listed in **Table 2.2**. In both type of films, the π-stacking order can be influced by the choice of R.

Table 2.2. $A^{0\rightarrow0}/A^{0\rightarrow1}$ values of amorphous glassy PDIs

ID	$A^{0\rightarrow0}/A^{0\rightarrow1}$	
	fast-cooled	spin-coated
DBala	0.832	0.696
DB2bu	0.895	0.721
DBval	1.012	0.949
DBileu	0.909	0.873
Dbllеu	0.755	0.606
DBtleu	0.956	0.893

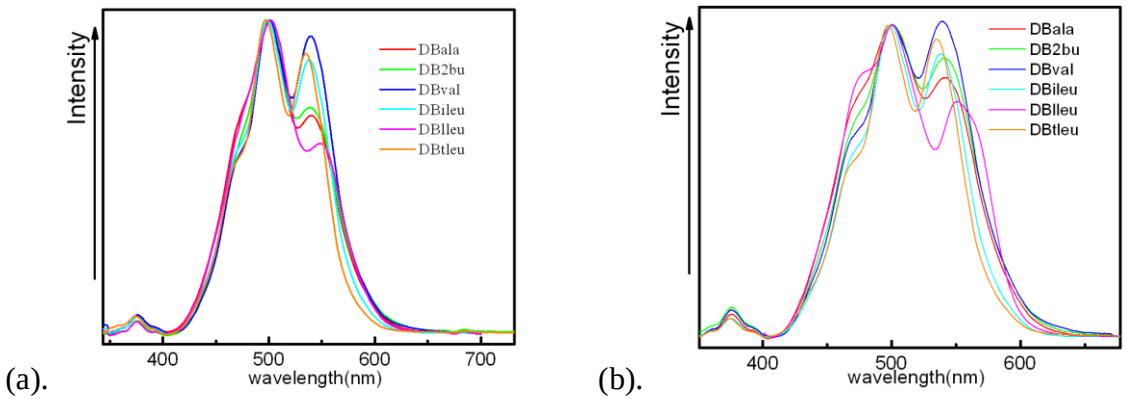

Figure 2.5. UV absorption spectra of amorphous PDIs from spin coating (a) and fast cooled from the melting (b)

The remarkable characteristic of aggregated chromophores is that they emit photoluminescence of completely different colors from that of the free monomeric molecules.[72] In **Figure 2.6**, the amorphous films prepared both from spin-coating and fast-cooling from the melt displayed peaks with positions varying from 628 – 656 nm which were largely red-shifted from that of monomeric PDIs.[71] More importantly, the absence of emission peaks below 600 nm substantiates the argument of all PDI molecules being π-stacked.

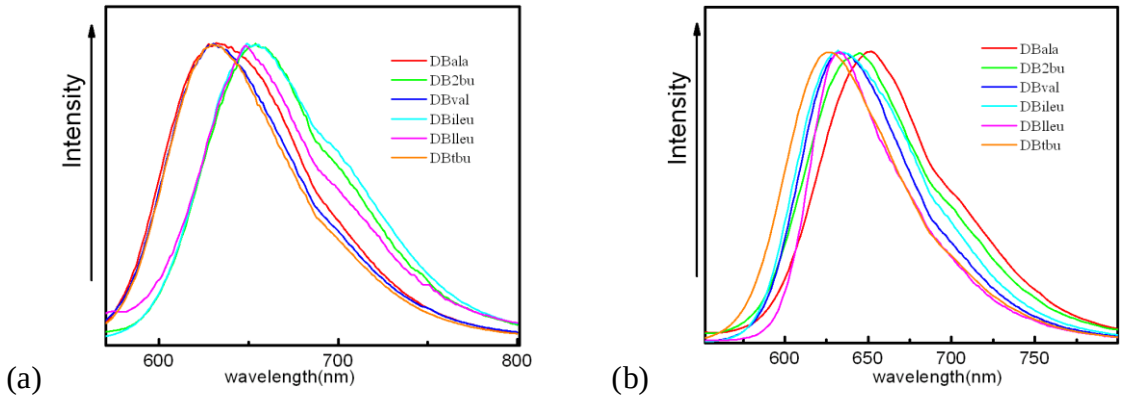

Figure 2.6. Fluorescence spectra of spin-coated (a) and fast-cooled PDI films (b) (Peaks were normalized to the same intensity, excited at 490 nm.)

In addition, FTIR experiments have been carried out to investigate how R affects the stacking of PDIs in these solid films. Here we use stretching frequency of the ester C=O as the spectroscopic probe. The ester C=Os in a tightly packed PDI π-stack would experience stronger dipole-dipole interaction and thus the $\nu_{C=O}$ band shifts to lower frequency.[73] The ester $\nu_{C=O}$ values are listed in **Table 2.3**. One can see that DBala, DB2bu and DBlleu possess the tightest π-stacks, while ester C=Os in DBval and DBtleu are engaged in a much weaker dipole-dipole interaction, probably due to larger intra-stack intermolecular separation.

Table 2.3. Ester $\nu_{C=O}$ values of amorphous glassy PDIs

ID	ester $\nu_{C=O}$ (cm^{-1})	
	fast-cooled	drop-cast
DBala	1747.7	1748.6
DB2bu	1747.7	1748.2
Dblleu	1747.7	1748.2
DBileu	1752.5	1753.0
DBval	1754.9	1754.0
DBtleu	1754.0	1754.0

2.3.3. Phase transition behavors of molecular glassy PDI films

The DSC traces of drop-cast samples are shown in **Figure 2.7** and the details are listed in **Table 2.4**. During the first heating, DBala displayed a T_g at 124 ^oC, one broad crystallization peak at 190 ^oC, and complicated melting peaks around 231 ^oC. For the DB2bu and DBval, besides the glass transition during the first heating the crystallization and melting peaks are very complex, therefore only the highest melting peak position was listed in **Table 2.4**. DBileu and DBlleu both displayed one crystallization and one

melting peak in addition to the glassy transition, whereas the peaks of DBileu were very small and DBlleu's melting peak was much larger. For DBtleu, the first heating trace only contains a step-wise glass transition.

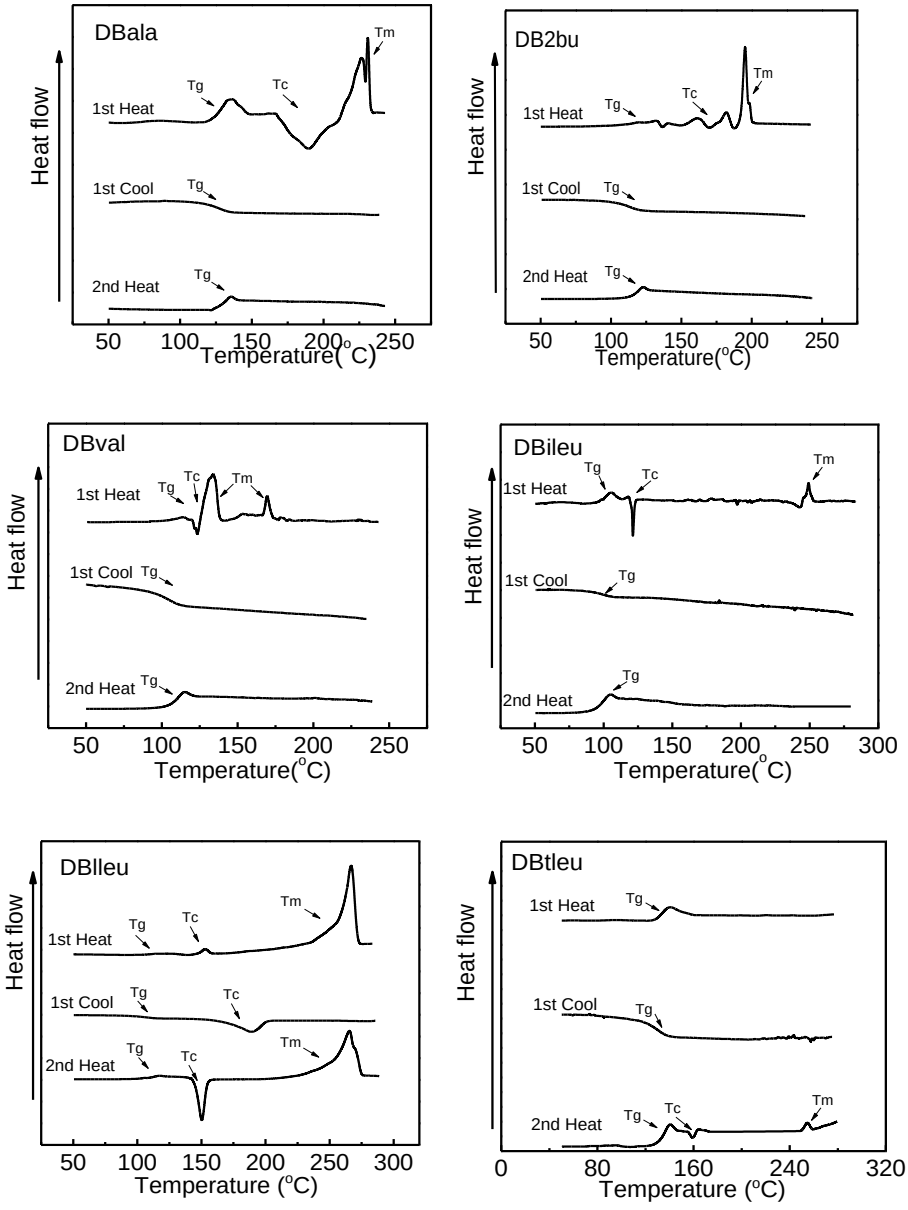

Figure 2.7. DSC data of amorphous materials (All the samples were prepared from $CHCl_3$ solution dried sample under vacuum at 50°C. The graphs contain: 1st heat from -50°C to melt, 1st cool after melt to -50°C, 2nd heat after cooled. All have the same rate

of 20°C/min.)

Table 2.4. Thermal analysis of amorphous materials based on DSC experiments

(T_g, T_c and T_m: °C, ΔH: kJ/mol)

Name	1st Heat			1st cool		2nd heat			Heat after annealed		
	T_g	T_c/(ΔH)	T_m(ΔH)	T_g	T_c(ΔH)	T_g	T_c(ΔH)	T_m(ΔH)	T_g	T_c(ΔH)	T_m(ΔH)
DBala	124	190(-13.2)	231(16.5)	130	-	130	-	-	131	201(3.2)	231(3.2)
DB2bu	111	A	198[b]	115	-	115	-	-	116	-	-
DBval	100	A	230[b]	105	-	105	-	-	112	-	223(6.1)
DBileu	100	121(-0.7)	249(0.9)	98	-	98	-	-	103	123(-0.8)	276(2.4)
DBlleu	110	139(-0.7)	267(37.1)	110	189(-13.1)	110	150(-13.0)	266(40.1)	109	138(-15.0)	266(40.4)
DBtleu	133	-	-	133	-	133	159(-0.4)	255(0.4)	134	155(-0.5)	267(0.6)

a: there are multiple small peaks including recrystallization and melting during heating.

b: the highest melting peak

To better understand the nature of these transitions, PLM observations were made when drop-cast samples were being heated at 20 ℃/min. At RT, small bright spots could be found in DB2bu and DBlleu while the rest of samples were completely dark. When temperature increased to about 190 °C, needle-like bifringent objects emerged in DBala as shown in **Figure 2.8a** probably indicating a crystallization process. Similarly, an ordering process is observed at 180 °C for DB2bu (**Figure 2.8b**) and at 245 °C for DBlleu (**Figure 2.8c**) in the form of appearance of birefringent objects. These phenomena were in agreement with the assignment of ordering processes to those exothermic thermo events.

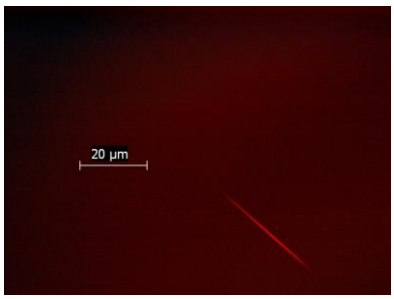

(a) DBala at 190 ^{o}C

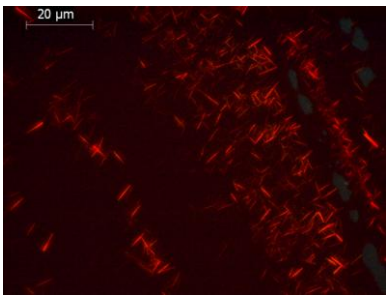

(b) DB2bu at 180 ^{o}C

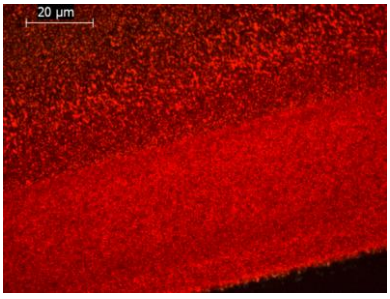

(c) DBlleu at 250 ^{o}C

Figure 2.8. PLM graphes displaying crystals appeared during the 1st heating

During cooling from the isotropic melt at 20 ^{o}C/min, only DBlleu displayed a prominent exothermic peak due to crystallization, which is in agreement with the PLM observation that only DBlleu was birefringent during cooling. All the other PDIs only exhibited a glass transition.

During the second heating, the step-wise glass transition has been observed for all PDIs. Additional thermo events have been observed for DBlleu and DBtleu. DBtleu displayed a tiny exothermic (probably due to crystallization) peak and a corresponding endothermic (probably due to melting) peak. The two peaks have nearly the same transition enthalpy, indicating the crystals that contributed to the melting peak entirely came from the crystallization process that took place during the second heating. DBlleu had a large recrystallization peak and an even larger melting peak, indicating that crystallization occurred during cooling from the melten state as well as during the second

heating, as was supported by the appearance of exothermic peak during the first cooling.

2.3.4. Stability and formation tendency of amorphous glassy PDIs

The amorphous glassy phase is always metastable. With the exception of some atactic polymers, such a phase is less stable than the corresponding thermodynamically stable ordered phase, typically a crystalline phase. This is particularly true for molecular glasses. Nevertheless, because large scale molecular motions are not allowed in a glassy phase, the transition from an amorphous glassy phase to the corresponding ordered phase is practically at rate of zero if the temperature of the molecular glass is substantially lower than T_g. Thus the T_g of an molecular glass itself does reflect the practical stability of the material. The higher the T_g is, the more stable the molecular glass. However, glass transition is not a purely thermodynamically controlled phase transition but instead it is strongly kinetic dependent. For instance, the T_g value from a dynamic mechanical analysis measurement is frequency dependent. Similary, the T_g measured by DSC depends on the heating/cooling rate. The slower the heating/cooling rate is, the lower the T_g. In other words, when a molecular glass is annealed at a temperature which is slightly lower than its T_g from a DSC scan with a heating/cooling rate of 20 ^oC/min, its temperature might be equal or higher than the real T_g due to the very low heating/cooling rate (annealing). All our molecular glassy PDIs possess a T_g near or higher than 100 ^oC (from DSC scans), it seems no need to worry about the application temperature being too close to RT. However, when intergrated in a device, the electric resistance heating effect during device operation could raise the temperature

considerably. In such a case, not only the T_g value which signifies the onset temperature of large scale molecular motion will influence the stability of a molecular glass, the rate of ordering process (for instance crystallization) in the vicinity of the T_g also needs to be considered.

In order to investigate the stability of the amorphous glassy PDIs in the vicinity of the T_g, annealing experiments were executed at 5 ^oC below corresponding T_gs for 12 hours after cooling at a rate of 20 ^oC/min from the isotropic liquid. A heating process at a rate of 20 ^oC/min was used to probe the transition behaviors after cooled to -50 ^oC at 20 ^oC/min. The results are shown in **Figure 2.9.** Glass transition had been observed for all these PDIs and DB2bu displayed only this transition. All the other PDIs exhibited additional transitions. For DBala, the crystallization peak area was equal to that of the melting peak, meaning the ordered structural formed was completely from the crystallization during heating. Similar conclusion could be drawn for DBtleu, the area of the melting peak was almost the same as that of the crystallization peak and both of them were very small. For DBval, there was no crystallization peak during the heating process thus the ordered structure must be developed exclusively during the annealing process. For DBileu and DBlleu, although the crystallization peak appeared during heating, the melting peak was still much larger, indicating the ordered structure was only partially developed during heating while the annealing process must also have made a substantial contribution.

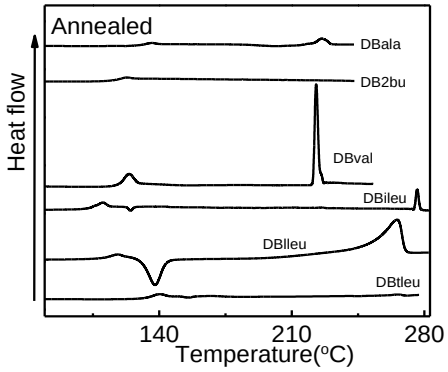

Figure 2.9. DSC traces of glassy PDIs after being annealed at 5 ℃ below T_gs for 12 hours

The annealing experiment results suggested that some of PDI molecular glasses crystallized so slowly that no detectable crystallinity had been developed even when they had been annealed for 12 hours at temperatures very close to their T_gs. Such an observation prompted us to carry out experiments under the condition that typically strongly favors the growth of crystals. Our original intention was to obtain highly crystalline PDIs as the standards for calculating the crystallinity of partially crystalline materials by DSC and/or WAXD. However, to our surprise, some of PDIs simply refuse to crystallize.

The samples were prepared as 1 mg/ml chloroform solutions. A small vial containg 1 ml such a solution was placed in a sealed bottle with a layer of methanol at the bottom. In such a setup, the chloroform in the vial had been slowly replaced by methanol which is a poor solvent for PDIs. The temperature had been maintained at RT. It took one week for a PDI to nearly fully precipitate from the solution. The solid samples were sparated from the nearly colorless solution, washed with methanol and

dried. The samples were examined by PLM, DSC and WAXD. Three of samples (DBala, DB2bu and DBlleu) were bright under crossed polarizers and other three (DBval, DBileu and DBtleu) were dark. According, 1D WAXD patterns presented in **Figure 2.10** fully agree with the PLM observations. DBala, DB2bu, DBlleu exhibit obvious sharp peaks indicating the at least partially crystalline structures while DBval, DBileu and DBtleu only displayed broad peaks, pointing out an amorphous phase.

DSC traces of these precipitated solids are illustrated in **Figure 2.11**. The glass transition has been observed for all samples. Additional enthalpic peaks showed up in the DSC traces of DBala, DB2bu and DBlleu. Since the area endothermic peak(s) is much larger than that of exothermic peak(s), DBala, DB2bu and DBlleu must be at least partially crystalline when slowly precipitated from the solution. In contrast, the absence of any enthalpic peaks in the DSC traces of DBval, DBileu and DBtleu confirms the amorphous glassy nature of their RT phase, as revealed by PLM and WAXD results. They simply refuse to crystallize.

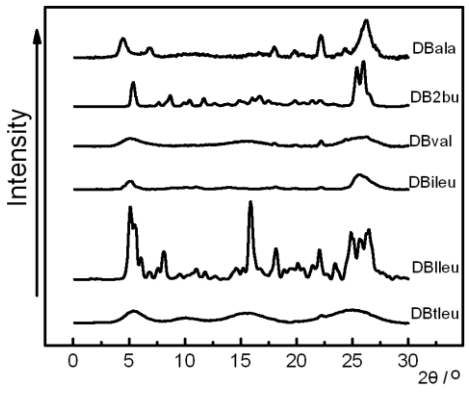

Figure 2.10. 1D WAXD patterns of the precipitated samples prepared by exposing 1 mg/ml $CHCl_3$ solutions in methanol vapor at RT for a week at RT

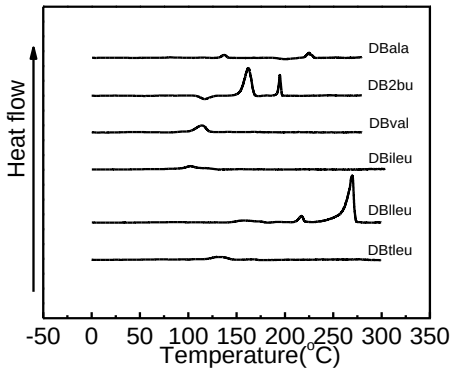

Figure 2.11. DSC curves of the precipitated samples prepared by exposing 1 mg/ml $CHCl_3$ solutions in methanol vapor at RT for a week at RT

2.4. Discussion

2.4.1. Amorphous glassy forming tendency and its dependence on R

Isotropic, amorphous glassy films of all PDIs have been successfully obtained by spin-coating from chloroform solution. Rapid cooling from the isotropic melt can also render all PDIs except DBlleu completely amorphous. In contrast, drop-casting leads to at least partially ordered DBlleu and DB2bu, while other PDIs remain amorphous. In a spin-coating process, a drop of solution solidifies in a fraction of a second, giving the shortest time for an ordered structure to nucleate and grow. Therefore it is the most efficient method out of three methods used by us to produce an amorphous PDI film. Drop-casting, on the other hand, gives PDI molecules the longest time to organize before the solidification occurs. Furthermore, the existence of solvent molecules increases the mobility of PDI molecules noticeably, which also favors the formation of a thermodynamically more stable ordered phase. Consequently it is the method that is most vulnerable to crystallization. The interesting observation here is that the

amorphous glassy forming ability of PDIs clearly exhibited R group dependence. When R is an isobuyl group, the PDI (DBlleu) is the most susceptible to crystallization, only spin-coating is able to produce a truly amorphous DBlleu film. In this series, when R is an ethyl group, the PDI (DB2bu) can be made amorphous by either spin-coating or rapid-cooling from the melt, but drop-casting produces an at least partially crystalline film. DBala is more willing to crystallize than DBileu, DBval and DBtleu. The latter three compound refuse to crystallize even when precipitate very slowly (oven the course of several days) from solution.

Apparenty, the crystallization rate is fastest for DBlleu having the isobutyl group. The isobutyl group uses its two methylene units to connect to the carbon atom which directly attaches to the imide nitrogen. This arrangement provides large conformational flexibility with little increase to the steric hindrance toward the PDI π-stack formation thus has the best ability to encourage the formation of ordered PDI π-stacks. DB2bu, having ethyl group as the R, offers less conformational flexibility and therefore slower crystallization rate. DBala, having methyl group as the R, does not enjoy much conformational flexibility from methyl group so that it crystallizes slower than DB2bu. On the other hand, methyl group does not create too much steric demand toward the formation of PDI π-stacks. As the results, DBala crystallizes faster than DBileu, DBval and DBtleu. The latter three PDIs have either secondary or tertiary alkyl group as the R group which demands significantly more space along the π-stacking axis than a methyl or primary alkyl group does. Such a large steric demand makes it difficult for an ordered

PDI π-stack to form, thus DBileu DBval and DBtleu crystallize slower than other PDIs. DBtleu features the most space demanding tertiary butyl as the R group which makes it most difficult to form ordered PDI π-stacks, consequently, it has the strongest glassy forming tendency.

To smmerize, the glassy forming tendency of a PDI can be understood by considering both the flexibility and the steric demand of an R group toward the PDI π-stack formation. The more flexible the R is, the more likely for the PDI to crystallize. On the countary, the more steric demand the R group has toward the PDI π-stack formation, the stronger glassy forming ability the PDI has.

2.4.2. Stability of the glassy phase and its dependence on R

For small glassying forming molecules, since the amorphous glassy phase is always a metastable phase, its practical stability is guranteed by kinetic factors that slow down the transition from the amorphous glassy phase to a corresponding ordered phase so much that practially is not considered happening. Thus the parameter that has the largest impact on the practical stability is the glass transition temperature, T_g. Since the T_g value of a specimen depends on its prior thermal history, only T_g values measured during 1st cooling are considered.

DBtleu exhibits the highest T_g, thanks to its highest molecular mass and the absence of any flexible substituents. DBala, although features the lowest molecular mass, the absence of flexible alkyl group and the strongest π-π interaction due to the smallest steric hindrance result in a respectable T_g of 130 ℃. DB2bu having R = ethyl

displays a T_g of 115 ℃. The somewhat lexible ethyl group reduced the T_g by 10 ℃ with respect to DBala. DBval exhibits a T_g of 105 ℃. The R group is isopropyl. Considering the very limited conformational flexibility of this group, the lower T_g of DBval when compared wit DB2bu where R = ethyl group can be attributed to weaker π-π interaction caused by the larger steric hindrance of isopropyl group.

It is quite interesting to see that although DBileu and DBlleu possess the same molecular mass as DBtleu, their T_gs are evidently lower. The R groups in DBileu and DBlleu are 1-methylpropyl and 2-methylpropyl (isobutyl), respectively. In the comparison with tertiary butyl group in DBtleu, the R groups in DBileu and DBlleu are markedly more flexible due to a larger number of conformers, which reduces the T_gs considerably. Since methyl substitudent on the 2-methylpropyl group in DBlleu is one methyelen unit further from the PDI core than that on the 1-methylpropyl group in DBileu, the PDI π-π interaction in DBlleu is stronger than that in DBileu, resulting the relatively higher T_g of 110 ℃ verus 98 ℃ for DBileu. Note that all PDIs exhibit T_gs near or higher than 100 ℃ which is much higher than RT.

Apparently, the R dependence of T_g values can also be understood by considering both the flexibility and steric demand of the R, in addition to the molecular mass factor. The more flexible the R is, the lower the T_g. At the same time, weaker π-π stacking interaction is, the lower the T_g. Besides, a higher molecular mass tends to result in a higher T_g.

These PDI films demonstrated remarkable phase stability when being annealed at

a temperature 5 ℃ below their T_gS. DBtleu and DB2bu were completey amorphous after annealing while DBala, DBileu and DBlleu were only partially crystalline as indicated by the presence of the exothermic peak during heating. DBval exhibited the poorest stability in the annealing experiment. For many PDIs, exothermic peak(s) was(were) observed during heating after annealing. Without such an annealing process, the exothermic peak was not observed for DBlleu. Such exothermic peaks were also observed when heating drop-cast samples. The appearance eof such exothermic peak(s) indicates the occurance of crystallization.

When directly cooled from the isotropic melt as a rate of 20 ℃/min, the nucleation rate for most of PDIs is too slow to even form nuclei. The exception is DBlleu, due to the relative strong PDI π-π stacking interaction and the mobile isobutyl group, it crystallize readily even during cooling from the isotropic melt at a rate of 20 ℃/min, as evidented by the exothermic peak during the first cooling. However, even for DBlleu, the crystallization is far away from completion under such a cooling condition. Thus, the crystallization continued when the temperature of the sample was raised to high enough during the second heating. For other PDIs, because there were not enough nuclei formed during cooling, the homogeneous nucleation during heating was too slow to produce any sizable amount of crystals.

During a drop-casting process, although crystallization rate was still slow for most of PDIs, it was significantly faster than that in cooling from the melt. Aparently, the presence of sovent molecules inceases the mobility of PDI molecules and facilitates the

crystallization. This can be clearly seen by comparing the heating and second DSC traces of drop-cast DBlleu. The exothermic peak observed during the first DSC trace is much smaller than the exothermic peak observed during the second heating, while the endothermic peaks observed during the first and the second heating are of the similar area. This means most of DBlleu molecules already crystallized in the process of drop-casting, while during cooling from the melt a significant part of DBlleu molecules remained amorphous. For DBala, DBval and DBileu, the drop-casting could not produce any measurable crystallinity. However, tiny nuclei formed. During the second heating process, those tiny nuclei acted as the seeds for heterogeneous nucleation which features less energy barrier than homogeneous nucleation.

2.4.3. PDI π-stacks and their tuning

Many attractive properties of organic semi-conducting materials can be attributed to their ability to from π-stacks. Although orientation ordered PDI π-stacks do not exist in amorphous glassy PDIs, disordered π stacks could present. At least orientationally ordered PDI π-stacks can be considerated as the fundations of ordered (LC or crystalline) PDI. An orientationaly ordered π-stack means all PDI molecules in the stack maintain the same orientation. On the other hand, if such a long-range orientation correlation is lost, the phase will not longer be optically anisotropic and an amorphous phase may result. One can consider orientationaly ordered PDI π-stacks as rigid rods while π-stacks without such orientational order can be considered as noodles.

The existence of PDI π-stacks was first evidented by the observation of the

WAXD diffraction peak around 3.5 Å d-spacing. This d-spacing is indicative of stacked π-systems with intra-stack separation of 3.5 Å. This peak is most prominent in the case of DBala. The exact location and the width of this peak is R dependent. Generally speaking, the smaller the steric demand the R has toward the PDI π-stack formation, the smaller the d-spacing is. Among both drop-cast and rapid-cool samples, DBala features the tightest PDI π-stacks. π-Stacks in DB2bu and DBlleu are not as tight as DBala, but tighter than that in DBval, DBileu and DBtleu. This trend can be correlated to the R grups: methyl in DBala; ethyl and isobutyl in DB2bu and DBlleu; isopropyl, 1-methylpropyl and tertiary butyl groups in DBval, DBileu and DBtleu, respectively.

PDI π-stacks in a drop-cast glassy film are generally tighter than that in a corresponding rapid cooled film. This is because a drop-casting process, molecules have more chance to find a relative low position in the energy landscape so it tends to produce a more stable glass. A most stable glass tends to have stronger intermolecular interaction and here π-π stacking interaction is one of the most important intermolecular interactions. The R group dependence of PDI π-stack tightness is also supported by FT-IR results. Since the stretching vibration frequency of an ester C=O is sensitive to the dipole-dipole interaction, plus a tighter PDI π-stack usually translates into a stronger ester dipole-dipole interaction, $\nu_{C=O}$ can be correlated to the tightness of PDI π-stacks. As we can see in the **Table 2.3**, the $\nu_{C=O}$ of DBala and DB2bu are significantly lower than that of DBileu, DBval and DBtleu, which suggests that the dipole-dipole attraction force experienced by the ester C=O in DBala and DB2bu is clearly stronger than that in

DBileu, DBval and DBtleu. This is most likely caused by a tighter π-stacking arrangement in DBala and DB2bu than that in DBileu, DBval and DBtleu. The different steric effects of the R groups toward the PDI π-stack formation may be the root cause.

Not only the peak position at ~ 3.5 Å is R group dependent, the peak width only varies with the R group. The width of an X-ray diffraction peak is inversely proportional to the correlation length of the periodic structure from which the diffraction arises, if the instrumental broadening effect is removed. Among the rapid cooled films, the PDI π-stack diffraction peak is the narrowest when R = methyl and ethyl (DBala and DB2bu). Such a diffraction peak in DBlleu (R = isobutyl) is somewhat broader. DBval, DBileu and DBtleu exhibit much broader diffraction peak at d-spacing ~ 3.5 Å. For drop-cast films, DBleu and DB2bu are not considered here because of their crystallinity. The diffraction at ~ 3.5 Å of DBala is substantially sharper than other three amorphous glassy PDIs (DBval, DBileu and DBtleu). These observations suggest that when the R group is more steric demanding toward the PDI π-stack formation, it leads to the formation of PDI π-stacks with shorter correlation.

The R-dependence of the correlation length of PDI π-stacks was also confirmed by UV absorption spectroscopy results. It has been found that the more PDI molecules are added to a stack, the smaller is the $A^{0\rightarrow0}/A^{0\rightarrow1}$. Thus we may use $A^{0\rightarrow0}/A^{0\rightarrow1}$ to estimate the degree of aggregation in the amorphous glassy PDI films. Among the rapid-cooled glassy PDI films, the $A^{0\rightarrow0}/A^{0\rightarrow1}$ ratio of DBala is the lowest one which is followed (in the order of increasing value) by DB2bu, DBileu, DBtleu and DBval. The

spin-coated films exhibited the similar trend.

2.5. Conclusions

A series of glass forming PDIs has been designed and successfully synthesized. The design was on basis of introducing steric hindrance toward PDI π-stack formation as the means of avoiding the formation of ordered structures. The controlled introduction of such steric hindrance was materialized by using a steric controlling group R with tunable space demand toward PDI π-stack formation. Highly smooth, transparent amorphous glassy films were prepared by drop-casting, spin-coating from solution and fast cooling from the melt. The glass forming tendency of a PDI is strongly dependent upon the nature of the steric control group R as expected. A rigid and steric demanding R group leads to the strongest glass forming tendency. In fact, the PDI with R = tertiary butyl group exhibited exceptional glass forming tendency. Completely amorphous glassy materials were always obtained from this compound no matter what procedures were used including one that was typically reserved for the growth of crystals. Glass transition temperatures of the formed glassy materials are all near or above 100 ℃ and they are R group dependent as well. Furthermroe, the nature of R group not only strongly affects the glass forming tendency, but also influences the structure of the formed glassy phase. The smallest R corresponds to the amorphous glassy phase with the tightest and most ordered PDI π-stacks. Such an ability to tune π-stacks in the amorphous glassy phase enables us to tailor the properties of glassy forming semi-conducting molecules according to our needs. For instance, DBala might be the most appealing candidate due

to the tightest and most ordered PDI π-stacks when charge transport performance is considered the most important. On the other hand, if the glassy forming tendency is considered the most important, DBtleu would be the best pick.

2.6. Experimental section

Instruments and Characterizations

^{1}H and ^{13}C NMR spectra were recorded on Varian 300 MHz NMR spectrometer with deuterated chloroform ($CDCl_3$) as the solvent at 25 ^{o}C. The chemical shifts were reported using TMS as the internal standard of 0 ppm. Infrared radiation spectra were obtained from Vertex 70 V FT-IR spectrometer at the resolution of 1 cm^{-1}. UV spectra were collected on a Varian UV spectrometer, ave time was set to 0.333 nm/s and we scanned from 700 nm to 300 nm. Fluorescence spectra were collected on Varian Cary Eclipse Fluorescence Spectrophotometer with a resolution of 1 nm and excitation wavelength of 490 nm. Polarized optical microscopy (POM) was performed on a Leica DM LB2 microscope equipped with a Mettler Toledo hot stage with a FP82HT temperature controller. DSC experiments were performed on a Perkin-Elmer PYRIS Diamond differential scanning calorimeter. The samples for the first scans were prepared as follows: place drops of the 80 mg/ml chloroform solution into a DSC pan, evaporate the solvent by vacuum drying at 50 ^{o}C until constant weight. During DSC experiments the scan rate was 20 ^{o}C/min. The specimens were continually used for the following DSC experiments of cooling and reheating processes. Elementary analysis data has been collected in Atlantic Microlab. High resolution mass spectrometry(HRMS)

were performed on Agilent 6520 Q-TOF in Hunter College, CUNY.

Materials and Synthesis

Materials: ALIQUAT 336 was kindly provided by Cognis Corporation. All the other reagents and chemicals were purchased from Fisher scientific or VWR international and used as received.

Synthesis procedure of **1** is outlined below:

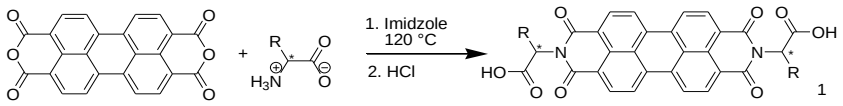

1a, R= CH3
1b, R= CH_2CH_3
1c, R= $CH(CH_3)_2$
1d, R= $CH(CH_3)C_2H_5$
1e, R= $CH_2CH(CH_3)_2$
1f, R= $C(CH_3)_3$

General synthesis procedure of **1**

Into a 50 ml Schlenk flask were charged corresponding amino acid (21 mmol), 3,4:9,10-perylenetetracarboxyldianhydride (PTCDA) 3.92 g (10 mmol), and imidazole (28 g). The mixture was purged with argon for 15 minutes before the reaction. The mixture was heated at 120 ^{o}C with argon purged on until the mixture was tested to be completely soluble in water. Subsequently, the reaction mixture was cooled to 90 ℃. Deionized water was then added with the protection of argon. The dark red solution was filtered to remove the trace amount of unreacted PTCDA. The solution was then acidified with 2 M HCl aqueous solution to a pH value of 3-4, the precipitate was collected by suction-filtration and thoroughly washed with deionized water until the filtrate was neutral; the red solid was collected and dried at 75 ℃ in vacuum oven until

constant weight.

N, *N'*-di((*S*)-1-carboxylethyl)-3,4:9,10-perylenetetracarboxyldiimide (**1a**) The corresponding amino acid was L-alanine, R = CH3, yield **1a** 5.15 g (96.4%).

N, *N'*-di((*S*)-1-carboxylpropyl)-3,4:9,10-perylenetetracarboxyldiimide (**1b**) The corresponding amino acid was L-2aminobutyricacid, R = CH_2CH_3, yield **1b** 5.37 g (95.6%).

N, *N'*-di((*S*)-1-carboxyl-2-methylpropyl)-3,4:9,10-perylenetetracarboxyldiimide (**1c**) The corresponding amino acid was L-valine, R = isopropyl, yield **1b** 5.60 g (94.8%).

N, *N'*-di((*1S, 2S*)-1-carboxyl-2-methylbutyl)-3,4:9,10-perylenetetra carboxyl-diimide (**1d**) The corresponding amino acid was L-isoleucine, R = 1-methylpropyl, yield **1d** 5.82 g (94.1%)

N, *N'*-di((*S*)-1-carboxyl-3-methylbutyl)-3,4:9,10-perylenetetracarboxyldiimide (**1e**) The corresponding amino acid was L-leucine, R = 2-methylpropyl, yield **1e** 5.9 g (95.4%)

N, *N'*-di((*S*)-1-carboxyl-2, 2-dimethylpropyl)-3,4:9,10-perylenetetracarboxyl-diimide (**1f**) The corresponding amino acid was L-tert-leucine, R = 2, 2-dimethylpropyl, yield **1f** 5.69 g (92.1%)

2a (DBala), 2d (DBileu), 2e (DBlleu) were synthesized in the following method:

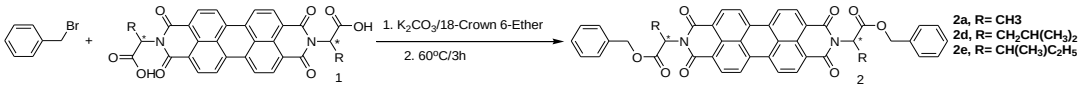

First, 534 mg (1 mmol) 1a was dissolved in 5 ml DMF with 0.138 mg K_2CO_3.

After all the 1a dissolved, 5.8 g 10% 18-crown-6 ether DMF solution was poured into the mixture. Subsequently, 513 mg (3 mmol) Benzylbromide was added to the mixture and the vial was sealed. The vial was heated in oil bath at 60 ^{o}C for 3 hours. 40ml methanol was poured into the mixture and red solid precipitated out. After the methanol solution was removed by filtration, the solid was dried at 75 ℃ in vacuum oven until constant weight. The crude product was purified by column chromatography on silica gel using 3% (volume) acetone/$CHCl_3$ as the eluent.

2c (DBval) was synthesized as below:

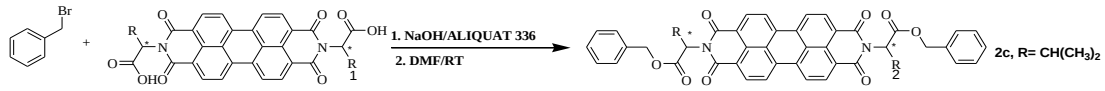

590 mg (1 mmol) **1c** was dissolved in 10 mL 1 % NaOH aqueous solution. 0.9 g (~ 2 mmol) ALIQUAT336 was dissolved in 10 ml 2:1 (v/v) ethanol/H_2O mixture. Two solutions were mixed and stirred at RT for 30 minutes. Then the mixture was extracted three times by using petroleum ether (3 ×10 mL) and the combined petroleum ether solution was evaporated to dryness. Subsequently, the residue was further dried at 75 ℃ for 2 hours in a vacuum oven. Then the residue was dissolved in 10 mL DMF followed by adding 0.4 g (3 mmol) benzylbromide. The mixture was stirred at RT for 12 hours. 40 mL methanol was poured into the mixture and the solid precipitated out. The solid was collected by suction-filtration and washed thoroughly with methanol. After being dried at 75 ℃ in vacuum oven until constant weight, the crude product was purified by column chromatography on silica gel using 3% (volume) acetone/$CHCl_3$ as

the eluent.

2b (DB2bu), 2f (DBtleu) were synthesized as below:

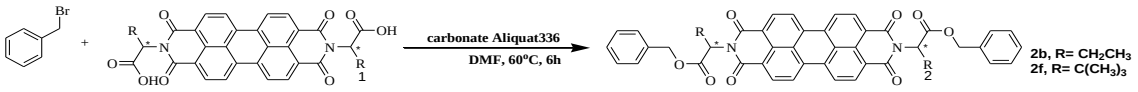

48 g (50 mmol) Aliquat336 was dissolved in 200 ml hexane. The hexane solution was continuously washed by saturated K_2CO_3 aqueous solution until there was not Cl^{-1} left in hexane phase. The hexane was removed by rotate evaporator and the produced carbonate Aliquat336 was dried thoroughly in vacuum oven at 50 ^oC overnight. Yield was 86 g (90 %).

562 mg (1mmol) **1b** was mixtured with 1 g (~1 mmol) carbonate Aliquat336 in 10 ml DMF and the mixture was stirred for 0.5 hour. After the solid dissolved, 0.4 g (3 mmol) benzylbromide was added into the mixture. The solution was stirred at 60 ^oC for 6 hours. 40 ml methanol was poured into the mixture. 40 mL methanol was poured into the mixture and the solid precipitated out. The solid was collected by suction-filtration and washed thoroughly with methanol. After being dried at 75 ^oC in vacuum oven overnight, the crude product was purified by column chromatograph on silica gel using 3 % (volume) acetone/$CHCl_3$ as the eluent.

2g was synthesized as below:

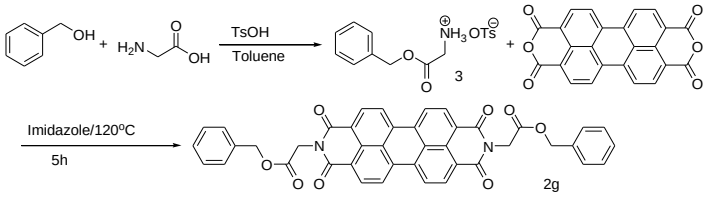

2.16 g (20 mmol) benzyl alcohol, 1.5 g (20 mmol) glycine and 4.18 g (22 mmol)

p-toluene sulfonic acid monohydrate were mixed in 25 ml toluene and the mixture was stirred and refluxed for 6 hours. Produced water was removed by water separator. After removing the toluene by rotate evaporator, the solid was recrystallized in acetone. 4.72 g (70.0%) product **3** was collected by suction-filtration. 392 mg (1mmol) PTCDA, 1.01 g (3 mmol) **3** and 3 g imidizole were mixture in a 25 ml Schlenk flask. The mixture was purged with argon for 15 minutes before reaction. Then the mixture was heated at 120 ℃ for 1.5 hours with argon purged on. Subsequently, the reaction mixture was cooled to 90 ^{o}C. Deionized water was then added with the protection of argon. The dark red suspension was transferred to a 200 ml beaker and diluted with additional 100 ml 5 % K_2CO_3 aqueous solution. The solid was washed and centrifuged until the up-layer solution became colorless.

N, N'-di((*S*)-2-benzyloxy-1-methyl-2-oxoethyl)-3,4:9,10-perylene-tetracarboxyldiimide (**2a**) Crude product was collected by suction filtration. 100/2 (v/v) $CHCl_3$/acetone was used as the eluent in the column chromatography. Yield of **2a** was 0.850 g (97 %).

^{1}H and ^{13}C NMR, FT-IR and elemental analysis confirmed the structure and purity of **2a**. ^{1}H NMR ($CDCl_3$, 300 MHz): δ (ppm) = 8.47 (d, J = 8.06 Hz, 4H, Ar (perylene)), 8.16 (d, J = 8.06 Hz, 4H, Ar (perylene)), 7.41 – 7.28 (m, 10H, Ar (phenyl)), 5.84 (q, J = 6.94 Hz, 2H, N-C**H**(COO)(CH_3), 5.38 – 5.22 (m, 4H, CO2-C**H$_2$**-), 1.79 (d, J = 7.47 Hz, 6H, NCH(COO)(C**H$_3$**) ^{13}C NMR (CDCl3, 75 MHz): δ (ppm) = 170.180 (ester C=O), 162.171 (imide C=O), 135.776 (Ar), 133.708 (Ar), 131.080 (Ar), 128.751 (Ar), 128.564

(Ar), 128.411 (Ar), 128.276 (Ar), 125.374 (Ar), 122.615 (Ar), 122.499 (Ar), 67.260 (-O-**C**H_2), 49.734 (N-**C**H (CH_3)), 14.909 (N-CH (**C**H_3)).

FT-IR (cm^{-1}): 3090, 3065, 3032 (aromatic stretch CH), 2942 (antisymmetric CH_2), 2894 (symmetric CH_2), 1747 (ester C=O), 1700 (symmetric imide C=O symmetric), 1661 (antisymmetric imide C=O), 1593 (aromatic ring stretch).

Anal. Calcd for C44H30N2O8: C, 73.94; H, 4.23; N, 3.92; Found: C, 73.43; H, 4.48; N, 3.93.

N, N'-di((*S*)-2-benzyloxy-1-ethyl-2-oxoethyl)-3,4:9,10-perylenetetracarboxyl-diimide (**2b**) Crude product was collected by suction filtration. 100/4 (v/v) $CHCl_3$/acetone was used as the eluent in the column chromatography. Yield of **2b** was 286 mg (38.6 %).

^{1}H and ^{13}C NMR, FT-IR and elemental analysis confirmed the structure and purity of **2b**. ^{1}H NMR ($CDCl_3$, 300 MHz): δ (ppm) = 8.20 (d, J = 7.88 Hz, 4H, Ar (perylene)), 7.60 (d, J = 8.26 Hz, 4H, Ar (perylene)), 7.28 – 7.49 (m, 10H, Ar (phenyl)), 5.80 – 5.75 (m, 2H, N-C**H**(COO)(CH_2CH_3)), 5.49 – 5.25 (m, 4H, CO_2-C**H$_2$**-), 2.60 – 2.47 and 2.40 – 2.24 (m, 4H, NCH(COO)(C**H$_2$**CH_3)), 1.05 (t, J=7.24 Hz, 6H, NCH(COO)(CH_2C**H$_3$**)). ^{13}C NMR ($CDCl_3$, 75 MHz): δ (ppm) = 170.218 (ester C=O), 163.002 (imide C=O), 136.021 (Ar), 134.236 (Ar), 131.684 (Ar), 129.315 (Ar), 128.841 (Ar), 128.683 (Ar), 128.574 (Ar), 125.913 (Ar), 122.937 (Ar), 122.827 (Ar), 67.452 (-O-**C**H2), 55.458 (N**C**H(COO)(CH_2CH_3)), 22.553 (NCH(COO)(**C**H_2CH3)), 11.303 (NCH(COO)(CH_2**C**H_3)).

FT-IR (cm^{-1}): 3090, 3063, 3031 (aromatic stretch CH), 2971 (antisymmetric CH_3), 2934, (antisymmetric CH_2), 2876 (symmetric CH_2), 1746 (ester C=O), 1701 (symmetric imide C=O symmetric), 1662 (antisymmetric imide C=O), 1593 (aromatic ring stretch).

Anal. Calcd for $C_{46}H_{34}N_2O_8$: C, 74.38; H, 4.61; N, 3.77; Found: C, 74.10; H, 4.68; N, 3.74.

N,N'-di((*S*)-2-benzyloxy-1-(1-methylethyl)-2-oxoethyl)-3,4:9,10-perylenetetra-carboxyldiimide (**2c)** Crude product was collected by suction filtration. 100/4 (v/v) $CHCl_3$/acetone was used as the eluent in the column chromatography. Yield of **2c** was 0.407 g (69 %).

^1H and ^{13}C NMR, FT-IR and elemental analysis confirmed the structure and purity of **2c**. ^1H NMR ($CDCl_3$, 300 MHz): δ (ppm) = 8.43 (d, J = 7.95 Hz, 4H, Ar (perylene)), 8.06 (d, J = 7.95 Hz, 4H, Ar (perylene)), 7.38 – 7.23 (m, 10H, Ar (phenyl)), 5.51 – 5.38 (m, 4H, CO_2-C**H**$_2$-), 5.19 (d, J=12.53, 2H, NC**H**(COO)), 3.01 – 2.89 (m, 2H, NCH(COO)(C**H**$(CH_3)_2$)), 1.37 and 0.86 (d, J=6.28 and 6.85 Hz, 12H, NCH(COO)(CH(C**H**$_3)_2$)). ^{13}C NMR ($CDCl_3$, 75 MHz): δ (ppm) = 169.682 (ester C=O), 162.930 (imide C=O), 135.808 (Ar), 134.251 (Ar), 131.634 (Ar), 129.209 (Ar), 128.494 (Ar), 128.379 (Ar), 128.187 (Ar), 125.915 (Ar), 122.839 (Ar), 122.533 (Ar), 66.948 (-O-**C**H2), 58.877 (N**C**H(COO)(CH$(CH_3)_2$)), 27.835 (NCH(COO)(**C**H$(CH_3)_2$)), 22.193 and 19.168 (NCH(COO)(CH(**C**H$_3)_2$)).

FT-IR (cm^{-1}): 3090, 3066, 3031 (aromatic stretch CH), 2966 (antisymmetric CH_3), 2928 (antisymmetric CH_2), 2875(symmetric CH_2), 1748 (ester C=O), 1701 (symmetric

imide C=O symmetric), 1662 (antisymmetric imide C=O), 1594 (aromatic ring stretch).

HRMS $(M+H)^+$: calcd for $C_{48}H_{39}N_2O_8$ 771.2701; found 771.2702.

N,N'-di((*S*)-2-benzyloxy-1-((*S*)-1-methylpropyl)-2-oxoethyl)-3,4:9,10-perylene-tetracarboxyldiimide (**2d**) Crude product was collected by suction filtration. 100/3 (v/v) $CHCl_3$/acetone was used as the eluent in the column chromatography. Yield of **2d** was 0.638 g (80 %).

^1H and ^{13}C NMR, FT-IR and elemental analysis confirmed the structure and purity of **2d**. ^1H NMR ($CDCl_3$, 300 MHz): δ (ppm) = 8.27 (d, J = 7.90 Hz, 4H, Ar (perylene)), 7.68 (d, J = 8.43 Hz, 4H, Ar (perylene)), 7.46 – 7.23 (m, 10H, Ar (phenyl)), 5.60 – 5.51 (m, 4H, CO_2-C**H$_2$**-), 5.20 (d, J=12.37, 2H, NC**H**(COO)), 2.79 – 2.64 (m, 2H, N-CH(COO)C**H**(CH_3)(CH_2CH_3)), 1.40 – 1.33 and 1.13 – 1.01 (m, 10H, N-CH(COO)CH(C**H$_3$**)(C**H$_2$**CH_3)), 0.87 (t, J=7.26, 6H, N-CH(COO)CH(CH_3)(CH_2C**H$_3$**)). ^{13}C NMR ($CDCl_3$, 75 MHz): δ (ppm) = 169.828 (ester C=O), 162.941 (imide C=O), 136.022 (Ar), 134.120 (Ar), 131.606 (Ar), 129.180 (Ar), 128.631 (Ar), 128.580 (Ar), 128.338 (Ar), 125.823 (Ar), 122.785 (Ar), 122.619 (Ar), 67.077 (-O-**C**H2), 58.652 (N-**C**H(COO)CH(CH_3)(CH_2CH_3)), 34.070 (NCH(COO)**C**H(CH_3)(CH_2CH_3)), 25.389 (N-CH(COO)CH(CH_3)(**C**H_2CH_3)), 18.191 (N-CH(COO)CH(**C**H_3)(CH_2CH_3)), 11.326 (N-CH(COO)CH(CH_3)(CH_2**C**H_3)).

FT-IR (cm^{-1}): 3091, 3066, 3031 (aromatic stretch CH), 2968 (antisymmetric CH_3), 2932 (antisymmetric CH_2), 2876 (symmetric CH_2), 1747 (ester C=O), 1702 (symmetric imide C=O symmetric), 1661 (antisymmetric imide C=O), 1594 (aromatic ring stretch).

Anal. Calcd for $C_{50}H_{42}N_2O_8$: C, 75.17; H, 5.30; N, 3.51; Found: C, 74.79; H, 5.16; N, 3.54.

N,N'-di((*S*)-2-benzyloxy-1-(2-methylpropyl)-2-oxoethyl)-3,4:9,10-perylene-tetracarboxyldiimide (**2e**) Crude product was collected by suction filtration. 100/3 (v/v) $CHCl_3$/acetone was used as the eluent in the column chromatography. Yield of **2e** was 0.630 g (79 %).

^1H and ^{13}C NMR, FT-IR and elemental analysis confirmed the structure and purity of **2e**. ^1H NMR ($CDCl_3$, 300 MHz): δ (ppm) = 8.62 (d, J = 7.82 Hz, 4H, Ar (perylene)), 8.50 (d, J = 8.01 Hz, 4H, Ar (perylene)), 7.31 – 7.25 (m, 10H, Ar (phenyl)), 5.89 – 5.84 (m, 2H, NC**H**(COO)), 5.30 – 5.18 (m, 4H, CO_2-C**H₂**-), 2.35 – 2.14 (m, 4H, NCH(COO)(C**H₂**CH(CH_3)$_2$)), 1.60 (broad, 2H, NCH(COO)(CH_2C**H**(CH_3)$_2$)), 1.04 and 0.95 (d, J=6.64 and 6.61 Hz, 12H, NCH(COO)(CH_2CH(C**H₃**)$_2$). ^{13}C NMR ($CDCl_3$, 75 MHz): δ (ppm) = 170.292 (ester C=O), 162.683 (imide C=O), 135.785 (Ar), 133.951 (Ar), 131.393 (Ar), 129.029 (Ar), 128.551 (Ar), 128.344 (Ar), 128.254 (Ar), 125.644 (Ar), 122.647 (Ar), 67.247 (-O-**C**H_2), 52.476 (N**C**H(COO)), 38.158 (NCH(COO)(**C**H_2CH(CH_3)$_2$)), 25.536 (NCH(COO)(CH_2**C**H(CH_3)$_2$)), 23.200 and 22.182 (NCH(COO)(CH_2CH(**C**H_3)$_2$)).

FT-IR (cm^{-1}): 3090, 3064, 3032 (aromatic stretch CH), 2958 (antisymmetric CH_3), 2937 (antisymmetric CH_2), 2872 (symmetric CH_2), 1747 (ester C=O), 1703 (symmetric imide C=O symmetric), 1662 (antisymmetric imide C=O), 1593 (aromatic ring stretch).

Anal. Calcd for $C_{50}H_{42}N_2O_8$: C, 75.17; H, 5.30; N, 3.51; Found: C, 74.92; H, 5.35;

N, 3.61.

N, N'-di((*S*)-2-benzyloxy-1-tbutyl-2-oxoethyl)-3,4:9,10-perylenetetracarboxyl-diimide (**2f**) Crude product was collected by suction filtration. 100/3 (v/v) $CHCl_3$/acetone was used as the eluent in the column chromatography. Yield of **2f** was 0.506 g (63.4 %).

^1H and ^{13}C NMR, FT-IR and elemental analysis confirmed the structure and purity of **2f**. ^1H NMR ($CDCl_3$, 300 MHz): δ (ppm) = 8.46 – 7.78 (m, 8H, Ar (perylene)), 7.39 – 7.19 (m, 10H, Ar (phenyl)), 5.66 – 5.28 (m, 4H, CO_2-C**H$_2$**-), 5.19 and 5.15 (s, 2H, NC**H**(COO)(C(CH_3)$_3$)), 1.26 (broad, 18H, NCH(COO)(C(C**H$_3$**)$_3$)). ^{13}C NMR ($CDCl_3$, 75 MHz): δ (ppm) = 168.488 (ester C=O), 163.324 (imide C=O), 137.625 (Ar), 136.059 (Ar), 134.343 (Ar), 131.956 (Ar), 128.585 (Ar), 128.272 (Ar), 123.065 (Ar), 122.752 (Ar), 66.738 (-O-**C**H2), 60.242 (N**C**H(COO)), 36.592 (NCH(COO)(**C**(CH_3)$_3$)), 28.607 (NCH(COO)(C(**C**H_3)$_3$).

FT-IR (cm^{-1}): 3091, 3065, 3031 (aromatic stretch CH), 2950 (antisymmetric CH_3), 2918 (antisymmetric CH_2), 2874 (symmetric CH_2), 1753 (ester C=O), 1704 (symmetric imide C=O symmetric), 1665 (antisymmetric imide C=O), 1594 (aromatic ring stretch).

Anal. Calcd for $C_{50}H_{42}N_2O_8$: C, 75.17; H, 5.30; N, 3.51; Found: C, 75.05; H, 5.41; N, 3.48.

N, N'-di(2-benzyloxy-2-oxoethyl)-3,4:9,10-perylenetetracarboxyldiimide (**2g**)

FT-IR (cm^{-1}): 3064, 3033, 3005 (aromatic stretch CH), 2959 (antisymmetric CH_3), 2923 (antisymmetric CH_2), 2854 (symmetric CH_2), 1728 (ester C=O), 1693 (symmetric

imide C=O symmetric), 1662 (antisymmetric imide C=O), 1593 (aromatic ring stretch).

HRMS $(M+H)^+$: calcd for $C_{42}H_{27}N_2O_8$ 687.1762; found 687.1770.

CHAPTER 3. THE 2D CRYSTALLINE SMECTIC LIQUID CRYSTALLINE PHASE AND TRANSITION BEHAVIORS OF A SERIES OF PERYLENE TETRACARBOXYLIC DIIMIDES: THE *n*-ALKYL CHAIN LENGTH DEPENDENCE

3.1. Introduction

In the past decades, perylene tetracarboxylic diimide (PDI) derivatives have captured a great deal of attentions due to their outstanding optical and electronic properties. For example, they are excellent materials for organic photovoltaic cells,[1] field-effect transistors,[2] n-type semiconductors,[3] light-emitting diodes,[4] and liquid crystals.[5]

It is well known that the optical and electronic properties of π-conjugated materials are directly and greatly affected by different π-stacking arrangements.[6] For instance the charge migration along the π-stacking direction is accelerated as a result of significant orbital overlap between adjacent π systems. Naturely, the charge transport efficiency is a function of (a) the degree of frontier orbital overlap and (b) the order of π-stacks. Therefore the control of local π-stacking arrangements of PDIs is a very important topic. Generally speaking, the properties of π-aggregated molecules rely on a few factors such as intrinsic optical and electronic properties of the constituent molecules (affected by carbocyclic scaffold or so called bay-area substituents[7]), intermolecular interactions such as hydrogen bonding,[8] metal ion coordination[9] and the nature of intermolecular π orbital overlap, as well as global morphology (various packing ways).[10] Since the attachment of bay-area substituents leads to a twisted PDI core which is generally considered negative for charge transport, varying the N-substituents becomes

an attractive alternative. Although the substituents at the two nitrogen atoms have little influence to the optical and electronic properties of the single molecule because of the existence of the HOMO and LUMO nodes at the nitrogen atoms,[6] a N-substituent can greatly influences intermolecular interactions and structure/morphology of the PDIs, which enables researchers to tune the properties of PDIs.

Liquid crystalline (LC) PDIs have advantages of easy processing and self-healing characteristics. In the past decades, LC PDIs have been successfully generated by introducing substituents in the bay-area,[11] bulky groups at imide nitrogen atoms,[12] or both.[13] As the consequence, varous LC phases have been obtained, such as discotic columnar,[14,17] smectic[15] and lamellar columnar.[16] Due to the strong tendency to form π-stacks, LC PDIs are promising charge transport materials. Among these PDIs, discotic columnar PDIs exhibit charge carrier mobility as high as 1.7 $cm^2V^{-1}S^{-1}$.[17] On the other hand, these LC PDIs also have disadvantages. The bay-area substituents reduced π-orbital overlapping due to the twisted perylene ring. Moreover, there is no long-range positional order exists along the π-stack axis in any of these LC PDIs. It is expected that PDI π-stacks with long-range positional order along the stacking axis would have even better ability to conduct electric charges than a conventional LC PDI due to the improved order. However, it has been theoretically stated that

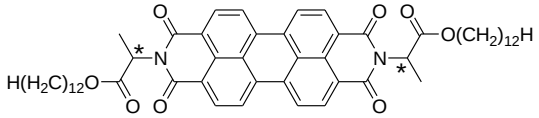

The structure of the first columnar smectic LC PDI

one-dimensional (1D) crystalline order cannot not exist in a columnar phase.[20] Even in a more order biaxial smectic phase, only short-range positional order exists in the π-stacking direction.[21] Nevertheless, we have developed a PDI (structure shown below)

that exhibits a highly ordered smectic LC phase, in which a long-range lamellar order coexists with quasi long range two-dimensional (2D) intra-layer crystalline order including crystalline π-stacking order.[22] We found that in the RT LC phase, the PDI cores pack into rigid layers. Inside each layer, the plate-like PDI cores aggregate into a 2D crystal due to strong inter-chromophore interaction. The *n*-alkyl chains are micro-phase separated from the rigid core part. A PDI core is forced to rotate about 30 ° along the ring normal with respect to its immediate neighbor before stacking to avoid the steric hindrance caused by a steric controlling group. Such a rotation imposes a large cross-section area to every alkyl chain. Consequently, *n*-alkyl chains have to adopt a conformation with a large number of gauche bonds to fill up the space appropriately. Such liquid-like disordered chains play a critical role of decoupling inter-layer molecular correlation so that the crystalline order of PDI cores is restricted in a single layer. If the conformation of *n*-alkyl chains were highly ordered, the intra-layer crystalline order of PDI cores would have extended to the adjacent layers and the phase would have been genuine crystalline instead of LC. Due to the importance of *n*-alkyl chains, it is imperative for us to understand how the length of alkyl chains influences phase transition behaviors including the phase stability of such novel LC PDIs. Thus further investigations have been performed by systematically adjusting the *n*-alkyl chain length from 4 carbons to 16 carbons. This series of compounds are denoted as CnAla where n is the number of carbon atoms in the *n*-akyl chain.

3.2. Results

3.2.1. Differential scanning calorimetry

The phase behavior of all the compounds has been probed with DSC and PLM

measurements. After sample preparation, it was a surprise to discover that C4-C8Alas and C16Ala were dark-red, while C9-C13Alas were orange and C14Ala had orange particles within the dark-red matrix. The DSC results are listed in **Table 3.1**.

Table 3.1. Phase transition temperatures (onset, ^{o}C), enthalpy changes (ΔH, kJ/mol) and entropy changes (ΔS) of CnAlas. (The PLM measurements confirmed the isotropization temperatures as complete dark pictures.)

n	1st heating		2nd heating	
	T_1 /^{o}C (ΔH_1/kJ mol^{-1})	T_i */^{o}C (ΔH_i/kJ mol^{-1})	T_1/^{o}C (ΔH_1/kJ mol^{-1})	T_i*/^{o}C (ΔH_i/kJ mol^{-1})
4		270.81(28.95)		280.93(30.21)
5		258.11(27.80)		269.07(28.70)
6		233.17(25.73)		234.22(25.99)
7		215.75(22.52)		222.39(24.00)
8		206.2(20.94)		212.76(20.23)
9	145.0(23.49)	201.5(20.86)		211.1(20.59)
10	132.8(35.86)	200.53(20.58)	-1.80(5.47)	205.8(20.75)
11	140.7(51.77)	194.52(20.49)	-4.30(9.11)	200.56(20.93)
12	120.0(68.45)	195.8(21.22)	20.62(21.18)	201.58(21.14)
13	107.8(61.08)	191.8(21.39)	29.08(26.72)	198.07(21.17)
14	112.96(1.44)	186.5(21.26)	37.73(30.97)	194.05(21.09)
16		184.42(20.81)	50.04(41.61)	189.86(21.05)

* T_i/ ΔH_i: isotropization temperature/enthalpy change

In addition to the isotropization transitions that all CnAlas display, orange C9 – C14Alas exhibit a phase transition at a lower temperature before the isotropization during the first scan as displayed in **Figure 3.1**. The molar enthalpy change of this transition increases with n when n is between 9 and 12. Afterward, further increase of n leads to increasingly smaller ΔHs. This phase transition is always accompanied by a color change from orange to dark-red during heating.

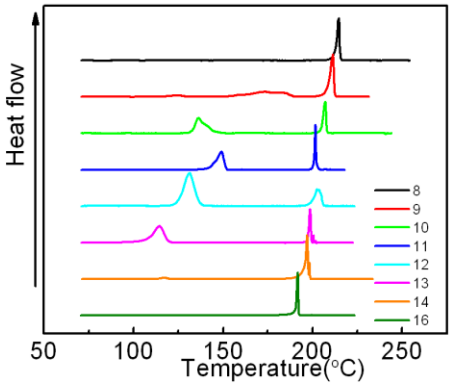

Figure 3.1. The first heating curves of orange solids (C9 – C14Alas). (C8 and C16Ala were also included in this graph as references.)

During the cooling and the second heating, a new phase transition was observed for C10 – C16Alas as depicted in **Figure 3.2**. Both the transition temperature and the molar enthalpy change increase with n.

As C12Ala had the largest molar ΔH when being heated from the orange phase to the dark-red phase, it was chosen as the representative compound and further investigated. During the first heating, the orange phase did not change until the temperature reaches 120 ^{o}C at which a phase transition occurs. During cooling, the orange phase did not appear, even when the temperature is cooled to RT. Furthermore, during the second heating, no thermal events were observed at about 120 ^{o}C. This means that the orange phase is the stable phase and the dark-red phase is the metastable one when the temperature is below 120 ^{o}C. However, the phase transition from the dark-red phase to the orange phase is slow. To qualitatively evaluate the rate of such a transition, C12Ala orange solid was first heated to slightly above the isotropization temperature and cooled it to RT. Then the dark-red solid was placed in several DSC pans and annealed for

different period of time at RT in a dark and dry place. DSC heating scans were subsequently employed to examine the conversion from the dark-red phase to the orange phase by monitoring the ΔH of the transition at 120 ^{o}C. The corresponding DSC thermograms are shown in **Figure 3.3**. Such a transition is indeed very slow at RT. After 49 days, the ΔH is zero. After being annealed at RT for 147 days, a small peak appeared with an enthalpy change of 1.49 kJ/mol. This value is only 2 % of what was observed during the first heating of the orange phase. After 1077 days, a profound peak showed up with an enthalpy change of 56.6 kJ/mol, indicating 89 % of the orange phase has been recovered.

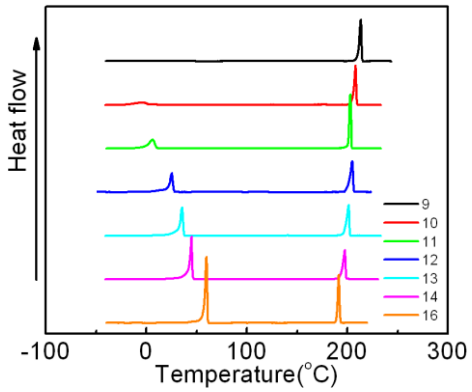

Figure 3.2. The second heating scan of C10 - C16Alas. (C9Ala was included as a reference.)

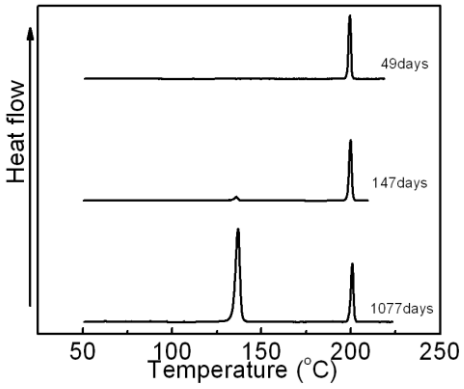

Figure 3.3. After cooled from melt, C12Ala samples were annealed at RT for different periods of time. (Scan rate: 10 ^{o}C/min)

DSC and color changes provided us valuable information about the phase transitions. However, they provide neither direct structural information of phases nor the molecular origin of phase transitions. We need spectroscopic and diffraction techniques to answer these questions.

3.2.2. X-ray diffraction

To understand phase structures of these PDIs, WAXD measurements were first carried out on those phases formed after cooling from the isotropic melt. For C4-C9Alas, only RT 1D WAXD patterns were taken since they only exhibit one endothermic peak during second heating (see **Figure 3.2**). For C10-C16Alas, there are two transitions on the second heating. For C10-C12Alas, 1D WAXD pattern was only taken at 140 ^{o}C because the lower transition temperature is lower than RT. In contrast, 1D WAXD patterns were taken at two temperatures for C14Ala and C16Ala. One is at 140 ^{o}C and the other is at RT.

1D WAXD patterns of C4-C9Alas at RT were shown in **Figure 3.4**. The

wide-angle region of all diffraction patterns consist of sharp peaks only, indicating that C4-C9Alas are crystalline at RT.

In contrast, as shown in **Figure 3.5**, the wide-angle region of C10-C16Alas consists of both sharp peaks and broad peaks, suggesting that they might be LC at 140 ^{o}C. A closer look at the region around 20 °2θ angle further supports this assignment, since only a broad peak could be found around 20 °2θ angle, demonstrating disordered alkyl chains. A pronounced peak could be observed at about 26 ° 2θ angle for all six compounds. This peak (d-spacing = 3.44 Å) is attributed to the spacing between adjacent PDI cores inside PDI π-stacks. On the other hand, the most intense peak at the small range exhibits *n*-alkyl chain length dependence. In order to obtain more precise results, small-angle X-ray diffraction (SAXD) experiments were executed. As in **Figure 3.6**, the peak position shifted to smaller angle region with an increasing n.

To investigate the effect of the lower temperature phase transition on the small-angle diffraction peak, a varying temperature SAXD study on C16Ala has been done and results were presented in **Figure 3.7**. In agreement with the DSC measurement showing a transition peak at 50.04 ^{o}C, the peak position changed abruptly at this temperature while at both two sides of the transition the d-spacing increases when a increasing temperature.

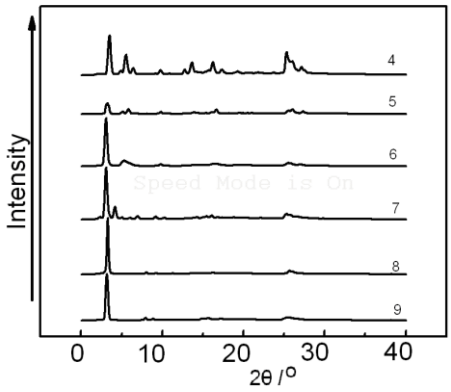

Figure 3.4. 1D WAXD of C4-C9Alas in the second heating

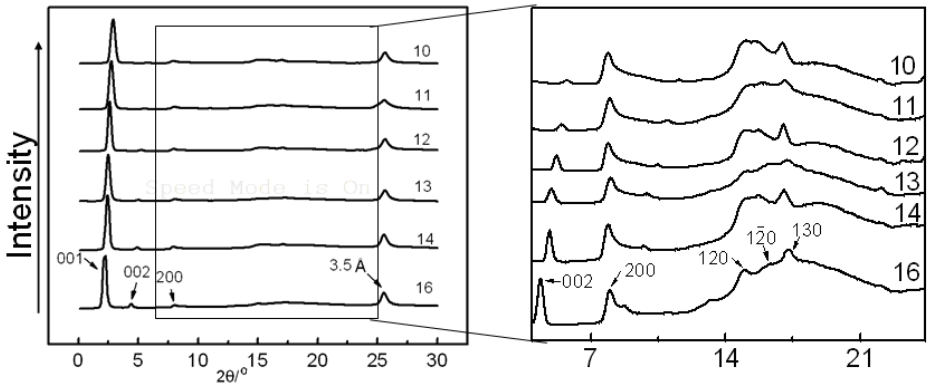

Figure 3.5. 1D-WAXD patterns of C10-C16Alas at 140 ℃

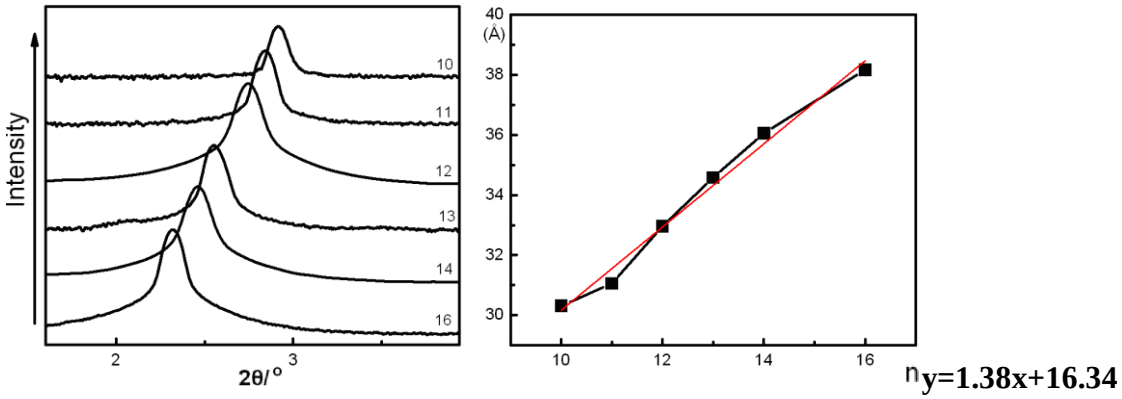

Figure 3.6 SAXD of C10-C16 Ala at 70°C (a); d-spacing of the small-angle diffraction plotted versus n.

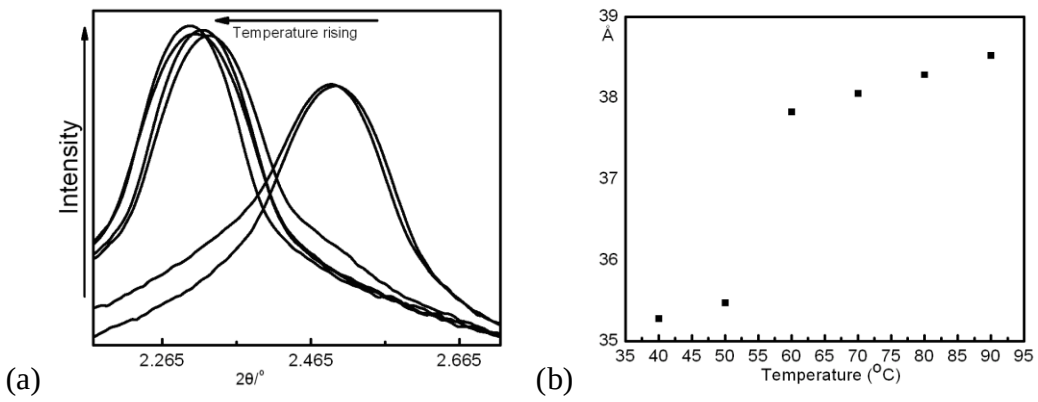

Figure 3.7. VTSAXD of C16Ala (a); plot of d-spacing versus n (b)

If the 1D WAXD patterns shown in **Figure 3.5** were inspected carefully, it can be found that the many diffract peaks are at essentially the same positions for C10-C16 Alas. More interestingly, only diffraction peaks that do show *n*-alkyl chain length dependence are the strongest peak at the small-angle region and its higher order harmonics with d-spacing ratios of $1:\frac{1}{2}:\frac{1}{3}\ \ldots\frac{1}{n}$. This set of peaks can be attributed to a layered structure with a long-range positional order along the layer normal direction. The rest of diffraction peaks are indexable using a 2D oblique crystalline lattice, just as we did with C12Alas in our previous work. The LC nature of C10-C14 and C16Alas at 150 ℃ was confirmed by the absence of any (*hkl*) diffractions with *l* and *h* or $k \neq 0$. Thus, C10, C11, C13, C14, C16Alas are in the same highly ordered LC phase as the RT LC phase exhibited by C12Ala. The key feature of this phase is that PDI cores pack into 2D oblique crystalline layers. However, only the rigid PDI cores not the flexible *n*-alkyl chains are experiencing the crystalline order, probably due to the flexible and disordered nature of *n*-alkyl chains in this phase. Moreover, even for the rigid PDI cores, such a crystalline order is only operative inside each PDI layer. The extension of this

crystalline order along the 3rd direction, i.e., along the layer normal direction, is prohibited by disordered alkyl chains. Consequently, the phase is LC instead of crystalline. PDI π-stacking order is also of crystalline nature as it is a part of 2D intra-layer crystalline order.

LC nature of the phase is also supported by the easy of achieving molecular orientation by applying mechanical shearing force. **Figure 3.8** illustrates two PLM micrographs of mechanically sheared C10Ala at RT after being cooled from the isotropic liquid state. The sample is uniformly red when the shearing direction is aligned 45 ° with respect to both the polarizer and the analyzer. However, when the shearing direction is parallel to either polarizer, the sample is completely dark. Such observations mean that nearly perfect molecular alignment could be achieved by simply mechanical shearing the C10Ala at RT, which is typical behavior for a LC phase. Since this phase features both long-ranged lamellar (smectic) order and 2D crystalline intra-layer order including crystalline π-stacking order, we would name as 2D crystalline smectic phase.

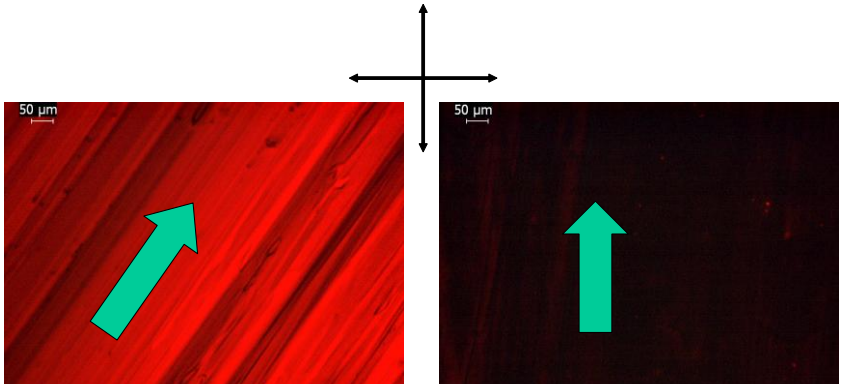

Figure 3.8. PLM micrographs of a mechanically sheared C10Ala at RT with different

alignment with respect to the polarizer.

When such a LC PDI is further cooled, the *n*-alkyl chains may become ordered enough that the original 2D intra-layer crystalline ordered extends to the 3rd dimension can convert the phase into a true 3D crystalline phase. This is probably the structure of the lowest temperature phase during the second heating. The RT WAXD patterns of C14 and C16Alas shown below in **Figure 3.9** do support this argument. Not only the original broad peak around 2θ 20° becomes sharper, but also a peak with an index of $(1\,\bar{2}\,2)$ could be identified in both patterns, signifying the 3D crystalline order. Note that the both the lamellar structure and the PDI π-stacks are retained in this crystalline phase. The preservation of lamellar structure is evidenced by the presence of strong $(00l)$ diffractions, while the existence of PDI π-stacks is indicated by the dark-red color and the appearance of diffractions at about 3.5 Å d-spacing.

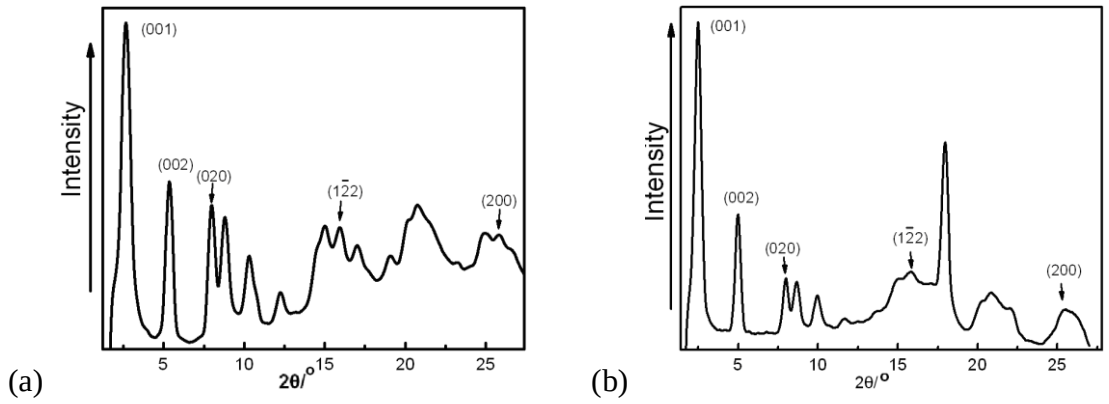

Figure 3.9. 1D WAXD of (a) C14Ala and (b) C16Ala

WAXD patterns of C9-C13Alas in their orange solid form were taken at RT and displayed in **Figure 3.10**. It is quite clear that all of them are crystalline because only sharp peaks can be found in the wide-angle region. Being quite different from the

dark-red phase, there are no diffractions below 5 °2θ angle which is often considered arising from the electron density contrast between the PDI region and the *n*-alkyl region. Moreover, there are no diffraction peaks in the region of 25-26 °2θ angle suggesting the absence of PDI π-stacks.

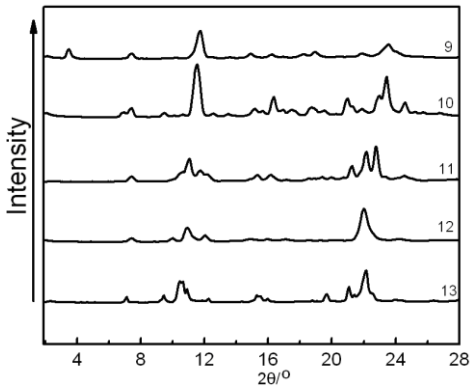

Figure 3.10. WAXD of orange solid of C9-C13Alas

Table 3.2. Indices of C10-C16Alas

Name	001[a]	002	020	003	004	120	$1\bar{2}0$	130	200
C10	28.97	14.49	11.19	9.66	7.23	5.95	5.75	5.22	3.44
C11	30.52	15.30	11.08	10.18	7.66	5.97	5.64	5.18	3.44
C12	32.37	16.19	10.98	10.80	8.11	5.95	5.70	5.13	3.44
C13	33.53	16.83	10.93	10.20	8.41	5.93	5.69	5.21	3.44
C14	32.72	16.36	10.92	10.91	8.19	6.01	5.60	5.11	3.42
C16	35.34	17.67	11.12		8.84	6.01	5.62	5.08	3.47

[a]: measured d-spacing of corresponding index, unit: Å

3.2.3. FT-IR

FT-IR provides important molecular information such as conformation and intermolecular interaction and it is a very useful technique that is complementary to scattering and thermoanalysis techniques.

It is known that the frequencies of asymmetric stretching $v_{as}(CH_2)$ and symmetric

stretching $v_s(CH_2)$ of *n*-alkyl chains depend on their conformation.[23] The $v_{as}(CH_2)$ and $v_s(CH_2)$ values for an all-anti alkyl chain are typically in the ranges of 2916 to 2920 and 2846 to 2850 cm^{-1}, respectively. These ranges shift to 2924-2928 and 2854-2856 cm^{-1} for liquid *n*-alkyl chains. To probe *n*-alkyl chains conformation changes, varying temperature FT-IR experiments were carried out.

For C10-C16Alas, as they had two phase transitions in the seconding heating, IR experiments were supposed to provide very useful information about the molecular origin of transitions. However, due to the difficulty to cool a sample below RT, the lower temperature transition was only explored for C16Ala. In **Figure 3.11**, the $v_{as}(CH_2)$ and $v_s(CH_2)$ values shifted from 2918 and 2850 cm^{-1} to 2923 and 2853 cm^{-1} during this transition and these two values slightly shifted to 2926 and 2854 cm^{-1} upon heating, clearly showing that *n*-alkyl chains undergoing a disordering process at the transition.

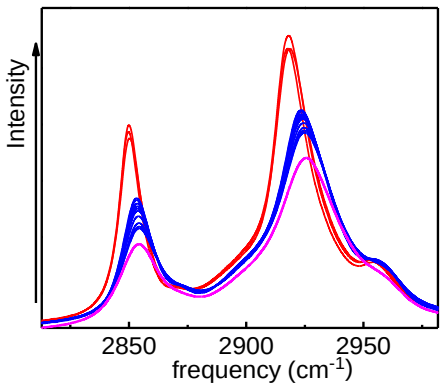

Figure 3.11. IR of *n*-alkyl chain stretching band shift of C16Alas during 2nd heating from RT to melt. (red: crystalline state, blue: LC phase, purple: isotropic phase)

During the first heating orange compounds also displayed two transitions and C12Ala was chosen as an example here. The $v_{as}(CH_2)$ and $v_s(CH_2)$ frequencies of orange

C12Ala were 2918 and 2850 cm^{-1}, indicating the crystalline alkyl chains, as depicted in **Figure 3.12**. When it was heated over the transition temperature the $v_{as}(CH_2)$ and $v_s(CH_2)$ values became 2925 and 2855 cm^{-1}, meaning the alkyl chains are in the liquid conformation and the positions maintained in this region with little shift until the solids were heated to melt.

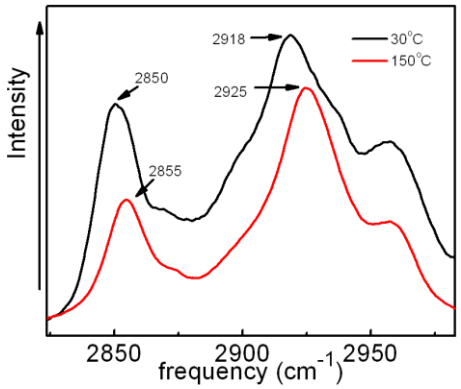

Figure 3.12. FT-IR of *n*-alkyl chain stretching bands of C12Ala during phase transition from crystalline state to disordered state

3.2.4. Solubility test

Solubility measurements provide a reliable means to compare the packing energy in different materials. Especially in the case of CnAlas, when using the same solvent, there will be no difference in terms of the nature of solvent-solute interaction, thus the solubility of a material directly reflects the relative strength of cohesive energy. To maximize the solubility difference among CnAlas, *n*-heptane was chosen because it is a weak solvent for CnAlas. If one assumes that both the rigid PDI core and the flexible *n*-alkyl chain have the same form of organization/conformation, the solubility would continuously change with increasing n in a monotone fashion. The solubility values

were given in **Figure 3.13**. When n increased from 4 to 8, the solubility increased almost linearly. However, when n reached 9 and further continually increased to 13, the solubility fell to very small values, meanwhile the precipitated solids were orange from the solutions. If n increased to 14 and 16, the solubility jumped up and increased to higher values. Those orange solids exhibit remarkably lower solubility in comparison to their dark-red counter parts. In other words, the enthalpic factor in orange solids is much greater than that of a dark-red material with comparable *n*-alkyl chain length.

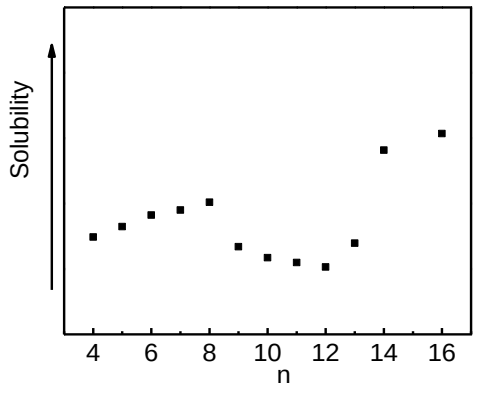

Name	Relative solubility
4	16.18
5	21.6
6	27.3
7	29.9
8	33.9
9	11.3
10	5.7
11	3.3
12	1
13	13.1
14	60.3
16	68.8

Figure 3.13. Relative solubility of CnAlas in heptane, C12Ala was set to 1 and the real solubility of C12Ala is 1.87×10^{-7} mol/L

3.3. Discussion

3.3.1. *n*-Alkyl chain length dependence of the 2D crystalline smectic phase

Since it is critically important for disordered *n*-alkyl chains to decouple the

possible inter-layer intermolecular correlation to avoid the 3D crystalline order, the chose of *n*-alkyl chains is important. When an *n*-alkyl chain is shorter than decyl group, it does not provide sufficient flexibility to decouple the inter-layer intermolecular correlation of PDI cores. Ten methylene units in an *n*-alkyl chain is the lower limit for an *n*-alkyl chain to effectively prevent the appearance of inter-layer intermolecular chromophore correlation.

As shown in **Figure 3.2**, there is a phase that appears at a lower temperature than this 2D crystalline smectic LC phase. Since both the transition temperature and enthalpy increase with n, this transition probably can be assigned to the melting of crystalline *n*-alky chains. In other words, in the low temperature phase, the *n*-alkyl chains are ordered. Upon heating, they become disordered, leading to the formation of the LC phase. This assignment for C16Ala is supported the varying temperature FT-IR results shown in **Figure 3.11** and WAXD results given in **Figure 3.9**. For C10-C13Alas which had lower transition temperature than RT, we could not directly observe the conformation-related IR band shifts due to the instrument limit, but as the DSC data showed the similar behavior and they were in the same trend with C14 and C16Alas, it is reasonable to deduce that C10-C13Ala have the similar ordered alkyl chains in the crystalline low temperature phase.

As the *n*-alkyl chain melting point increases steadily with the increasing length of *n*-alkyl chain, plus the clearing point of CnAlas does not change significantly when n increases from 10, the longer the *n*-alkyl chain is, the narrower the temperature range

over which the compound is LC. The phase boundary diagram of CnAlas is summarized in **Figure 3.14**.

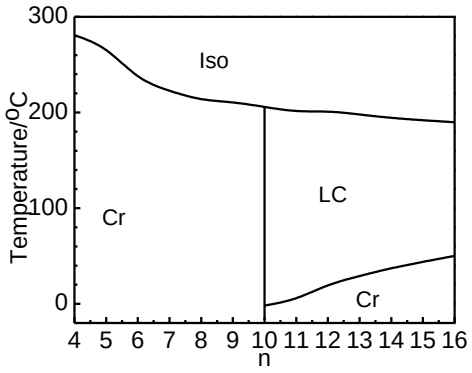

Figure 3.14. The phase boundary diagram of CnAlas

The *n*-alkyl chain length dependence of isotropization is also worth discussion. If one plots the ΔH and ΔS of this transition against the length of *n*-alkyl chains, the contribution of *n*-alkyl chains can be estimated. Such a plot is presented in **Figure 3.15**. The key observation is that the transition enthalpy and entropy values exhibit little dependence on the number of methylene groups in the *n*-alkyl chains. For instance, the difference of ΔS values between C10Ala and C16Ala is only 2.14 $JK^{-1}mol^{-1}$. Every methylene unit contributes 0.18 $JK^{-1}mol^{-1}$ to the isotropization transition. This is in sharp contrast with the contribution of 1.54 $JK^{-1}mol^{-1}$ per methylene to the isotropization of a nematic phase that features a rod-like mesogen.

ΔS of the isotropization transition reflects the difference in order between the isotropic liquid and the LC phase. Approximately, the total ΔS can be treated as the combination of ΔS_{core} and $\Delta S_{n\text{-alkyl}}$. Since the packing schemes of PDI cores in LC phases of C10-C16Alas are essentially the same, the ΔS_{core} can be considered as constant

among all homologues. Therefore, the $\Delta S_{n\text{-alkyl}}$ term causes the different ΔS values. $\Delta S_{n\text{-alkyl}}$ is directly related to the order difference between the *n*-alkyl chains in the LC phase and that in the isotropic liquid. It is reasonable to assume the *n*-alkyl chains in the isotropic liquid state are truly liquid. Therefore, the $\Delta S_{n\text{-alkyl}}$ contains the quantitative information about the degree of disorder of *n*-alkyl chains. If the *n*-alkyl chains in the LC phase possess the conformation exactly the same as in the isotropic liquid state, $\Delta S_{n\text{-alkyl}} = 0$. At the other end, if the *n*-alkyl chains in the LC phase are in all-anti conformation as that in crystalline *n*-alkanes, a very large $\Delta S_{n\text{-alkyl}}$ value is expected. For instance, adding every methylene group to an *n*-alkane with an even number of carbon atoms would contribute 10.9 $JK^{-1}mol^{-1}$ to the melting entropy change of the *n*-alkane.

Although the conformation of *n*-alkyl chains were already investigated using FT-IR, the degree of disorder (or order) of *n*-alkyl chains obtained from thermoanalysis offers much better resolution. The 0.18 $JK^{-1}mol^{-1}$ per CH_2 contribution (especially when compared with 1.54 $JK^{-1}mol^{-1}$ per methylene in a nematic->liquid transition and 10.9 $JK^{-1}mol^{-1}$ per CH_2 in melting of n-alkane crystals) strongly suggests that the *n*-alkyl chains in the 2D crystalline smectic LC phase are indeed nearly the same as that in isotropic liquid.

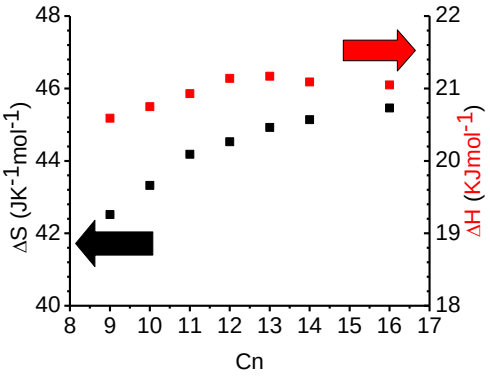

Figure 3.15. n-Dependent transition enthalpy and entropy

Such liquid *n*-alkyl chains decouple inter-layer PDI correlation and can be considered as the origin of the molecular mobility of this LC phase. Thanks to the molecular mobility, when annealed in such a 2D crystalline smectic LC phase, self-alignment may occur. On this regard, C16Ala might be a particularly promising material, because it has an easily accessible LC temperature range over which self-organization could occur, after which that it could be cooled from the LC phase to a crystalline phase to immobilize the achieved form of organization. To test this possibility, a drop of 20 mg/ml C16Ala $CHCl_3$ solution was spin-coated on a piece of silicon wafer. Then the specimen was heated to the liquid state and cooled to 150 ^oC at the rate of 20 ^oC/min. Subsequently, the specimen was annealed at 150 ^oC for 24 hours. After cooled to RT, the 2D WAXD pattern was obtained by running the X-ray beam parallel to the silicon wafer surface. From the pattern, the orientation of the lamellar structure is obvious. All (00*l*) diffractions are in the form of short arcs in stead of rings and the arcs are perpendicular to the surface of silicon wafer. At the same time, (200) arcs which can be attributed to the PDI π-stacks are parallel to the surface of silicon wafer.

Such an alignment is highly desired for field effect transistors because the conduction pathways are parallel to the substrate surface. Usually such a favorite alignment can only be achieved by an energy-intensive vacuum vapor deposition process with careful substrate temperature and evaporation rate control. However, we have achieved it using a convenient solution process. The crystalline nature of C16Ala provides a necessary structural stability. We speculate that the self-alignment in the 2D crystalline smectic LC phase is mainly driven by the desire of the relatively low energy *n*-alkyl chains to occupy the air/sample interface. When the entire air/sample interface is occupied by *n*-alkyl chains, the PDI layers are forced to be parallel to this interface and thus the substrate. This arrangement is retained when the sample is cooled to RT where C16Ala is its crystalline phase.

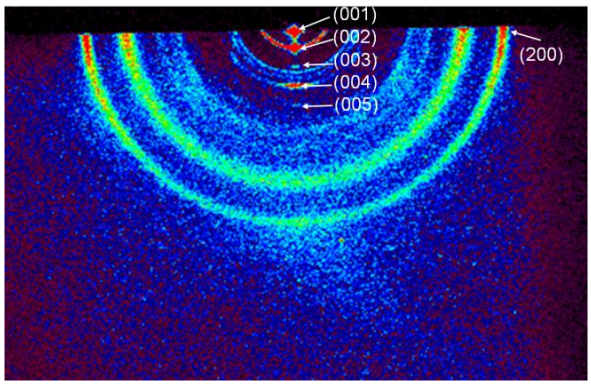

Figure 3.16. 2D WAXD pattern of C16Ala on silica waver after annealed for 24h at 150 ^{o}C.

3.3.2. *n*-Alkyl chain length dependence of the orange phase

The orange color caught our attention because it is known that the color of a pigment could be strongly affected its packing. For PDIs, an orange color suggests very

weak or no PDI π-stacks in the material. On the basis of the RT annealing experiment results shown in **Figure 3.3**, the orange phase of C12Ala is the thermodynamic stable phase at RT and the 2D crystalline smectic LC phase is metastable. IR spectra suggest that the *n*-dodecyl chains are in their all-anti conformation in the orange phase. WAXD result and the color indicate that there are no PDI π-stacks in the orange phase. When the orange phase was heated to the first transition temperatures forming the LC phase, the alkyl chains undergo a disordering process while PDI π-stacks form as evidenced by IR spectra (**Figure 3.12**) and WAXD pattern (**Figure 3.5**) as well as color change from orange to dark-red. When such a LC phase is cooled to RT, although the orange phase is more stable, its formation from the LC phase is extremely slow. This is because to form the orange phase in which there are no PDI π-stacks, the PDI π-stacks must be disassembled first. Since PDIs have a strong tendency to stack together, it requires a large amount of energy to break PDI π-stacks. This constitutes large activation energy for the formation of the crystalline phase from the LC phase. When such a precipitation process is induced by adding methanol (poor solvent) to chloroform solution of C12Ala, orange solid can be directly obtained, because the PDI molecules don't have to overcome the π-stacking interaction to crystallize.

When orange C12Ala disorders into the dark-red LC phase, the *n*-dodecyl chains change their conformation from all-anti to a gauche-containing disordered conformation. Therefore, the melting enthalpy *n*-dodecyl chains must be a very important part of the ΔH (68.45 kJ/mol). However, since in the orange state there are no PDI π-stacks but PDI

cores do stack in the LC phase, one could consider the π-stack formation would make a negative contribution to the ΔH. Here we take the ΔH at the isotropization as the approximate value of exothermic contribution of PDI π-stack formation. Thus the corrected ΔH for converting two dodecyl chains from the all-anti crystalline conformation into the disordered conformation is 90.0 kJ/mol, almost the exact same value as the melting enthalpy change of *n*-$C_{24}H_{50}$ (90.7 kJ/mol) at the same heating rate of 5 ^{o}C/min.[24] This match directed us to the following speculation: The orange phase is favored by the *n*-alkyl chains because in this phase the *n*-alkyl chains are in the most stable all-anti conformation which makes it possible for them to pack well. The dark-red phase is favored by the PDI π-stacks. In the dark-red phase, PDI cores stack together via strong π-π stacking interactions and thus stabilize the phase. Due to the limit of the molecular structure, it is difficult for the all-anti *n*-alkyl chains and the tight packed PDI π-stacks form simultaneously. For C12Ala, the all-anti dodecyl chains and their packing offer more stabilization than what PDI π-stacking can when the temperature is below the melting point of the orange phase so that it is thermodynamically stable.

In the solubility experiment, the solubility increased when n increased from 4 to 8 and further included 14 and 16. This is due to the entropy driving force of the increased number of CH_2 units. However, when n = 9 – 13, most of the dissolved compounds precipitated and turned to orange, leaving light yellow-green solution of very low concentration. The new formed orange crystals have a reduced solubility. This reduced solubility implies that the enthalpic factor holding PDI molecules together is

especially strong.

However, while this speculation can explain why C4-C8Alas do not form the orange phase, it cannot explain why C16Ala does not crystallize into the orange form because *n*-hexadecyl chains would offer more driving force toward the orange phase. This model also cannot explain how the transition enthalpy/entropy values of orange phase vary with the length of *n*-alkyl chains as shown in **Table 3.3**. Certainly this model does not explain among all PDIs that could form the orange phase, only C11 and C12Alas form the orange form most readily. For C11 and C12Alas, the chloroform drop-cast dark-red films can be readily converted to the orange form by annealing in methanol vapor at RT. The orange solids of C10 and C13Alas can only obtained by slowly precipitating from methanol/chloroform mixture. The solid C14Ala precipitated from methanol/chloroform was orange particles as the minority dispersed in the dark-red matrix. While for C9Ala, dark-red particles in the orange matrix were observed. When n is smaller than 8, only dark-red solids were observed, same as C16Ala. It seems that only *n*-alkyl chains with certain length have the tendency to become orange crystals, in which the crystalline *n*-alkyl chains overwhelm the π-π interactions. The C12Ala is the most typical one.

Table 3.3 Enthalpy and entropy change of n-alkyl chain melting

n	$(H_1+\Delta H_i)^a$ kJ/mol	ΔS^b J/mol K
9	43.75	104.66
10	57.26	141.10
11	73.66	178.04
12	89.86	228.64
13	83.47	219.16
14	24.08	62.39

To explain the above observations, a crystalline structure is proposed for the orange phase and has been supported by simulation, which is depicted in **Figure 3.17** and C12Ala is the example molecule applied in this structure. In this structure, there are interdigitated crystalline *n*-alkyl chains facing above or below the PDI cores. In this structure *n*-alkyl chains pack with the PDI cores alternatively resulting in absence of π-stacks. These fully crystallized *n*-alkyl chains offer large enthalpic stabilitization that is more than enough to compensate the absence of π-stacks.

Furthermore, the *n*-alkyl chains must be of certain length so that they are able to cover the entire PDI core appropriately, with a correct angle to the PDI long axis. This unique structure of PDIs has never been discovered before.

Based on the above assumption, molecular simulation has been carried out. A reasonable 3×3 crystal lattice of orange C12Ala has been caculated with energy minimization. The model has been presented in **Figure 3.17**. During heating, the crystalline *n*-alkyl chains melt and became disordered when the no longer restricted PDI cores formed crystalline π-stacks, leading to a dark-red phase like the other PDIs.

(a) models

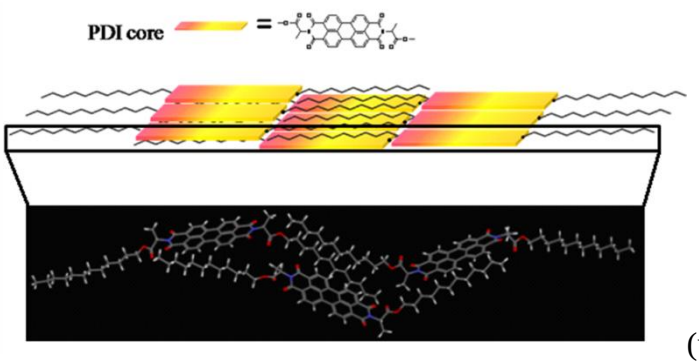

(unit cell)

(b) Topview

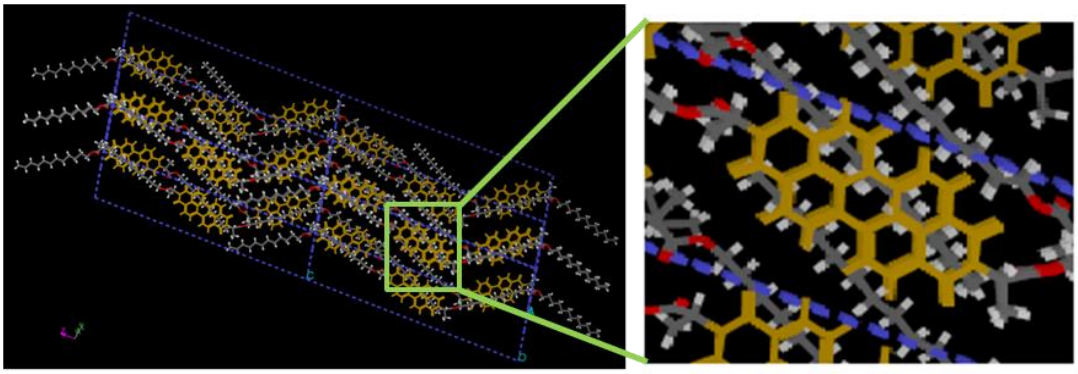

SideView

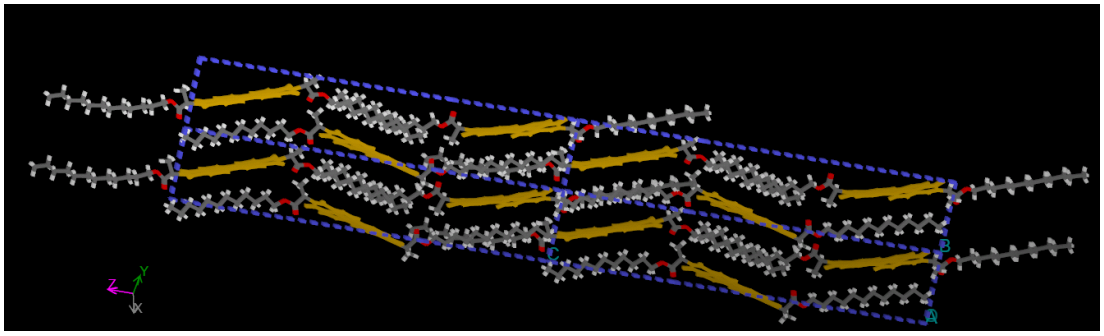

Figure 3.17. Orange crystalline structure of C12Ala. (a)model (b) simulation results The cell is under energy minimization treatment with compass force field.

When *n* further increases, the alkyl chains become too long to cover the PDI cores. Consequently, the orange phase is minor component in solution precipitated C14Ala and no orange phase C16Ala was observed.

3.4. Conclusions

We have investigated the influences of lengths of *n*-alkyl chain substituents (n = 4 – 14 and 16) to the structure and phase transition of CnAlas.

The formation of the novel 2D crystalline LC phase requires the *n*-alkyl chains no shorter than decyl to decouple the inter-layer intermolecular correlation. With shorter *n*-alkyl chains, only crystalline phases can form when cooling from the isotropic melt, probably due to the insufficient flexibility. FT-IR, WAXD and DSC results suggested *n*-alkyl chains in this LC phase are nearly as disordered as that in the isotropic liquid phase. Further cooling the LC phase results in the formation of a crystalline phase in which ordered *n*-alkyl chains, the layered structure and PDI π-stacks coexist. The melting point that separates such a crystalline phase and its corresponding LC phase increases with the length of *n*-alkyl chain. When n > 13, the melting point is above RT.

When the PDI π-π stacking interaction provides the major enthalpic driving force in the formation 2D crystalline LC phase, with an appropriate length, *n*-alkyl chains could be the dominating structuring factor. When n = 9-14, an orange crystalline phase can form and it is thermodynamically more stable the LC phase when the temperature is lower than the melting point of the orange phase (~ 120 ℃). However, the formation of the orange phase from the LC phase is kinetically trapped. In the orange phase, *n*-alkyl chains are in crystalline, all anti form and PDI π-stacks are not present. The formation tendency of CnAlas is *n*-alkyl length dependent. C11 and C12Alas are most readily to form the orange phase. The formation tendency of the orange phase decreases rapidly

when *n*-alkyl chains are longer or shorter than these optimum lengths. A model was proposed for the orange phase to explain the abovementioned observations and was supported by the simulation results.

3.5. Experimental section

Materials

All reagents and chemicals were purchased from Fisher scientific or VWR international and used as received.

Sample characterization

^{1}H NMR and ^{13}C NMR spectra were recorded on a Varian 300 MHz NMR spectrometer with deuterated chloroform ($CDCl_3$) as solvent at 25 ^{o}C. For ^{1}H NMR, the chemical shifts were reported using $CHCl_3$ residue (δ = 7.26 ppm) in deuterated chloroform as the internal standard. For ^{13}C NMR, the chemical shifts were reported using the $CDCl_3$ signal (δ = 77.16 ppm) as the reference.

DSC measurements were conducted on a PerkinElmer Diamond DSC calorimeter. A nitrogen purge was maintained over the samples during the measurement. For preparation, each compound of CnAlas was dissolved in 1:1 hot chloroform/methanol mixture and the solution was then cooled to RT. Subsequently, the solvent was allowed to evaporate at RT slowly. Since chloroform evaporates faster than methanol and methanol is a very poor solvent for CnAlas, precipitation occurred slowly over the course of evaporation. After vacuum dried over night at RT, the samples for DSC measurement were ready. For each sample, three scans have been operated by running empty pan,

standard sapphire and the sample. All the samples were sequentially heated from -50 ^{o}C to about 15 ^{o}C above the isotropization temperature, then cooled back to -50 ^{o}C and heated to above the isotropization temperature at the constant rate of 5 ^{o}C/min. Because for all the compounds the cooling scans coincide with the next heating scans, they were not discussed here. Every DSC trace was generated by subtracting the corresponding empty run and calibrating against the sapphire run. The onset temperatures and integrated areas of the peaks were recorded as transition temperatures and enthalpies for the transitions.

Polarized light microscopy (PLM) observations were performed on a Leica DM LB2 microscope equipped with a Mettler Toledo hot stage with a FP82HT temperature controller. The heating/cooling rate was 10 ^{o}C/min and it was reduced to 1 ^{o}C/min manually when it is close to the DSC-observed transition temperatures.

Infrared spectra were obtained from Vertex 70V FT-IR spectrometer at a resolution of 1 cm^{-1}. To perform an IR experiment, the sample was initially dissolved in $CHCl_3$ at a concentration of 20 mg/ml and the solution was drop-cast on a KBr pallet and dried to form a film. The film was then annealed in methanol vapor at RT overnight (only C11 and C12Ala were orange and all the rest were dark-red) before scanning.

X-ray diffraction measurements were performed on a Bruker X-ray instrument using Cu Kα radiation (λ = 0.1542 nm). The samples were prepared in the same way as that for DSC experiments.

The molecular modeling was carried out using a Cerius 2 software package

(version 4.10) with the Compass force field.

Solubility measurements were done using the following procedure. 1 mg of CnAla was added to vials containing 5ml *n*-haptane and sealed and heated to 80 ^{o}C for one hour. Subsequently, the solution was cooled to RT. After staying at RT for one day, 1 ml of the top clear solution was taken out and filtered for UV test. The absorbance at 527 nm was measured using an ultraviolet visible spectrometer. An $\varepsilon = 8.5 \times 10^4$ was used for all CnAla when calculating solubility.

Synthesis

The perylene derivatives CnAla (*n* = 4-14, 16) were synthesized according to the route as shown in **Scheme 3.1**, following the previous work in ref [22] with some modifications. This route provided high yields about 80%.

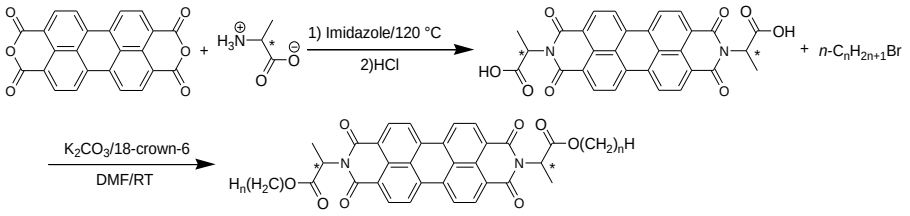

n = 4 - 14，16

Scheme 3.1. Synthesis of CnAlas (*n* = 4 – 14, 16). DMF = *N*,*N*-dimethylformamide

Synthesis of *N, N'*-di((*S*)-1-carboxyethyl)-3,4:9,10-perylenetetracarboxyldiimide (PDI-L-ala)

Into a 50 ml Schlenk flask were charged 1.87 g L-alanine (21 mmol), 3,4:9,10-perylenetetracarboxyldianhydride (PTCDA) 3.92 g (10 mmol), and imidazole (28 g). The mixture was purged with argon for 15 minutes before being heated at

120 ℃ until the reaction mixture was completely soluble in water. Subsequently, the reaction mixture was cooled to 90 ℃. Deionized water was added under the protection of argon. The dark-red solution was filtered to remove the trace amount of unreacted PTCDA. The solution was then acidified with 2 M HCl aqueous solution to a pH value of 3-4, the formed precipitate was collected by suction-filtration and thoroughly washed with deionized water until the filtrate was neutral; the red solid was collected and dried at 75 ℃ in vacuum oven until constant weight. 5.131 g (96 %) PDI-L-Ala was obtained as a dark-red solid.

General synthetic procedure of CnAlas

Into a N_2-purged 20 mL vial were charged 0.5 mmol PDI-L-Ala (MW: 534), 76 mg (0.55 mmol) K_2CO_3 and 2.9 g DMF solution containing 290 mg (1.1 mmol) 18-crown-6. The mixture was stirred for 30 minutes at RT, forming a deep purple solution. 1.5 mmol 1-bromo-C_nH_{2n+1} was then added to the solution. The reaction mixture was sealed and stirred in dark at 60 ^oC for 12 hours before being poured into 20 ml methanol. The solid precipitate was collected by centrifugation and dried at RT in a vacuum oven for 12 hours. The crude product is purified by column chromatography on silica gel using 40/1 (v/v) chloroform/acetone as the eluent.

N, N'-di((*S*)-2-(butyloxyl)-1-methyl-2-oxoethyl)-3,4:9,10-perylenetetracarboxyl- diimide (C4Ala) Yield 0.259 g (80.1 %)

^{1}H NMR ($CDCl_3$, 300 MHz): δ (ppm) = 8.59 (d, J = 7.90 Hz, 4H, Ar), 8.45 (d, J = 7.98 Hz, 4H, Ar), 5.78 (q, J = 6.96 ,2H, NC**H**(COO)CH_3), 4.18- 4.26 (m, 4H,

(COO)C**H$_2$**), 1.76 (d, J = 6.68 Hz, 6H, NCH(COO)C**H$_3$**), 1.59 – 1.68 (m, 4H, (COO)CH$_2$C**H$_2$**), 1.25 – 1.41 (m, 4H, (COO)CH$_2$CH$_2$C**H$_2$**), 0.89 (t, J = 7.41 Hz, 6H, CH$_2$C**H$_3$**). ^{13}C NMR ($CDCl_3$, 75 MHz): δ (ppm) = 170.45 (ester C=O), 162.78 (imide C=O), 134.73 (Ar), 131.73 (Ar), 129.47(Ar), 126.39 (Ar), 123.18 (Ar), 65.53 ((COO)**C**H$_2$), 49.78(N**C**H(COO)CH$_3$), 30.68((COO)CH$_2$**C**H$_2$), 19.27 (**C**H$_2$CH$_3$), 14.97 (NCH(COO)(**C**H$_3$)), 13.84 (CH$_2$**C**H$_3$). FT-IR: ν (cm^{-1}) = 2958 (antisymmetric CH_3), 2875 (symmetric CH_3), 1743 (ester C=O), 1706 (symmetric imide C=O), 1655 and 1664 (antisymmetric imide C=O), 1594 (aromatic ring).

N,N'-di((*S*)-2-(pentyloxyl)-1-methyl-2-oxoethyl)-3,4:9,10-perylene-tetracarboxyldiimide (C5Ala) Yield 0.278 g (82.4 %)

^{1}H NMR ($CDCl_3$, 300 MHz): δ (ppm) = 8.59 (d, J = 8.04 Hz, 4H, Ar), 8.44 (d, J = 8.04 Hz, 4H, Ar), 5.78 (q, J = 6.93 ,2H, NC**H**(COO)CH$_3$), 4.18- 4.24 (m, 4H, (COO)C**H$_2$**), 1.77 (d, J = 6.90 Hz, 6H, NCH(COO)C**H$_3$**), 1.59 – 1.69 (m, 4H, (COO)CH$_2$C**H$_2$**), 1.26 – 1.31 (m, 8H, (COO)CH$_2$CH$_2$C**H$_2$**C**H$_2$**), 0.82 (t, J = 6.98 Hz, 6H, CH$_2$C**H$_3$**). ^{13}C NMR ($CDCl_3$, 75 MHz): δ (ppm) = 170.43 (ester C=O), 162.73 (imide C=O), 134.68 (Ar), 131.73 (Ar), 129.44(Ar), 126.35 (Ar), 123.19 (Ar), 65.82 ((COO)**C**H$_2$), 49.78(N**C**H(COO)CH$_3$), 28.31((COO)CH$_2$**C**H$_2$), 28.18 ((COO)CH$_2$CH$_2$**C**H$_2$), 22.39 (**C**H$_2$CH$_3$), 14.95 (NCH(COO)(**C**H$_3$)), 14.09 (CH$_2$**C**H$_3$). FT-IR: ν (cm^{-1}) = 2953 (antisymmetric CH_3), 2872 (symmetric CH_3), 1746 (ester C=O), 1708 (symmetric imide C=O symmetric), 1655, 1664 (antisymmetric imide C=O), 1594 (aromatic ring stretch).

N, N'-di((*S*)-2-(hexyloxyl)-1-methyl-2-oxoethyl)-3,4:9,10-perylenetetracarboxyl-diimide (C6Ala) Yield 0.321 g (91.4 %)

^{1}H NMR ($CDCl_3$, 300 MHz): δ (ppm) = 8.52 (d, J = 7.69 Hz, 4H, Ar), 8.32 (d, J = 8.27 Hz, 4H, Ar), 5.78 (q, J = 6.98 ,2H, NC**H**(COO)CH_3), 4.15- 4.28 (m, 4H, (COO)C**H$_2$**), 1.77 (d, J = 6.87 Hz, 6H, NCH(COO)C**H$_3$**), 1.60 – 1.69 (m, 4H, (COO)CH_2C**H$_2$**), 1.19 – 1.33 (m, 12H, (COO)CH_2CH_2C**H$_2$**C**H$_2$**C**H$_2$**), 0.81 (t, J = 6.46 Hz, 6H, CH_2C**H$_3$**). ^{13}C NMR ($CDCl_3$, 75 MHz): δ (ppm) = 170.40 (ester C=O), 162.66 (imide C=O), 134.48 (Ar), 131.64 (Ar), 129.32 (Ar), 126.18 (Ar), 123.14 (Ar), 65.84 ((COO)**C**H_2), 49.79(N**C**H(COO)CH_3), 31.51 ((COO)$CH_2CH_2CH_2$**C**H_2), 28.59((COO)CH_2**C**H_2), 25.69 ((COO)CH_2CH_2**C**H_2), 22.67 (**C**H_2CH_3), 14.97 (NCH(COO)(**C**H_3)), 14.06 (CH_2**C**H_3). FT-IR: ν (cm^{-1}) = 2935 (antisymmetric CH_2), 2860 (symmetric CH_2)), 1746 (ester C=O), 1708 (symmetric imide C=O symmetric), 1655, 1664 (antisymmetric imide C=O), 1594 (aromatic ring stretch).

N, N'-di((*S*)-2-(heptyloxyl)-1-methyl-2-oxoethyl)-3,4:9,10-perylenetetracarboxyl-diimide (C7Ala) Yield 0.340 g (93.0 %)

^{1}H NMR ($CDCl_3$, 300 MHz): δ (ppm) = 8.41 (d, J = 7.96 Hz, 4H, Ar), 8.16 (d, J = 8.13 Hz, 4H, Ar), 5.78 (q, J = 6.95 ,2H, NC**H**(COO)CH_3), 4.16- 4.29 (m, 4H, (COO)C**H$_2$**), 1.78 (d, J = 6.94 Hz, 6H, NCH(COO)C**H$_3$**), 1.61 – 1.72 (m, 4H, (COO)CH_2C**H$_2$**), 1.19 – 1.30 (m, 16H, (COO)CH_2CH_2C**H$_2$**C**H$_2$**C**H$_2$** C**H$_2$**), 0.80 (t, J = 6.84 Hz, 6H, CH_2C**H$_3$**). ^{13}C NMR ($CDCl_3$, 75 MHz): δ (ppm) = 170.40 (ester C=O), 162.52 (imide C=O), 134.22 (Ar), 131.41 (Ar), 129.12(Ar), 125.85 (Ar), 122.97 (Ar),

65.90 ((COO)**C**H_2), 49.76(N**C**H(COO)CH_3), 31.82 (**C**H_2), 28.96(**C**H_2), 28.62(**C**H_2), 25.99 (**C**H_2), 22.65 (**C**H_2CH_3), 14.97 (NCH(COO)(**C**H_3)), 14.19 (CH_2**C**H_3). FT-IR: ν (cm^{-1}) = 2929 (antisymmetric CH_2), 2858(symmetric CH_2), 1746 (ester C=O), 1707 (symmetric imide C=O symmetric), 1655, 1664 (antisymmetric imide C=O), 1594 (aromatic ring stretch).

N, N'-di((*S*)-2-(octyloxyl)-1-methyl-2-oxoethyl)-3,4:9,10-perylenetetracarboxyl-diimide (C8Ala) Yield 0.319 g (84.1 %)

^{1}H NMR ($CDCl_3$, 300 MHz): δ (ppm) = 8.37 (d, J = 8.27 Hz, 4H, Ar), 8.08 (d, J = 7.99 Hz, 4H, Ar), 5.76 (q, J = 6.94 ,2H, NC**H**(COO)CH_3), 4.16- 4.29 (m, 4H, (COO)C**H₂**), 1.78 (d, J = 6.76 Hz, 6H, NCH(COO)C**H₃**), 1.62 – 1.71 (m, 4H, (COO)CH_2C**H₂**), 1.18 – 1.28 (m, 20H, (COO)CH_2CH_2C**H₂**C**H₂**C**H₂** C**H₂** C**H₂**), 0.80 (t, J = 6.63 Hz, 6H, CH_2C**H₃**). ^{13}C NMR ($CDCl_3$, 75 MHz): δ (ppm) = 170.37 (ester C=O), 162.40 (imide C=O), 134.06 (Ar), 131.34 (Ar), 128.99(Ar), 125.71 (Ar), 122.91 (Ar), 65.86 ((COO)**C**H_2), 49.78(N**C**H(COO)CH_3), 31.82 (**C**H_2), 29.29(**C**H_2), 28.64(**C**H_2), 26.04(**C**H_2), 22.72(**C**H_2), 14.92 (NCH(COO)(**C**H_3)), 14.17 (CH_2**C**H_3). FT-IR: ν (cm^{-1}) = 2929 (antisymmetric CH_2), 2856(symmetric CH_2), 1747 (ester C=O), 1706 (symmetric imide C=O symmetric), 1658, (antisymmetric imide C=O), 1594 (aromatic ring stretch).

N, N'-di((*S*)-2-(nonyloxyl)-1-methyl-2-oxoethyl)-3,4:9,10-perylenetetracarboxyl-diimide (C9Ala) Yield 0.374 g (95.1 %)

^{1}H NMR ($CDCl_3$, 300 MHz): δ (ppm) = 8.38 (d, J = 8.00 Hz, 4H, Ar), 8.10 (d, J = 8.18 Hz, 4H, Ar), 5.76 (q, J = 7.05 ,2H, NC**H**(COO)CH_3), 4.16- 4.29 (m, 4H,

(COO)C**H$_2$**), 1.78 (d, J = 6.89 Hz, 6H, NCH(COO)C**H$_3$**), 1.61 – 1.70 (m, 4H, (COO)CH$_2$C**H$_2$**), 1.17 – 1.33 (m, 24H, (COO)CH$_2$CH$_2$C**H$_2$**C**H$_2$**C**H$_2$** C**H$_2$**C**H$_2$**C**H$_2$**), 0.80 (t, J = 6.67 Hz, 6H, CH$_2$C**H$_3$**). ^{13}C NMR ($CDCl_3$, 75 MHz): δ (ppm) = 170.35 (ester C=O), 162.43 (imide C=O), 134.11 (Ar), 131.38 (Ar), 129.05(Ar), 125.76 (Ar), 122.93 (Ar), 65.89 ((COO)**C**H$_2$), 49.80(N**C**H(COO)CH$_3$), 31.96 (**C**H$_2$), 29.60(**C**H$_2$), 29.29 (**C**H$_2$), 28.62 (**C**H$_2$), 26.05(**C**H$_2$), 22.72 (**C**H$_2$CH$_3$), 14.92 (NCH(COO)(**C**H$_3$)), 14.18 (CH$_2$**C**H$_3$). FT-IR: ν (cm^{-1}) = 2925 (antisymmetric CH_2), 2855 (symmetric CH_2), 1748 (ester C=O), 1707 (symmetric imide C=O symmetric), 1661 (antisymmetric imide C=O), 1594 (aromatic ring stretch).

N, N'-di((*S*)-2-(decyloxyl)-1-methyl-2-oxoethyl)-3,4:9,10-perylenetetracarboxyl-diimide (C10Ala) Yield 0.361 g (88.6 %)

^{1}H NMR ($CDCl_3$, 300 MHz): δ (ppm) = 8.64 (d, J = 7.81 Hz, 4H, Ar), 8.53 (d, J = 8.03 Hz, 4H, Ar), 5.80 (q, J = 7.03 ,2H, NC**H**(COO)CH$_3$), 4.11- 4.27 (m, 4H, (COO)C**H$_2$**), 1.75 (d, J = 6.98 Hz, 6H, NCH(COO)C**H$_3$**), 1.57 – 1.66 (m, 4H,(COO)CH$_2$C**H$_2$**), 1.14 – 1.25 (m, 28H, (COO)CH$_2$CH$_2$C**H$_2$**C**H$_2$**C**H$_2$**C**H$_2$**C**H$_2$**C**H$_2$**C**H$_2$**), 0.80 (t, J = 6.59 Hz, 6H, CH$_2$C**H$_3$**). ^{13}C NMR ($CDCl_3$, 75 MHz): δ (ppm) = 170.42 (ester C=O), 162.77 (imide C=O), 134.83 (Ar), 131.82 (Ar), 129.55(Ar), 126.51 (Ar), 123.31 (Ar), 65.82 ((COO)**C**H$_2$), 49.70(N**C**H(COO)CH$_3$), 31.98 (**C**H$_2$), 29.69(**C**H$_2$), 29.45(**C**H$_2$), 29.31 (**C**H$_2$), 26.06 (**C**H$_2$), 22.78 (**C**H$_2$CH$_3$), 14.94 (NCH(COO)(**C**H$_3$)), 14.23 (CH$_2$**C**H$_3$). FT-IR: ν (cm^{-1}) = 2925 (antisymmetric CH_2), 2854 (symmetric CH_2), 1749 (ester C=O), 1701 (symmetric imide C=O symmetric), 1661 (antisymmetric imide C=O), 1594

(aromatic ring stretch).

N, N'-di((*S*)-2-(undecyloxyl)-1-methyl-2-oxoethyl)-3,4:9,10-perylenetetracarboxyl-diimide (C11Ala) Yield 0.378 g (89.7 %)

^{1}H NMR ($CDCl_3$, 300 MHz): δ (ppm) = 8.38 (d, J = 7.91 Hz, 4H, Ar), 8.09 (d, J = 8.18 Hz, 4H, Ar), 5.76 (q, J = 7.14 ,2H, NC**H**(COO)CH_3), 4.16- 4.27 (m, 4H, (COO)C**H$_2$**), 1.78 (d, J = 6.98 Hz, 6H, NCH(COO)C**H$_3$**), 1.58 – 1.70 (m, 4H, (COO)CH_2C**H$_2$**), 1.15 – 1.26 (m, 32H, (COO)CH_2CH_2C**H$_2$**C**H$_2$**C**H$_2$** C**H$_2$**C**H$_2$**C**H$_2$**C**H$_2$** C**H$_2$**), 0.82 (t, J = 6.86 Hz, 6H, CH_2C**H$_3$**). ^{13}C NMR ($CDCl_3$, 75 MHz): δ (ppm) = 170.37 (ester C=O), 162.40 (imide C=O), 134.07 (Ar), 131.33 (Ar), 129.00(Ar), 125.75 (Ar), 122.92 (Ar), 65.84 ((COO)**C**H_2), 49.78(N**C**H(COO)CH_3), 32.01 (**C**H_2), 29.73(**C**H_2), 29.65(**C**H_2), 29.42(**C**H_2), 29.34(**C**H_2), 28.63(**C**H_2), 26.06 (**C**H_2), 22.75 (**C**H_2CH_3), 14.91 (NCH(COO)(**C**H_3)), 14.20 (CH_2**C**H_3). FT-IR: ν (cm^{-1}) =2919 (antisymmetric CH_2), 2850(symmetric CH_2), 1749 (ester C=O), 1695 (symmetric imide C=O symmetric), 1660 (antisymmetric imide C=O), 1591 (aromatic ring stretch).

N, N'-di((*S*)-2-(dodecyloxyl)-1-methyl-2-oxoethyl)-3,4:9,10-perylenetetracarboxyl-diimide (C12Ala) Yield 0.407 g (93.4 %)

This compound has been confirmed in [16]

N, N'-di((*S*)-2-(tridecyloxyl)-1-methyl-2-oxoethyl)-3,4:9,10-perylenetetracarboxyl-diimide (C13Ala) Yield 0.415 g (92.3 %)

^{1}H NMR ($CDCl_3$, 300 MHz): δ (ppm) = 8.65 (d, J = 7.95 Hz, 4H, Ar), 8.54 (d, J = 8.18 Hz, 4H, Ar), 5.78 (q, J = 7.09 ,2H, NC**H**(COO)CH_3), 4.11- 4.26 (m, 4H, (COO)C**H$_2$**),

1.75 (d, J = 6.96 Hz, 6H, NCH(COO)C**H$_3$**), 1.58 – 1.66 (m, 4H, (COO)CH$_2$C**H$_2$**), 1.14 – 1.26 (m, 40H, (COO)CH$_2$CH$_2$C**H$_2$**C**H$_2$**C**H$_2$** C**H$_2$**C**H$_2$**C**H$_2$**C**H$_2$**C**H$_2$**C**H$_2$**C**H$_2$**), 0.85 (t, J = 6.96 Hz, 6H, CH$_2$C**H$_3$**). ^{13}C NMR ($CDCl_3$, 75 MHz): δ (ppm) = 170.43 (ester C=O), 162.78 (imide C=O), 134.84 (Ar), 131.84 (Ar), 129.57(Ar), 126.53 (Ar), 123.32 (Ar), 65.83 ((COO)**C**H$_2$), 49.70(N**C**H(COO)CH$_3$), 32.03 (**C**H$_2$), 29.78(**C**H$_2$), 29.64(**C**H$_2$), 29.47(**C**H$_2$), 29.33(**C**H$_2$), 28.62(**C**H$_2$), 26.06 (**C**H$_2$), 22.82 (**C**H$_2$CH$_3$), 14.94 (NCH(COO)(**C**H$_3$)), 14.26 (CH$_2$**C**H$_3$). FT-IR: ν (cm^{-1}) = 2922 (antisymmetric CH$_2$), 2853 (symmetric CH$_2$), 1748 (ester C=O), 1699 (symmetric imide C=O symmetric), 1661(antisymmetric imide C=O), 1593 (aromatic ring stretch).

N, N'-di((*S*)-2-(tetradecyloxyl)-1-methyl-2-oxoethyl)-3,4:9,10-perylenetetracarboxyl-diimide (C14Ala) Yield 0.420 g (90.6 %)

^{1}H NMR ($CDCl_3$, 300 MHz): δ (ppm) = 8.53 (d, J = 7.96 Hz, 4H, Ar), 8.35 (d, J = 8.29 Hz, 4H, Ar), 5.78 (q, J = 6.97 ,2H, NC**H**(COO)CH$_3$), 4.14- 4.28 (m, 4H, (COO)C**H$_2$**), 1.77 (d, J = 6.97 Hz, 6H, NCH(COO)C**H$_3$**), 1.59 – 1.68 (m, 4H, (COO)CH$_2$C**H$_2$**), 1.15 – 1.29 (m, 44H, (COO)CH$_2$CH$_2$C**H$_2$**C**H$_2$**C**H$_2$** C**H$_2$**C**H$_2$**C**H$_2$**C**H$_2$**C**H$_2$**C**H$_2$**C**H$_2$**), 0.86 (t, J = 6.75 Hz, 6H, CH$_2$C**H$_3$**). ^{13}C NMR ($CDCl_3$, 75 MHz): δ (ppm) = 170.40 (ester C=O), 162.52 (imide C=O), 134.22 (Ar), 131.41 (Ar), 129.12(Ar), 125.85 (Ar), 122.97 (Ar), 65.90 ((COO)**C**H$_2$), 49.76(N**C**H(COO)CH$_3$), 31.82 (**C**H$_2$), 28.96(**C**H$_2$), 28.62(**C**H$_2$), 25.99 (**C**H$_2$), 22.65 (**C**H$_2$CH$_3$), 14.97 (NCH(COO)(**C**H$_3$)), 14.19 (CH$_2$**C**H$_3$). FT-IR: ν (cm^{-1}) = 2924 (antisymmetric CH$_2$), 2853 (symmetric CH$_2$), 1750 (ester C=O), 1702 (symmetric

imide C=O symmetric), 1662 (antisymmetric imide C=O), 1594 (aromatic ring stretch).

N, N'-di((*S*)-2-(hexadecyloxyl)-1-methyl-2-oxoethyl)-3,4:9,10-perylenetetracarboxyl-diimide (C16Ala) Yield 0.401 g (81.6 %)

^{1}H NMR ($CDCl_3$, 300 MHz): δ (ppm) = 8.61 (d, J = 8.06 Hz, 4H, Ar), 8.48 (d, J = 8.18 Hz, 4H, Ar), 5.78 (q, J = 6.93 ,2H, NC**H**(COO)CH_3), 4.12- 4.27 (m, 4H, (COO)C**H$_2$**), 1.76 (d, J = 7.03 Hz, 6H, NCH(COO)C**H$_3$**), 1.57 – 1.66 (m, 4H, (COO)CH_2C**H$_2$**), 1.14 – 1.29 (m, 52H, (COO)CH_2CH_2C**H$_2$**C**H$_2$**C**H$_2$** C**H$_2$**C**H$_2$**C**H$_2$**C**H$_2$**C**H$_2$**C**H$_2$**C**H$_2$**C**H$_2$**C**H$_2$**C**H$_2$**C**H$_2$**), 0.86 (t, J = 6.57 Hz, 6H, CH_2C**H$_3$**). ^{13}C NMR ($CDCl_3$, 75 MHz): δ (ppm) = 170.42 (ester C=O), 162.73 (imide C=O), 134.76 (Ar), 131.79 (Ar), 129.49(Ar), 126.41 (Ar), 123.24 (Ar), 65.83 ((COO)**C**H_2), 49.75 (N**C**H(COO)CH_3), 32.06 (**C**H_2), 29.78(**C**H_2), 29.65(**C**H_2), 29.48 (**C**H_2), 29.34(**C**H_2), 28.63(**C**H_2), 26.08 (**C**H_2), 22.85 (**C**H_2CH_3), 14.96 (NCH(COO)(**C**H_3)), 14.28 (CH_2**C**H_3). FT-IR: ν (cm^{-1}) = 2923 (antisymmetric CH_2), 2853(symmetric CH_2), 1750 (ester C=O), 1701 (symmetric imide C=O symmetric), 1661 (antisymmetric imide C=O), 1594 (aromatic ring stretch).

CHAPTER 4. BLACK CRYSTALLINE PERYLENE TETRACARBOXYLIC DIIMIDES WITH EXCEPTIONAL RED-SHIFT ABSORPTION

4.1. Introduction

Core-unsubstituted perylene tetracarboxylic diimides (PDIs) have found their applications as high quality colorants.[1,2] These lightfast pigments or dyes display a large range of shades in the solid-state from orange, red, maroon to even black.[3-7] If these shades are examined spectroscopically, their absorption maxima (λ_{max}) cover a wide wavelength range from 500 to 678 nm.[7] The changes in the color of these crystalline compounds are remarkable, as these PDIs exhibit essentially the same absorption spectrum in solutions when PDI molecules exist in the monomeric state.[8] This is because the N-substituents are electronically decoupled from the PDI chromophore so that HOMO and LUMO levels of individual core-unsubstituted PDI exhibit little dependence on the nature of N-substituents.[8] Thus the large variation of colors in the solid state can be mainly attributed to different packing schemes in crystals. This so-called crystallochromic effect was associated with different intermolecular interactions in long-ranged ordered PDI stacks. Since the intra-stack inter-planar d-spacing of PDI rings is always around 3.4 Å, the mutual orientation of adjacent PDI cores inside a π-stack becomes the governing factor. An empirical function was first derived to establish the correlation between the λ_{max} and the transverse (along the short axis of the PDI ring) and longitudinal (along the long axis of the PDI ring) offset of a PDI unit relative to its immediate intra-stack neighbor.[7] Later a quantum chemical approach was able to

reveal that the degree of inter-chromophore frontier orbitals overlap is the crucial parameter.[9] Generally speaking, a larger inter-chromophore LUMO overlap inside a stack results in a broader conduction band. Likewise, a broader valence band can be attributed to a larger inter-molecular HOMO overlap. Broadening of either conduction or valence band reduces the band gap and produces a longer λ_{max}.

Longer λ_{max}s or in other words, broader frontier orbitals have implications far beyond the absorption spectrum of solid PDIs.[10] For instance, a broader valence band correlates to more efficient hole transport, while a broader conduction band can speed up electron transport. Moreover, band broadening would stabilize excitons and increase their lifetimes, which leads to a longer exciton diffusion length.[11] High charge carrier mobility and long exciton diffusion length are the two key parameters that would make PDIs even more appealing in the emerging area of organic electronics and optoelectronics.[12] Considering the fact that PDI already have attracted a great deal of attention in recent years in these fields, there are strong motivations to increase λ_{max}s of PDIs so that their charge and exciton transport performance can be improved. Moreover, since the solar flux that arrives at the surface of the Earth peaks at approximately 700 nm, the increase of λ_{max} itself would enhance a PDI's capability to absorb solar energy due to better spectroscopic match. This would enable the fabrication of more efficient PDI-based organic solar cells.

Although solid PDIs with even longer λ_{max} than 678 nm (the highest reported value so far) are clearly advantageous for many potential applications, to the best of our

knowledge, there are no literature reports on such experimental efforts. In contrast, the computational aspect has advanced considerably. In addition to the early empirical and quantum chemical approaches, force field and molecular dynamics simulations have been applied to predict crystal structures of PDIs. Density functional theory calculations have also been done on a dimer model to illustrate the oscillation strength of the molecular and charge-transfer transitions as the function of the longitudinal offset. Very recently, quantum chemical computations have been carried out to map the potential energy surface and corresponding λ_{max} values of an unsubstituted PDI dimer by varying both the longitudinal and transverse offset values.[13] The preferred geometric arrangement of PDIs in a stack for a very long λ_{max} has been suggested. As a rule of thumb, the best packing scheme should be: First, PDI rings are parallel to each other. Second, the transverse offset should be as small as possible. Third, the longitudinal offset should be in the vicinity of 2.6 Å. However, to materialize such an optimum setting experimentally remains a challenge. In fact, even a very slight change of imide substitution group could change the packing scheme and eventually λ_{max} considerably. For instance, the longitudinal offset, transverse offset and λ_{max} of crystalline N, N'-di(3-methoxypropyl)-3,4:9,10-perylenetetracarboxydiimide are 3.15 Å, 0.68 Å and 613 nm respectively. However, N, N'-di(2-ethoxyethyl)-3,4:9,10-perylenetetracarboxy-diimide crystallize into a structure in which longitudinal offset and transverse offset are 3.23 Å, 1.28 Å respectively. As the result, the λ_{max} changes significantly to 564 nm. Note that these two PDIs are constitutional isomers and the only difference in their

molecular structures is the position of the oxygen atom in the latter one has been moved toward the N by one atom. Such a high sensitivity of a crystal structure to the molecular structure can reasoned on the basis of the flat potential energy surface of a parallel π-stacked PDI dimer with respect to the off values along the longitudinal and transverse directions. This implies that even a small difference in the substituents could change the packing scheme noticeably, which probably can explain the fact that none of reported core-unsubstituted PDIs having strongly red-shifted λ_{max}s (> 600 nm) in their aggregated state were designed results. On the other hand, the flatness of potential energy surface of the PDI dimer may also provide a unique opportunity for one to achieve very large λ_{max} via a tuning mechanism, if two structuring factors can be incorporated into the N-substituent and the contribution of these two factors can be finely adjusted. Due to the varying contributions of two factors, the geometric arrangement of PDIs in a π-stack could be finely altered.

4.2. Molecular Design

Here ester and n-alkyl groups are chosen as the two structural units. The ester group is selected because it can engage in an attractive dipole-dipole interaction which can substantially influence the packing of PDIs. The ester dipole-dipole interaction is relatively strong. Therefore, the packing scheme directed by it would be robust. Gradual instead of abrupt structural changes are expected upon an incrementally adjusted contribution from the other structure unit. At the same time, ester dipole dipole interaction is not overwhelmingly strong so that the other structure factor cannot compete.

That is also why hydrogen bonding is not introduced into the system. *n*-Alkyl groups are picked due to their commercial availability with a wide-range of lengths, strong tendency to pack into a crystalline state in the all-anti conformation and good solubilizing power. The general structure of proposed molecules is shown below:

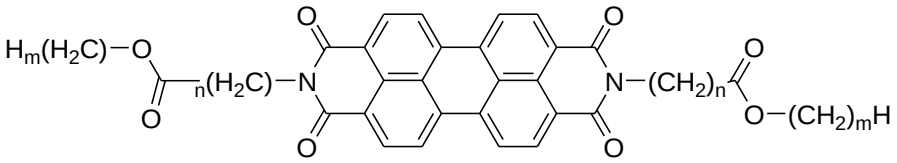

The key parameter m will be adjusted to tune the λ_{max}. However, an appropriate n value should be determined before starting the synthesis, if one wants to avoid the preparation of excessively large number of compounds. The n values were screened by the means of force field simulation. In such a simulation, a PDI was placed into a lattice in which intermolecular interactions were only allowed along the π-stacking direction (1D crystal). The preferred packing geometry in a PDI π-stack was extracted from the 1D PDI crystal with the lowest energy. The λ_{max} of such a π-stacked PDI was estimated by applying the quantum chemically generated offset-λ_{max} correlation. Although in the real world the packing is three-dimensional, a 1D π-stack can still be used as a guideline for us to see the packing preference of a PDI.

A zero value of n can be excluded because it would lead to an unstable compound. n = 1 can also be excluded because a compound with n = 1 and m = 12 has been synthesized in our previous work and it does not exhibit a large red-shifted λ_{max} in the solid state. Since the smaller n is, the stronger influence the ester group will have on the packing of PDI. Thus, only n = 2-6 were inspected. To reduce the calculation time,

the m was set as 1.

The simulation was carried out using Acceryls Cerius 2 (version 4.10) equipped with COMPASS force field. The first step was to find the most stable conformations of a PDI. Because the built-in symmetry of the molecule, when calculation the energy of conformations, molecules with the following general structure were used to speed up the energy minimization process.

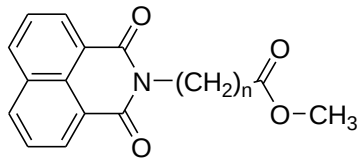

It is possible that a conformation that is not most stable one could pack into a crystalline phase with the lowest energy due to favorable intermolecular interactions. For this reason, all conformations that have energies no more than 0.5 kcal/mol above the most stable conformer were chosen to pack into one-dimensional crystals.

When calculating the energy of a PDI 1D crystal, a PDI molecule with preoptimized conformation was placed in a crystal lattice with $P\bar{1}$ symmetry. The π-stacking direction was designated as the c-axis. α, β, γ were all set as 90 °. The *a* and *b* axis were set as 5 nm. Only change of c axis is allowed during energy minimization. In this way, only intermolecular interaction along the stacking axis will be experienced by PDI molecules.

The most stable PDI crystals are shown below with their corresponding transverse and longitudinal offset values. It is apparent only when n = 3, the most stable packing scheme could lead to a significantly red-shifted λ_{max}.

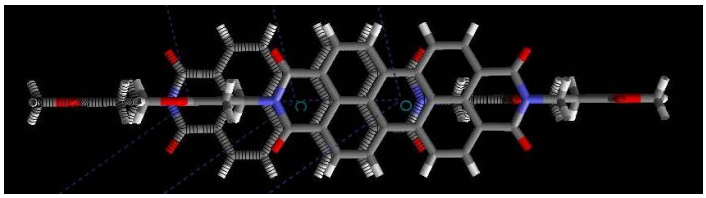

n = 2, *lo* (longitudinal offset) = 4.65 Å, *to* (transversal offset) = 0 Å

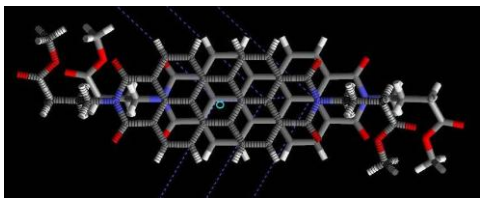

n = 3, *lo* = 2.67 Å, *to* = 0.12 Å

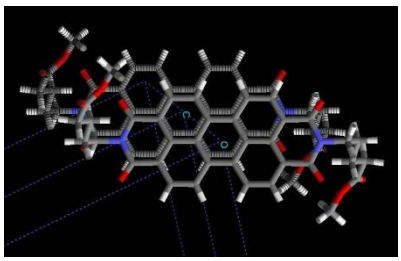

n = 4, *lo* = 2.18 Å, *to* = 1.70 Å

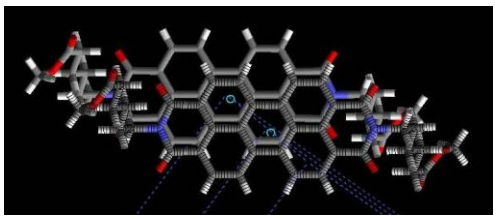

n = 5, *lo* = 2.15 Å, *to* = 1.78 Å

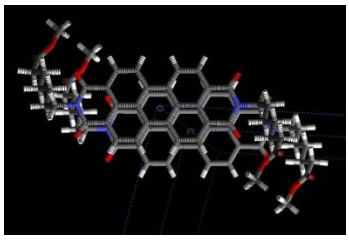

n = 6, *lo* = 2.16 Å, *to* = 1.65 Å

4.3. Results and Discussion

Guided by the simulation results, a PDI (G4) with n = 3 and m = 4 was synthesized. The UV spectrum of G4 in its dilute chloroform solution is presented in **Figure 4.1**. Just as any core un-substituted PDIs, the peaks at 527, 490 and 445 nm all originate from the π-π* electronic transition. The fine structure is due to vibrational coupling. Delightfully, a dramatically red-shifted peak (λ_{max} = 640 nm) appeared after the addition of methanol as shown in **Figure 4.2**. Clearly, methanol-induced crystallization produced G4 crystals having fairly strong frontier orbital interactions inside a PDI π-stack.

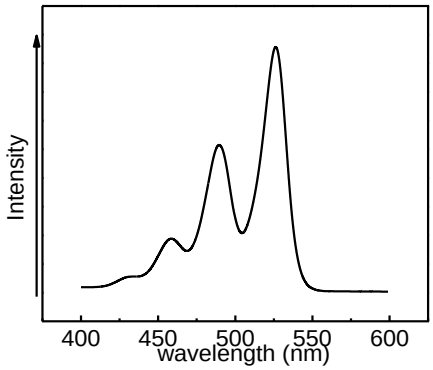

Figure 4.1. Absorption of G4 in dilute chloroform solution

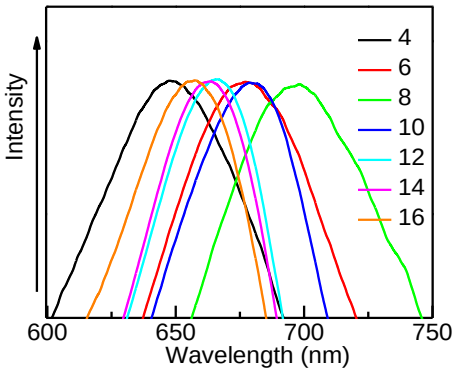

Figure 4.2. Absorption of dispersion of G4-16 in chloroform solution after adding

methanol (MeOH:$CHCl_3$ = 2:1) for 30 min

Encouraged by this observation, PDIs with n = 3 and m = 6, 8, 10, 12, 14, 16 (Gm) have been synthesized. The dilution solutions of all these PDIs in chloroform exhibit the essentially identical absorption spectrum as that of G4. In every case, a new peak with λ_{max} > 640 nm appeared upon the addition of methanol, as shown in **Figure 4.2**. The λ_{max} values of Gm were listed in **Table 4.1**. These observations strongly suggest that (4-n-alkyoxy)-4-oxobutyl group is a robust structural unit which is capable of directing PDIs to pack in a stable manner. Such a packing scheme consistently leads to large frontier orbital overlaps thus a large λ_{max}.

A more interesting observation is that the λ_{max} value of a homologue varies systematically with m. The λ_{max} first increases while m increases. The largest λ_{max} was observed at m = 8. Further increase of m beyond 8 results in a slight decrease of λ_{max}. λ_{max}s of G8, G10 and G12 are greater than any literature reported values. Among them the λ_{max} of G8 is 695 nm, which matches very well with the solar flux spectrum. This implies that incorporation of G8 into an organic solar cell might lead to a noticeable performance boost.

It is worth noting that all this PDIs are noticeably soluble in warm chloroform. Films cast from chloroform solution all exhibit λ_{max} > 640 nm, as illustrated in **Table 4.2**.

Table 4.1. Absorption peaks (λ_{max}) of dispersion of G4-16 in chloroform solution after adding methanol (MeOH:$CHCl_3$ = 2:1) for 30min

n	λ_{max} (nm)
4	647
6	680
8	**695**
10	687
12	676
14	670
16	667

Table 4.2. Absorption of drop-cast films

n	λ_{max} (nm)
4	662
6	686
8	692
10	691
12	692
14	692
16	691

Although the observed λ_{max}-m correlation suggests that a tuning mechanism is in operation, more details are needed to understand how PDIs pack. Certainly single crystal X-ray diffraction is the most powerful and informative approach. Unfortunately, our efforts on growing single crystals that are suitable for X-ray diffraction analysis were not successful. Nevertheless, the crystalline nature of these PDIs at RT can be firmly established by power X-ray diffraction. Moreover, with additional information from IR and UV spectroscopy, we can understand the structures and their tuning mechanism in

these PDIs to a certain degree.

The powder X-ray diffraction patterns are shown in **Figure 4.3**. Since only sharp peaks can be observed, all these PDIs are crystalline at RT. In every diffraction pattern, the peak at the smallest diffraction angle can be correlated to the inter-layer spacing. The d-spacing of this diffraction peak is plotted versus m and is depicted in **Figure 4.4**. When a PDI, for instance G8, crystallizes, the PDI cores tend to stack on top of each other forming tightly-packed PDI π-stacks, driven by the strong π-π interaction between adjacent PDI core. Those π-stacks further assemble into rigid layers. The essentially linear side groups pack between two adjacent PDI layers. The fact the d-spacing of the smallest angle peak continuously increases with increasing m also supports this assignment. The good linearity of this plot confirms that the structural difference among all homologues is incremental due to different lengths of n-alkyl chains. Otherwise, considerable deviations from the linearity would have been observed.

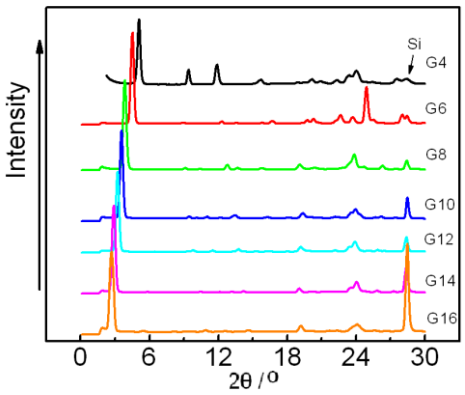

Figure 4.3. Powders WAXD of G4-G16

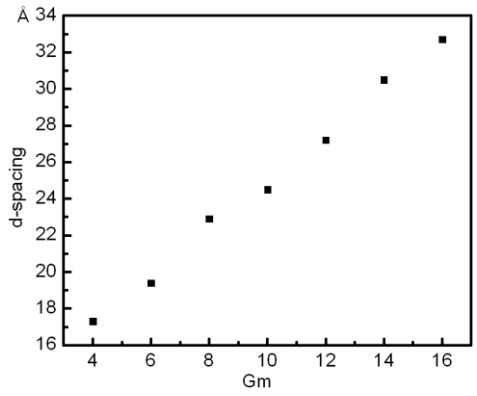

Figure 4.4. d-Spacing values of G4-G16

IR spectroscopy provides convincing evidences supporting structural tuning. It is known that the stretching frequency of the ester C=O ($\nu_{C=O}$) is sensitive to the dipole-dipole interaction. The stronger the dipole-dipole interaction is, the lower $\nu_{C=O}$. Of course, the electronic effect of the substituents that attach to the carbonyl carbon atom and the oxygen atom can also affect $\nu_{C=O}$. However, since the only structure difference among Gms is the length of alkyl chains having at least four methylene units, the resulted frequency shift due to the different electronic effect from n-alkyl groups should be too small to be detectable. Therefore, any observed frequency changes must be due to different dipole-dipole interaction originated from packing. The ester $\nu_{C=O}$ region of Gms is shown in **Figure 4.5**. The frequency values are listed in **Table 4.3**. The ester $\nu_{C=O}$ of G4 is 1738 cm^{-1}, with the increasing length of the n-alkyl chain, the ester $\nu_{C=O}$ continuously increases. The ester $\nu_{C=O}$ of G4 has the lowest frequency, implying that the ester group in G4 is experiencing the strongest dipole-dipole interaction. With the increasing length of the n-alkyl chain, the ester C=O is experiencing increasingly weaker dipole-dipole interaction. In G4, the *n*-alkyl chain is the shortest one. Therefore, the

packing of molecules is dominated by 4-oxobutyl fragment. As long as the transverse and longitudinal offset values corresponding to a relative low potential energy for an π-stacked PDI (and there are positions satisfy this requirement), the ordering of G4 molecules would be such that their 4-oxobutyl fragments are in a very low energy state. As one of major intermolecular attractive force providers, ester C=Os must have enjoyed the priority to have their needs satisfied. That is why G4 has the lowest $\nu_{C=O}$ frequency. However, when the *n*-alkyl chain becomes longer and longer, the enthalpic contribution from *n*-alkyl chains becomes greater and greater. Thus, it becomes increasingly important for n-alkyl chains to pack in their most preferred fashion, for instance, the similar arrangement that can be found in crystalline *n*-alkane or polyethylene. It just happened in Gms, the arrangement favored by the 4-oxobutyl fragment does not coincide with that is favored by the packing of *n*-alkyl chains. Consequently, there is a competition between two. When the *n*-alkyl chain is short, the competition is dominated by the 4-oxobutyl fragment. As the result, the ester C=O is enjoying a strong dipole dipole attractive force. With a longer alkyl chain, the alkyl part gains strength in its competition against the 4-oxobutyl part. To have the lowest free energy of entire crystalline solid, the ester C=O has to give up a fraction of its dipole dipole interaction so that the *n*-alkyl chains can pack more comfortably.

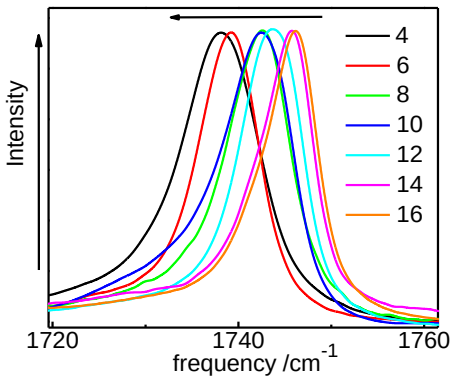

Figure 4.5. The ester $\nu_{C=O}$ region of Gms

Table 4.3. The frequency values of ester $\nu_{C=O}$ Gms

n	$\nu_{C=O}$ (cm^{-1})
4	1738.1
6	1739.0
8	1742.4
10	1742.9
12	1743.8
14	1745.6
16	1746.7

By increasing the length of the *n*-alkyl chain by every two methylene units, the ester C=O blue shifts for about 1 cm^{-1}. Such modest frequency change should be associated with a very small change in transverse and/or longitudinal offset values. Nevertheless, since the *n*-alkyl chains are accessible from inexpensive commercial products with a wide length range, we were able to tune the length of the alkyl chain from four to sixteen methylene units. This tuning leads to a 9 cm^{-1} frequency shift of $\nu_{C=O}$, which may be correlated to a sizable overall change in transverse and/or longitudinal offset values. The key advantage we have here is such a sizable overall change in packing geometry has been done in an incremental way: seven steps. As the result, we

have had good chance to capture a suitable geometry in this tuning process.

To summarize, we have identified the first functionality that can robustly lead to the formation of solid PDIs with strongly red-shifted λ_{max}. On this basis of this robust functionality, we have synthesized the first series of core-unsubstituted PDIs in which all homologues display strongly red-shifted λ_{max}. Three PDIs exhibit λ_{max} longer than any literature reported values. G8 has a λ_{max} that matches well with the solar flux spectrum. It is expected that these PDIs with an exceptionally long λ_{max} will demonstrated improved performance in organic electronic and optoelectronic devices. A competition-based tuning mechanism has been suggested and supported by the experimental evidence. The successful applications of tuning may lead to PDIs with even longer λ_{max} and other colorants with an exceptionally long λ_{max}.

4.4. Experimental section

Materials

All reagents were used as received. 1-butanol (99+ %), 1-hexanol (96 %), 1-octanol (98 %), 1-decanol (99 %) and 1-dodecanol (98 %) were purchased from ACROS ORGANICS. 1-tetradecanol (98+ %) and 3,7-dimethyl-1-octanol (98 %) were purchased from TCI. 1-hexadecanol (98 %) was purchased from Alfa Aesar. Toluene and acetone were purchased from Sigma-Aldrich. Imidizol was purchased from Fisher scientific.

Sample characterization

^{1}H NMR and ^{13}C NMR spectra were recorded on a Varian 600 MHz NMR

spectrometer with deuterated chloroform ($CDCl_3$) as solvent at 25 ^oC. For ^1H NMR, the chemical shifts were reported using $CHCl_3$ residue (δ = 7.26 ppm) in deuterated chloroform as the internal standard. For ^{13}C NMR, the chemical shifts were reported using the $CDCl_3$ signal (δ = 77.16 ppm) as the internal standard. Infrared radiation spectra were obtained from Vertex 70V FT-IR spectrometer at the resolution of 1 cm^{-1}. X-ray diffraction measurements were performed on a Brukerheaven X-ray instrument using Cu as radiation source providing a 0.154 nm beam, of which area was 0.5 mm^2. UV-visible spectra were collected on a Varian UV-Vis spectrometer.

Molecular Modeling

The molecular modeling was carried out using a Cerius 2 software package (version 4.10) with the Compass force field for multiple molecular packing.

Synthesis

Synthesis procedure of **1** and **2** is outlined below:

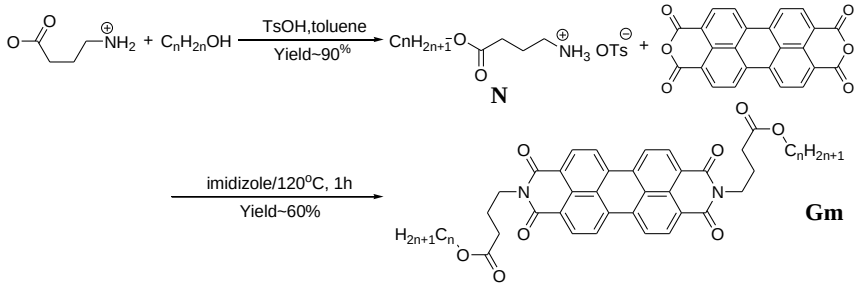

General procedure of **N**

Into a 100 ml Schlenk flask were charged corresponding alcohol (35 mmol), 2.06 g (20mmol) 4-aminobutyricacid, 4.2 g (22 mmol) p-toluene sulfonicacid monohydrate and 50 ml toluene. The mixture was purged with N_2 as protection when it

was heated to reflux (110 ^{o}C) for 8 hours. Subsequently the toluene was removed by vacuum rotate evaporator and the solid was dissolved in 80 ml acetone at 50 ^{o}C. The solution was cooled in refrigerator and the product crystallized. The crystals were collected on Buchner funnel by suction filtration and were rinsed by 5 ml cold acetone. The recrystallization process was performed again before drying process in vacuum oven at RT overnight.

4-(butyloxy)-4-oxobutyl-1-ammonium 4-toluenesulfonate (**4**) The corresponding alcohol was 1-butanol, n = 4, yield **4** 5.49g (83 %)

4-(hexyloxy)-4-oxobutyl-1-ammonium 4-toluenesulfonate (**6**) The corresponding alcohol was 1-hexanol, n = 6, yield **6** 6.39g (89 %)

4-(octyloxy)-4-oxobutyl-1-ammonium 4-toluenesulfonate (**8**) The corresponding alcohol was 1-octanol, n = 8, yield **8** 6.97g (90 %)

4-(decyloxy)-4-oxobutyl-1-ammonium 4-toluenesulfonate (**10**) The corresponding alcohol was 1-decanol, n = 10, yield **10** 7.64g (92 %)

4-(dodecyloxy)-4-oxobutyl-1-ammonium 4-toluenesulfonate (**12**) The corresponding alcohol was 1-dodecanol, n = 12, yield **12** 8.06g (91 %)

4-(tetradecyloxy)-4-oxobutyl-1-ammonium 4-toluenesulfonate (**14**) The corresponding alcohol was 1-tetradecanol, n = 14, yield **14** 8.67g (92 %)

4-(hexadecyloxy)-4-oxobutyl-1-ammonium 4-toluenesulfonate (**16**) The corresponding alcohol was 1-hexadecanol, n = 16, yield **16** 9.08g (91 %)

General procedure of **Gm**

Into a 25 ml Schlenk flask were charged corresponding **1** (2 mmol), 392 mg (1 mmol) 3,4:9,10-perylenetetracarobxyldianhydride (PDA) and 4 g imidizole. The mixture was purged with N_2 for 15 minutes before being heated at 120 ^oC for one hour. Subsequently the reaction mixture was cooled to 90 ^oC. Deionized water was then added with the protection of N_2. After suction filtration, solid has been collected and was dispersed in 150 ml H_2O. The dispersion was repeatedly washed with 3 % K_2CO_3 aqueous solution and filtrate until the solution part became colorless under UV light (no yellow-green emission light). The solid product was collected by suction-filtration and dried in vacuum oven over night at 60 ^oC. For each of **G4 – G16**, the dried solid was dissolved in 200 ml hot $CHCl_3$ (60 ^oC) and the insoluble residue was removed by hot suction filtration. After the filtered solution cooled down to RT and the product precipitated, it was heated at 60 ^oC until clear and suction filtration was performed again to remove trace insoluble particles. Afterwards, the solution cooled down and stayed overnight at RT for the product to precipitate. The solid was collected by suction filtration and rinsed with RT $CHCl_3$. This recrystallization process was applied again with 200 ml $CHCl_3$. The solid was collected and dried in vacuum oven at 40 ^oC overnight. For the further purification, the product was dissolved in hot chloroform (60 ^oC) to become a solution with a concentration of 5 mg/ml. Then the hot solution passed through a short column (3 cm long) quickly with air pressure when 10 % methanol/$CHCl_3$ hot solution (60 ^oC) was used as the eluent in the column

chromatography. ^{1}H and ^{13}C NMR, FTIR and MS confirmed the structure and purity of these compounds.

N,N'-di(4-(butyloxy)-4-oxobutyl)-3,4:9,10-perylenetetracarboxyldiimide (**G4**)

Yield 0.371 g (55 %)

^{1}H NMR ($CDCl_3$, 600 MHz): δ (ppm) = 8.66 (d, J = 7.92 Hz, 4H, Ar), 8.58 (d, J = 8.10 Hz, 4H, Ar), 4.29 (t, J = 7.29 Hz, 4H, $CH_2COOC\mathbf{H_2}$), 4.06 (t, J = 6.69 Hz, 4H, $NC\mathbf{H_2}CH_2CH_2COOCH_2$), 2.48 (t, J = 7.59 Hz, 4H, $NCH_2CH_2C\mathbf{H_2}COOCH_2$), 2.11 – 2.16 (m, 4H, $NCH_2C\mathbf{H_2}CH_2COOCH_2$), 1.57 – 1.62 (m, 4H, $CH_2COOCH_2C\mathbf{H_2}$), 1.34 – 1.40 (m, 4H, $CH_2COOCH_2CH_2C\mathbf{H_2}$), 0.92 (t, J = 7.38 Hz, 6H, $CH_2COOCH_2CH_2CH_2C\mathbf{H_3}$). ^{13}C NMR ($CDCl_3$, 150 MHz): δ (ppm) = 173.113 (ester C=O), 163.519 (imide C=O), 134.803 (Ar), 131.616 (Ar), 129.502 (Ar), 126.584 (Ar), 123.363 (Ar), 123.262 (Ar), 64.536 ($CH_2COO\mathbf{C}H_2$), 39.976 ($N\mathbf{C}H_2CH_2CH_2COOCH_2$), 32.113 ($\mathbf{C}H_2$), 30.797 ($\mathbf{C}H_2$), 23.627 ($\mathbf{C}H_2$), 19.262 ($\mathbf{C}H_2$), 13.859 ($CH_2\mathbf{C}H_3$). FT-IR ($cm^{-1}$): 2956 (antisymmetric CH_3), 2871 (symmetric CH_3), 1738 (ester C=O), 1691 (symmetric imide C=O symmetric), 1660 (antisymmetric imide C=O), 1593 (aromatic ring stretch). HRMS $(M+H)^+$: calcd for $C_{40}H_{39}N_2O_8^+$ 675.2701; found 675.2694.

N,N'-di(4-(hexyloxy)-4-oxobutyl)-3,4:9,10-perylenetetracarboxyldiimide (**G6**)

Yield 0.438 g (60 %)

^{1}H NMR ($CDCl_3$, 600 MHz): δ (ppm) = 8.70 (d, J = 7.92 Hz, 4H, Ar), 8.64 (d, J = 8.10 Hz, 4H, Ar), 4.29 (t, J = 7.14 Hz, 4H, $CH_2COOC\mathbf{H_2}$), 4.05 (t, J = 6.78 Hz, 4H, $NC\mathbf{H_2}CH_2CH_2COOCH_2$), 2.47 (t, J = 7.44 Hz, 4H, $NCH_2CH_2C\mathbf{H_2}COOCH_2$), 2.11 – 2.16

(m, 4H, $NCH_2C\mathbf{H_2}CH_2COOCH_2$), 1.57 – 1.62 (m, 4H, $CH_2COOCH_2C\mathbf{H_2}$), 1.25 – 1.34 (m, 12H, $CH_2COOCH_2CH_2C\mathbf{H_2}C\mathbf{H_2}C\mathbf{H_2}$), 0.87 (t, J = 6.82 Hz, 6H, $CH_2COOCH_2CH_2$-$CH_2CH_2CH_2C\mathbf{H_3}$). ^{13}C NMR ($CDCl_3$, 150 MHz): δ (ppm) = 173.126 (ester C=O), 163.601 (imide C=O), 134.912 (Ar), 131.693 (Ar), 126.694 (Ar), 123.396 (Ar), 123.336 (Ar), 64.877 ($CH_2COO\mathbf{C}H_2$), 39.962 ($N\mathbf{C}H_2CH_2CH_2COOCH_2$), 32.116 ($\mathbf{C}H_2$), 31.601 ($\mathbf{C}H_2$), 28.716 ($\mathbf{C}H_2$), 25.728 ($\mathbf{C}H_2$), 23.634 ($\mathbf{C}H_2$), 22.672 ($\mathbf{C}H_2$), 14.156 ($CH_2\mathbf{C}H_3$). FT-IR ($cm^{-1}$): 2951 (antisymmetric CH_3), 2869 (symmetric CH_3), 1739 (ester C=O), 1690 (symmetric imide C=O symmetric), 1661 (antisymmetric imide C=O), 1592 (aromatic ring stretch). HRMS $(M+H)^+$: calcd for $C_{44}H_{47}N_2O_8^+$ 731.3327; found 731.3327.

N,N'-di(4-(octyloxy)-4-oxobutyl)-3,4:9,10-perylenetetracarboxyldiimide (**G8**)

Yield 0.488 g (62 %)

^{1}H NMR ($CDCl_3$, 600 MHz): δ (ppm) = 8.66 (d, J = 7.93 Hz, 4H, Ar), 8.58 (d, J = 8.05 Hz, 4H, Ar), 4.29 (t, J = 7.08 Hz, 4H, $CH_2COOC\mathbf{H_2}$), 4.04 (t, J = 6.82 Hz, 4H, $NC\mathbf{H_2}CH_2CH_2COOCH_2$), 2.48 (t, J = 7.55 Hz, 4H, $NCH_2CH_2C\mathbf{H_2}COOCH_2$), 2.11 – 2.16 (m, 4H, $NCH_2C\mathbf{H_2}CH_2COOCH_2$), 1.57 – 1.62 (m, 4H, $CH_2COOCH_2C\mathbf{H_2}$), 1.22 – 1.33 (m, 20H, $CH_2COOCH_2CH_2C\mathbf{H_2}C\mathbf{H_2}C\mathbf{H_2}C\mathbf{H_2}C\mathbf{H_2}$), 0.86 (t, J = 7.08 Hz, 6H, $CH_2COOCH_2CH_2CH_2CH_2CH_2CH_2CH_2C\mathbf{H_3}$). ^{13}C NMR ($CDCl_3$, 150 MHz): δ (ppm) = 173.110 (ester C=O), 163.535 (imide C=O), 134.778 (Ar), 131.609 (Ar), 129.508 (Ar), 126.581 (Ar), 123.358 (Ar), 123.272 (Ar), 64.884 ($CH_2COO\mathbf{C}H_2$), 39.969 ($N\mathbf{C}H_2CH_2CH_2COOCH_2$), 32.108 ($\mathbf{C}H_2$), 31.940 ($\mathbf{C}H_2$), 29.388 ($\mathbf{C}H_2$), 29.340 ($\mathbf{C}H_2$), 28.765 ($\mathbf{C}H_2$), 26.057 ($\mathbf{C}H_2$), 23.613 ($\mathbf{C}H_2$), 22.786 ($\mathbf{C}H_2$), 14.243 ($CH_2\mathbf{C}H_3$). FT-IR

(cm^{-1}): 2927 (antisymmetric CH_2), 2850 (symmetric CH_2), 1743 (ester C=O), 1692 (symmetric imide C=O symmetric), 1659 (antisymmetric imide C=O), 1592 (aromatic ring stretch). HRMS $(M+H)^+$: calcd for $C_{48}H_{55}N_2O_8^+$ 787.3953; found 787.3948.

N,N'-di(4-(decyloxy)-4-oxobutyl)-3,4:9,10-perylenetetracarboxyldiimide (**G10**)

Yield 0.556 g (66 %)

^{1}H NMR ($CDCl_3$, 600 MHz): δ (ppm) = 8.63 (d, J = 7.93 Hz, 4H, Ar), 8.53 (d, J = 8.03 Hz, 4H, Ar), 4.28 (t, J = 7.18 Hz, 4H, $CH_2COOC\mathbf{H_2}$), 4.04 (t, J = 6.80 Hz, 4H, $NC\mathbf{H_2}CH_2CH_2COOCH_2$), 2.48 (t, J = 7.54 Hz, 4H, $NCH_2CH_2C\mathbf{H_2}COOCH_2$), 2.11 – 2.16 (m, 4H, $NCH_2C\mathbf{H_2}CH_2COOCH_2$), 1.57 – 1.62 (m, 4H, $CH_2COOCH_2C\mathbf{H_2}$), 1.24 – 1.33 (m, 28H, $CH_2COOCH_2CH_2C\mathbf{H_2}C\mathbf{H_2}C\mathbf{H_2}C\mathbf{H_2}C\mathbf{H_2}C\mathbf{H_2}C\mathbf{H_2}$), 0.87 (t, J = 7.05 Hz, 6H, $CH_2COOCH_2CH_2CH_2CH_2CH_2CH_2CH_2CH_2CH_2C\mathbf{H_3}$). ^{13}C NMR ($CDCl_3$, 150 MHz): δ (ppm) = 173.127 (ester C=O), 163.465 (imide C=O), 134.683 (Ar), 131.542 (Ar), 129.459 (Ar), 126.489 (Ar), 123.313 (Ar), 123.211 (Ar), 64.853 ($CH_2COO\mathbf{C}H_2$), 39.982 ($N\mathbf{C}H_2CH_2CH_2COOCH_2$), 32.120 ($\mathbf{C}H_2$), 32.018 ($\mathbf{C}H_2$), 29.690 ($\mathbf{C}H_2$), 29.454 ($\mathbf{C}H_2$), 28.779 ($\mathbf{C}H_2$), 26.079 ($\mathbf{C}H_2$), 23.616 ($\mathbf{C}H_2$), 22.839 ($\mathbf{C}H_2$), 14.268 ($CH_2\mathbf{C}H_3$). FT-IR (cm^{-1}): 2917 (antisymmetric CH_2), 2852 (symmetric CH_2), 1743 (ester C=O), 1692 (symmetric imide C=O symmetric), 1658 (antisymmetric imide C=O), 1592 (aromatic ring stretch). HRMS $(M+H)^+$: calcd for $C_{52}H_{63}N_2O_8^+$ 843.4579; found 843.4580.

N,N'-di(4-(dodecyloxy)-4-oxobutyl)-3,4:9,10-perylenetetracarboxyldiimide (**G12**)

Yield 0.548 g (61 %)

^{1}H NMR ($CDCl_3$, 600 MHz): δ (ppm) = 8.69 (d, J = 7.96 Hz, 4H, Ar), 8.62 (d, J =

8.04 Hz, 4H, Ar), 4.29 (t, J = 7.23 Hz, 4H, $CH_2COOC\mathbf{H_2}$), 4.04 (t, J = 6.74 Hz, 4H, $NC\mathbf{H_2}CH_2CH_2COOCH_2$), 2.47 (t, J = 7.59 Hz, 4H, $NCH_2CH_2C\mathbf{H_2}COOCH_2$), 2.11 – 2.16 (m, 4H, $NCH_2C\mathbf{H_2}CH_2COOCH_2$), 1.57 – 1.62 (m, 4H, $CH_2COOCH_2C\mathbf{H_2}$), 1.23 – 1.33 (m, 36H, $CH_2COOCH_2CH_2C\mathbf{H_2}C\mathbf{H_2}C\mathbf{H_2}C\mathbf{H_2}C\mathbf{H_2}C\mathbf{H_2}C\mathbf{H_2}C\mathbf{H_2}C\mathbf{H_2}$), 0.86 (t, J = 7.02 Hz, 6H, $CH_2COOCH_2CH_2CH_2CH_2CH_2CH_2CH_2CH_2CH_2CH_2CH_2C\mathbf{H_3}$). ^{13}C NMR ($CDCl_3$, 150 MHz): δ (ppm) = 173.128 (ester C=O), 163.567 (imide C=O), 134.884 (Ar), 131.697 (Ar), 129.583 (Ar), 126.665 (Ar), 123.377 (Ar), 123.310 (Ar), 64.889 ($CH_2COO\mathbf{C}H_2$), 39.967 ($N\mathbf{C}H_2CH_2CH_2COOCH_2$), 32.119 ($\mathbf{C}H_2$), 32.060 ($\mathbf{C}H_2$), 29.807 ($\mathbf{C}H_2$), 29.778 ($\mathbf{C}H_2$), 29.738 ($\mathbf{C}H_2$), 29.686 ($\mathbf{C}H_2$), 29.502 ($\mathbf{C}H_2$), 29.431 ($\mathbf{C}H_2$), 28.767 ($\mathbf{C}H_2$), 26.070 ($\mathbf{C}H_2$), 23.614 ($\mathbf{C}H_2$), 22.833 ($\mathbf{C}H_2$), 14.272 ($CH_2\mathbf{C}H_3$). FT-IR ($cm^{-1}$): 2916 (antisymmetric CH_2), 2852 (symmetric CH_2), 1744 (ester C=O), 1692 (symmetric imide C=O symmetric), 1660 (antisymmetric imide C=O), 1593 (aromatic ring stretch). HRMS $(M+H)^+$: calcd for $C_{56}H_{71}N_2O_8^+$ 899.5205; found 899.5199.

N,N'-di(4-(tetradecyloxy)-4-oxobutyl)-3,4:9,10-perylenetetracarboxyldiimide (**G14**) Yield 0.621 g (65 %)

^{1}H NMR ($CDCl_3$, 600 MHz): δ (ppm) = 8.70 (d, J = 7.99 Hz, 4H, Ar), 8.64 (d, J = 8.08 Hz, 4H, Ar), 4.29 (t, J = 7.20 Hz, 4H, $CH_2COOC\mathbf{H_2}$), 4.04 (t, J = 6.81 Hz, 4H, $NC\mathbf{H_2}CH_2CH_2COOCH_2$), 2.47 (t, J = 7.43 Hz, 4H, $NCH_2CH_2C\mathbf{H_2}COOCH_2$), 2.11 – 2.16 (m, 4H, $NCH_2C\mathbf{H_2}CH_2COOCH_2$), 1.57 – 1.62 (m, 4H, $CH_2COOCH_2C\mathbf{H_2}$), 1.23 – 1.33 (m, 44H, $CH_2COOCH_2CH_2C\mathbf{H_2}C\mathbf{H_2}C\mathbf{H_2}C\mathbf{H_2}C\mathbf{H_2}C\mathbf{H_2}C\mathbf{H_2}C\mathbf{H_2}C\mathbf{H_2}C\mathbf{H_2}$), 0.87 (t, J = 7.24 Hz, 6H, $CH_2COOCH_2CH_2CH_2CH_2CH_2CH_2CH_2CH_2CH_2CH_2CH_2C\mathbf{H_3}$).

^{13}C NMR ($CDCl_3$, 150 MHz): δ (ppm) = 173.106 (ester C=O), 163.579 (imide C=O), 134.899 (Ar), 131.712 (Ar), 129.610 (Ar), 126.686 (Ar), 123.400 (Ar), 123.335 (Ar), 64.890 ($CH_2COO\mathbf{C}H_2$), 39.952 ($N\mathbf{C}H_2CH_2CH_2COOCH_2$), 32.123 ($\mathbf{C}H_2$), 32.055 ($\mathbf{C}H_2$), 29.848 ($\mathbf{C}H_2$), 29.824 ($\mathbf{C}H_2$), 29.810 ($\mathbf{C}H_2$), 29.801 ($\mathbf{C}H_2$), 29.742 ($\mathbf{C}H_2$), 29.688 ($\mathbf{C}H_2$), 29.510 ($\mathbf{C}H_2$), 29.432 ($\mathbf{C}H_2$), 28.771 ($\mathbf{C}H_2$), 26.072 ($\mathbf{C}H_2$), 23.625 ($\mathbf{C}H_2$), 22.840 ($\mathbf{C}H_2$), 14.275 ($CH_2\mathbf{C}H_3$). FT-IR ($cm^{-1}$): 2916 (antisymmetric CH_2), 2852 (symmetric CH_2), 1746 (ester C=O), 1692 (symmetric imide C=O symmetric), 1660 (antisymmetric imide C=O), 1593 (aromatic ring stretch). HRMS $(M+H)^+$: calcd for $C_{60}H_{79}N_2O_8^+$ 955.5831; found 955.5823.

N,N'-di(4-(hexadecyloxy)-4-oxobutyl)-3,4:9,10-perylenetetracarboxyldiimide (**G16**) Yield 0.678 g (67 %)

^{1}H NMR ($CDCl_3$, 600 MHz): δ (ppm) = 8.68 (d, J = 7.89 Hz, 4H, Ar), 8.60 (d, J = 8.11 Hz, 4H, Ar), 4.29 (t, J = 7.20 Hz, 4H, $CH_2COOC\mathbf{H_2}$), 4.04 (t, J = 6.72 Hz, 4H, $NC\mathbf{H_2}CH_2CH_2COOCH_2$), 2.48 (t, J = 7.53 Hz, 4H, $NCH_2CH_2C\mathbf{H_2}COOCH_2$), 2.11 – 2.16 (m, 4H, $NCH_2C\mathbf{H_2}CH_2COOCH_2$), 1.57 – 1.62 (m, 4H, $CH_2COOCH_2C\mathbf{H_2}$), 1.23 – 1.33 (m, 52H, $CH_2COOCH_2CH_2C\mathbf{H_2}C\mathbf{H_2}C\mathbf{H_2}C\mathbf{H_2}C\mathbf{H_2}C\mathbf{H_2}C\mathbf{H_2}C\mathbf{H_2}C\mathbf{H_2}C\mathbf{H_2}C\mathbf{H_2}$-$C\mathbf{H_2}C\mathbf{H_2}$), 0.87 (t, J = 6.90 Hz, 6H, $CH_2COOCH_2CH_2CH_2CH_2CH_2CH_2CH_2CH_2CH_2CH_2$-$CH_2CH_2CH_2CH_2CH_2C\mathbf{H_3}$). ^{13}C NMR ($CDCl_3$, 150 MHz): δ (ppm) = 173.348 (ester C=O), 163.748 (imide C=O), 131.888 (Ar), 129.211 (Ar), 123.519 (Ar), 65.102 ($CH_2COO\mathbf{C}H_2$), 40.170 ($N\mathbf{C}H_2CH_2CH_2COOCH_2$), 32.296 ($\mathbf{C}H_2$), 30.062 ($\mathbf{C}H_2$), 30.044 ($\mathbf{C}H_2$), 30.023 ($\mathbf{C}H_2$), 29.960 ($\mathbf{C}H_2$), 29.904 ($\mathbf{C}H_2$), 29.725 ($\mathbf{C}H_2$), 29.648 ($\mathbf{C}H_2$), 28.983

(**C**H_2), 26.283 (**C**H_2), 23.842 (**C**H_2), 23.058 (**C**H_2), 14.492 (CH_2**C**H_3). FT-IR (cm^{-1}): 2916 (antisymmetric CH_2), 2852 (symmetric CH_2), 1746 (ester C=O), 1692 (symmetric imide C=O symmetric), 1659 (antisymmetric imide C=O), 1593 (aromatic ring stretch). HRMS $(M+H)^+$: calcd for $C_{64}H_{87}N_2O_8^+$ 1011.6457; found 1011.6453.

CHAPTER 5. SYNTHESIS AND CHARACTERIZATIONS OF THE FIRST SOLUBLE NONRACIMIC CHIRAL MAIN-CHAIN PERYLENE TETRACARBOXYLIC DIIMIDE POLYMERS

5.1. Introduction

Perylene tetracarboxylic diimides (PDIs) have been attracting considerable attention as lightfast colorants,[1-3] highly efficient fluorophores,[4-6] the best n-type organic semiconductors[7-9] and versatile building blocks in self-assembly.[10-14] From the application point of view, incorporation of PDIs into main chains of polymeric architectures will generate mechanical robust materials with the attractive functionalities. One potentially exciting application of such a material is to replace expensive and poor film-forming fullerene derivatives as the electron acceptor and electron transport material in plastic solar cells. This calls for well-defined solution processable main-chain PDI polymers with extensive π-stacked organization.

Although a number of PDI main-chain polymers have been reported,[15-27] most of them[15,17,19,20,26,28] are only soluble in special solvents such as concentrated sulfuric acid or *m*-cresol, mainly due to the strong PDI π-stacking interaction. As a matter of fact, even many low molecular weight PDI dyes including some with long *n*-alkyl chains have very low solubility in common organic solvents.[29-31] To obtain better processability, two general approaches have been developed to reduce PDI π-stacking interaction and render low molecule weight PDIs readily soluble. The first approach involves the attachment of solubilizing group to the carbocyclic scaffold (bay-area).[32-35] Usually this

modification leads to the distortion of the originally planar perylene ring so that the packing of PDI moieties becomes more difficult which contributes to pronouncedly increased solubility. In the second approach the solubilizing groups are connected to the imide nitrogen atoms.[4,6,36,37] In this case, the planarity of the PDI core is retained. Among all solubilizing substituents, sterically demanding groups as 2,6-di-*tert*-butylphenyl[38] and long chain symmetrically secondary alkyl groups (swallow tails)[36] exhibited extraordinary ability to generate highly soluble PDI dyes, presumably because of the significantly reduced PDI π-π interaction by a steric means. The first approach has been successfully implemented into preparation of well soluble main-chain PDI polymers.[16,18] However, as far as charge transport is concerned, planarity of PDI rings is preferred for establishing PDI π-stacks as efficient charge transport pathways. Thus, functionalization at the imide nitrogen atoms is a preferred option. Along this line, highly flexible polyether[22,25] or highly branched hydrocarbon segments[27] have been incorporated into main-chain PDI polymers and oligomers affording soluble materials with planar PDI rings. Note that swallow tails have not been integrated to main-chain PDI polymers as solubilizing groups probably because of difficulties in synthesis, although they have been extensively used in donor-acceptor dyads and triads,[39-41] donor-bridge-acceptor molecules,[42] fluorescent sensors and light switches,[43-45] supramolecular assemblies,[46,47] PDI multichromophores[48-50] and PDI side chain polymers.[51-53] Besides the above-mentioned approaches initially developed for low molecular weight PDIs, copolymerization with other monomers has also been proven

useful in giving soluble main-chain PDI polymers.[17,20,21,23,24,26,28]

Recently we have found that the incorporation of a library of nature-occurring α-amino acids into PDIs offers an efficient way to *tune* π-stacking interaction between adjacent rigid units, mainly by steric effects.[54,55] This tunability is highly desired as it allows us to achieve a delicate balance between good solubility and the ability to form PDI π-stacks with extensive intermolecular π orbital overlap, which is crucial for various optoelectronic applications. When an optically pure α-amino acid is used, nonracemic chiral PDI molecules result since the chirality centers do not participate in reactions. The configurational chirality may express as helical aggregates of PDI chromophores in a defined fashion, which could lead to increased charge carrier mobilities.[9] With the integration of the unique PDI π-stack tunability and the optical activity into polymers, we report the synthesis and characterization of the first solution-processable nonracemic chiral main-chain PDI polymers.

5.2. Results and discussion

PDI-L-Ala and PDI-L-Leu have been prepared in excellent yields by reacting perylene tetracarboxylic dianhydride with L-alanine and L-Leucine in molten imidazole. The methyl group in PDI-L-Ala and the isobutyl group in PDI-L-Leu can be considered as the π-stack controlling groups that direct the formation of PDI π stacks by a steric means. Because isobutyl group is more sterically demanding than methyl group, it is expected that the formation of PDI π-stacks in PDI-L-Leu (and its derivatives) is more difficult than that in PDI-L-Ala, which should lead to higher solubility. To increase the

processability, a long and flexible spacer is employed to connect the PDI units into semi-flexible main-chain polymers.

Acyclic diene metathesis (ADMET)[58, 59] was chosen to produce such semi-flexible polymers. ADMET has a few advantages over traditional polycondensation reactions. For instance, usually an ADMET reaction only involves one symmetrically substituted monomer equipped with two vinyl groups. Therefore there is no need to take great care on stoichiometric balance as in an AA/BB polycondensation or carry out a multi-step synthesis to obtain the unsymmetrically substituted monomer as in an AB polycondensation. In addition, since the ethylene gas is the only side product, it is relatively easy to obtain clean final products. In our case, one additional advantage of using ADMET is that the corresponding monomers, ML-Ala11 and ML-Leu11 exhibit high solubility in common organic solvents, which facilitates the preparation and purification of monomers, as well as the solution polymerization reactions. As shown in **Scheme 5.1**, the two monomers were synthesized in high yields from PDI-L-Ala and PDI-L-Leu, respectively.

Same as a conventional polycondensation reaction, an ADMET polymerization prefers high monomer concentration to minimize the formation of cyclic products, therefore bulk polymerization is the top choice. However, because of the melting points of ML-Ala11 (186.5 ℃) and ML-Leu11 (158.3 ℃) are too high to support an efficient bulk ADMET reaction, solution polymerizations were performed. Since ADMET is an equilibrium process, removal of ethylene gas is needed to shift the equilibrium to the

formation of high molecular weight polymers. Usually this is achieved either by using a reduced pressure, or purging the reactor with a nitrogen or argon flow. Here we chose to purge the reaction system with N_2. To prevent excessive loss of the solvent, 1, 2-dichlorobenzene is chosen as the solvent because of its high boiling point (180 ℃) and good ability to dissolve both monomers and the corresponding polymers. The polymerization reactions were catalyzed by Grubbs II catalyst with structure shown in **Scheme 5.1**.

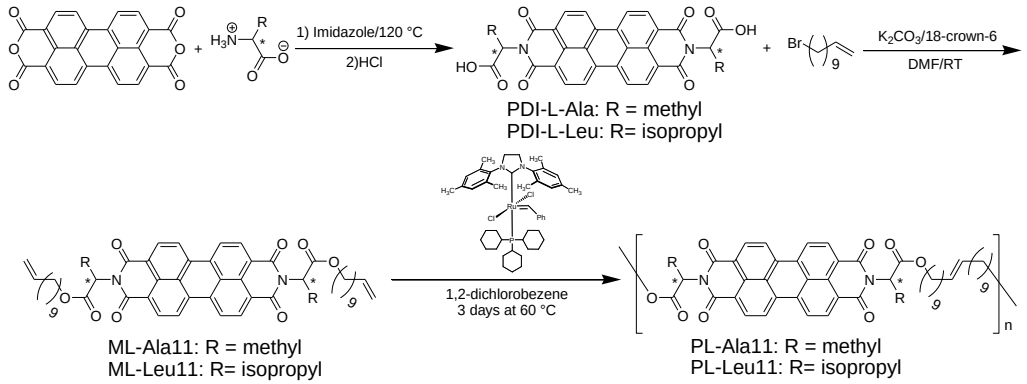

Scheme 5.1. ADMET synthesis of main-chain PDI polymers all labeled chirality centers are in *S* configuration

ADMET of ML-Ala11 was first carried out. The original clear solution turned cloudy during the first day. This is probably due to the rapidly decreased solubility of the oligomers of PL-Ala11 with the increased degree of polymerization. The reaction was stopped after three days. ^{1}H NMR spectroscopy confirmed the quantitative conversion of the monomer to polymer. As shown in **Figure 5.1A**, the vinyl group in the monomer displays its ^{1}H resonance at about 5.7 (overlapped with H_1) and about 4.9 ppm. After polymerization, the resonance peak at 4.9 ppm completely disappears and a

new resonance peak appears at 5.3 ppm, indicating the formation of internal carbon-carbon double bonds. Completion of polymerization has also been verified by FT-IR as shown in **Figure 5.2A**. The characteristic absorption bands of vinyl group of the monomer can be observed at 3077, and 909 cm^{-1}. These bands disappeared after polymerization, signifying the complete conversion of the diene monomer.

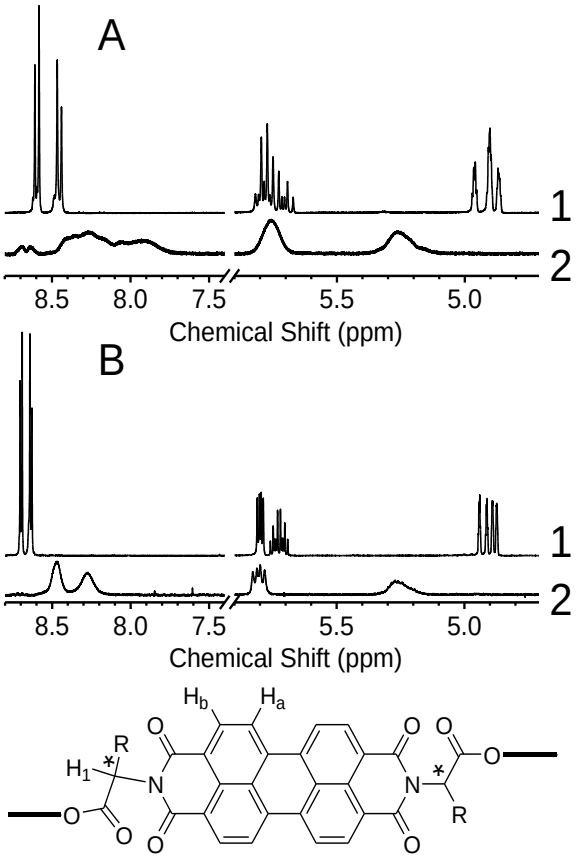

Figure 5.1. ^{1}H NMR spectra of ML-Ala11 (A1) and PL-Ala11 (A2); ML-Leu11 (B1) and PL-Leu 11 (B2)

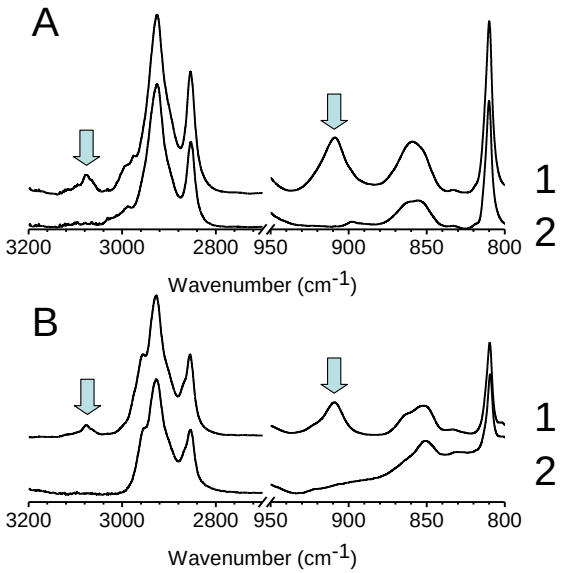

Figure 5.2. FT-IR spectra of ML-Ala11 (A1) and PL-Ala11 (A2); ML-Leu11 (B1) and PL-Leu 11 (B2). Absorption bands of vinyl groups were labeled with arrows.

ADMET of ML-Leu11 gave a viscous solution after 24 hours and no precipitations were observed during the entire polymerization process, which implies that PL-Leu11 are more soluble than PL-Ala11 in 1, 2-dichlorobenzene, likely because the bulkier isobutyl group can better reduce PDI π-stacking interaction. The reaction was stopped after three days. The completion of reaction is also confirmed by ^{1}H NMR and FT-IR, as shown in **Figure 5.1B** and **5.2B**.

PL-Ala11, is partially (~85 %) soluble in chloroform at about 10^{-3} M (in repeat units) concentration. The chloroform-soluble fraction is soluble partially in CH_2Cl_2, THF, acetone, pyridine and ethyl acetate, producing a colored solution up to about 10^{-5} M concentrations. PL-Leu11 is completely soluble in chloroform at 10^{-2} M concentration. It also partially dissolves in CH_2Cl_2, toluene, acetone at concentrations about 10^{-5} M. PL-Leu11's solubility in THF is very low, the concentration of the saturated solution at

RT is about 10^{-6} M.

Molecular weights and their distribution of PL-Ala11 and PL-Leu11 were characterized by size exclusion chromatography (SEC). The extracted molecular weight data were given in **Table 5.1**. The absorption coefficients of PL-Ala11 and PL-Leu11 at 527 nm are 5.6×10^4 and 6.5×10^4 L/(mol·cm), respectively. With such high extinction coefficients, we were able to record SEC traces with THF as eluent although both polymers exhibit low solubilities in this solvent. SEC curves of PL-Ala11 were presented in **Figure 5.3A**. A series of sharp peaks with low molecular weights strongly suggest that PL-Ala11 is mainly a mixture of oligomers. Since no vinyl groups were observed in ^{1}H NMR, these oligomers should possess a cyclic structure.

For PL-Leu11, as revealed by the SEC trace of the THF soluble part shown in **Figure 5.3B**, also consists of mostly oligomers. However, because only a small part (~25 %) of PL-Leu11 is soluble in THF, the THF soluble part only represents the low molecular weight end of the material. To better understand the overall molecular weight distribution, a fractionation experiment was carried out by adding THF into concentrated PL-Leu11 chloroform solution. Although the precipitated fraction (PL-Leu11A) is essentially insoluble in THF, its saturated THF solution was able to give the SEC trace illustrated in **Figure 5.3C**, thanks to PL-Leu11A's high extinction coefficient at 527 nm. The number-average and weight average molecular weight are 3.3 K and 6.9 K, respectively. It is reasonable to assume that THF is only able to dissolve the low molecular weight end of PL-Leu11A, the THF insoluble part must possess even higher

molecular weight. Because the molecular weight measurements were relative to a calibration with polystyrene standards, the molecular weights of PDI polymers could be notably underestimated. This is due to the formation of PDI π-stacks in solution (see below), which reduces the hydrodynamic volume of a polymer chain. A reduced hydrodynamic volume corresponds to a decreased molecular weight. This speculation is supported by the observation that the SEC molecular weight of ML-Leu11 is only 505, while its real molecular weight is 923. The true high molecular weight nature of PL-Leu11 is firmly backed by the film-casting experiments. Flexible and free-standing films of PL-Leu11 can be drop-cast from its chloroform solution. One of such free-standing drop-cast films is shown in **Figure 5.4**. They can be bent or folded without breaking, signifying the high molecular weight nature of PL-Leu11. In contrast, the same procedure on PL-Ala11 produced a very brittle film that could not be lifted from the substrate, due to the substantially lower molecular weight.

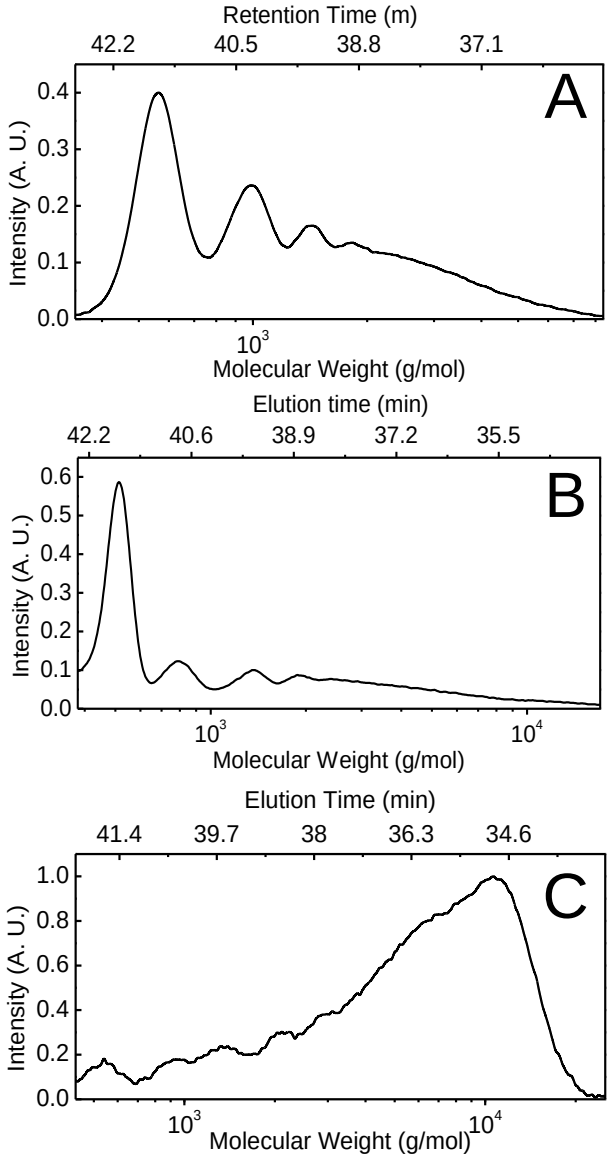

Figure 5.3. SEC curves of PL-Ala11 (A), PL-Leu11 (B) and PL-Leu11A(C)

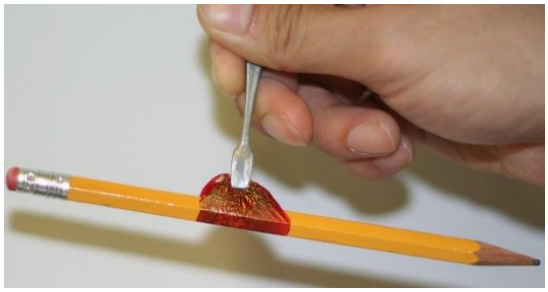

Figure 5.4. The photograph of a PL-Leu11 film cast from chloroform solution. The film was used to wrap around a pencil and hang it in air

Table 5.1. Molecular Weights and Polydispersity of PDI Polymers

Polymer	M_n (g/mol)	M_w (g/mol)	PDI
PL-Ala11	916	1470	1.60
PL-Leu11	810	1930	2.38
PL-Leu11A	3250	6920	2.13

Aggregation behavior of PL-Ala11, PL-Leu11 and their corresponding monomers were investigated by UV-visible (UV-vis) and circular dichroism (CD) spectroscopy. Aggregation of a PDI derivative in solution is strongly dependent upon the solvent-solute interaction. When the side chains are well-solvated by the solvent, PDI π-stacking interaction becomes the major driving force of aggregation, resulting in the formation of PDI π-stacks. Due to the intermolecular π-orbital overlap in π-stacks, the electronic spectrum of stacked PDI units is different from that of unassociated chromophores.[9,60-62] UV-vis spectra of monomers are shown in **Figure 5.5**. The spectra of two monomers are essentially identical. The spectra feature a series of absorption peaks at 527 nm, 490 nm and 458 nm. They can be attributed to the vibrational progression of the $S_0 \rightarrow S_1$ electronic transition of the PDI monomers.[61] The absorption maximum at 527 nm originates from the transition from the zero vibrational level of the S_0 state to the zero vibrational level of the S_1 state ($0 \rightarrow 0$). The peaks at 490 and 458 are due to the transition from the zero vibration level of the S_0 state to the first and the second vibrational excited levels of the S_1 state, respectively. They can be marked as $0 \rightarrow 1$ (490 nm) and $0 \rightarrow 2$ (458 nm). As reported earlier,[61,63] the intensity ratio A527/A490 decreases upon the formation of π-stacks. For both monomers, A527/A490 = 1.68 at

10^{-6} M concentration and this ratio changes very little when the concentration increases from 5.9 μM to 9.6 mM. This implies that over such a broad concentration range, PDI molecules are essentially all in the monomeric state.[61, 63] In contrast, A527/A490 changes appreciably when the concentration of bis-*N*,*N*-(2-(2-(2-(2-hydroxyethoxy)ethoxy)ethoxy)ethyl) perylene tetracarboxylic diimide chloroform solution changes from 0.48 mM to 7.7 mM.[61] This can be attributed to the existence of the π-stack tuning group in ML-Ala11 (methyl) and ML-Leu11(isobutyl), thus it is more difficult for ML-Ala11 and ML-Leu11 to assemble into PDI π-stacks owing to greater steric hindrance toward the formation of PDI π-stacks. Contrarily, the *N*-substituents in bis-*N*,*N*-(2-(2-(2-(2-hydroxyethoxy)ethoxy)ethoxy)ethyl) perylene tetracarboxylic diimide are much less sterically demanding.

The UV-vis spectrum of PL-Leu11 is illustrated in **Figure 5.5B**. Similar to that of monomers, the spectrum changes little when the concentration increases from 5.9 μM to 8.9 mM. However, the spectrum of the PL-Leu11 is considerably broader than that of ML-Leu11. In addition, A527/A490 for PL-Leu11 is about 1.46, which is clearly lower than 1.68 found for its monomer. Both the spectrum broadening and decreased A527/A490 value[61, 63] suggest the existence of PDI π-stacks in PL-Leu11 solution, even at a concentration as low as 5.9 μM. The organization of chromophore units in a PDI polymer is more complicated than monomeric PDIs. For a monomeric PDI, when concentration is the only variable, there is always a concentration below which the entropy contribution dominates and essentially all PDI molecules are in the unassociated

state. However, for a polymer, even at an extremely low concentration, PDI π-stacks still can form via a folding process because a PDI chromophore has an appreciable probability to meet another PDI unit in the same polymer chain due to the chemical connectivity.[62, 63] With increasing concentrations, folded PDI polymer chains could further self-assemble into larger aggregates. At μM concentration in chloroform, every PDI polymer chain can be considered to be well-separated from each other, thus intra-molecular π-stack formation or folding is the major form of aggregation. Although larger aggregates could form because of self-assembly of folded polymer chains, this was not observed for PL-Leu11 at concentrations up to 8.9 mM as evidenced by little change in UV-vis spectrum. The spectroscopic behavior of PL-Ala11 solution is essentially the same as that of PL-Leu11. The UV-vis spectrum shown in **Figure 5.5A** suggests that PL-Ala11 chains also fold into PDI π-stacks in chloroform solution.

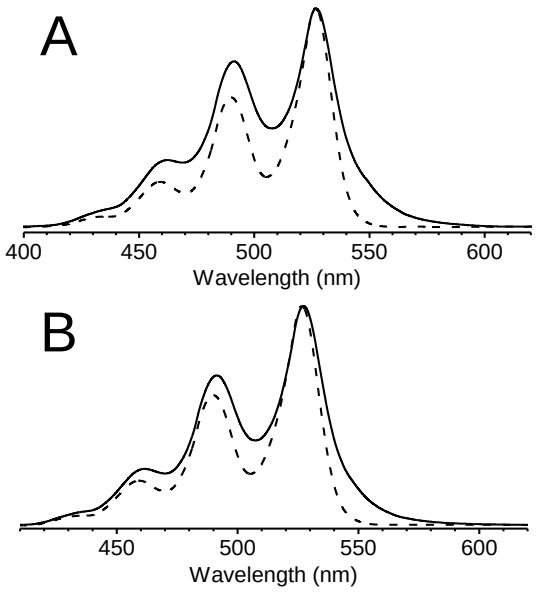

Figure 5.5. UV-vis spectra of PL-Ala11 (solid) and ML-Ala11 (dash) (A); PL-Leu11 (solid) and ML-Leu11 (dash) (B). All solutions are at a concentration of 5.9 μM in chloroform.

The formation of π-stacks in polymer solutions is also confirmed by solution ^{1}H NMR experiments. The chemical shifts of H_a and H_b (**Figure 5.1**) can be used to monitor π-stack formation of PDIs. Upon π-stack formation, both δ_a and δ_b decrease, accompanied by an increase of δ_b-δ_a.[61-63] For ML-Ala11, the perylene aromatic protons can be found as two doublets at δ_a = 8.45 and δ_b = 8.6. At the same time, the corresponding protons appear at 7.92 and 8.26 ppm as two very broad peaks in PL-Ala11. The significantly decreased chemical shift values and the increased δ_b-δ_a, from 0.15 ppm in the monomer to 0.34 ppm in the polymer, strongly support the existence of PDI π-stacks in the polymer solution. In the aromatic region, there are two additional relative sharp, weak peaks at 8.64 and 8.69 pm. They may be attributed to the perylene

aromatic protons from the monocyclic PDI as a result of unimolecular ring-closing metathesis of the ML-Ala11. Similar behaviors were observed in NMR spectra of ML-Leu11 and PL-Leu11. The perylene aromatic protons were observed at 8.63 and 8.7 ppm for ML-Leu11, while the corresponding protons appeared at 8.27 and 8.47 ppm as two broad peaks for PL-Leu11. However, the fact that no perylene proton peaks other than the two broad ones appeared in ^{1}H NMR of PL-Leu11 implies that hardly any monocylic PDI formed during polymerization.

When organizing into π-stacks, a PDI unit will either slip and/or rotate with respect to the adjacent PDI to minimize the energy.[37,64,65] If a rotation occurs, both left and right-handed rotations are possible. Nonchiral molecules must take the two rotation directions at the equal probability. Consequently, either no helical organization will be developed, or right-handed and left-handed helices will form at the exactly same population. Contrarily nonracemic chiral PDIs may favor a particular rotation direction over the other, leading to helically arranged chromophores with a well-defined handedness. ML-Ala11, ML-Leu11, PL-Ala11 and PL-Leu11 are nonracemic chiral materials because the optically pure amino acids were used as the starting materials and the chirality centers are not involved in the reactions. As a result of the nonracemic chiral nature, a distinct helical arrangement of PDI units may exist in their π-stacks, which can be readily detected by CD spectroscopy. CD spectra of two polymers and their corresponding monomers were given in **Figure 5.6**. No CD signals were observed for the monomers, whereas a pronounced CD signal was observed for both polymers with

a positive maximum at 491 nm and a negative maximum at 548 nm. The bisignated CD signals are characteristic for helically stacked chromophores. The negative sign of the signal, which characterized by a positive to negative change with increasing wavelength, indicates the helical arrangement is left-handed.[66]

Combining UV-Vis, ^{1}H NMR and CD results, a putative picture of aggregation behaviors of four PDIs in chloroform solution can be given. On one hand, the vast majority of monomer molecules exist in chloroform solution as the unassociated species, thus the configurational chirality does not express into chiral arrangement of PDI molecules. On the other hand, PDI π-stacks form in polymers, even at a very low concentration, probably as the consequence of an intra-molecular folding process. Due to the nonracemic chiral nature of the polymers inherited from the L-form α amino acids, the dye units favor the left-handed helical arrangement, which gave the negative bisignated CD signal.

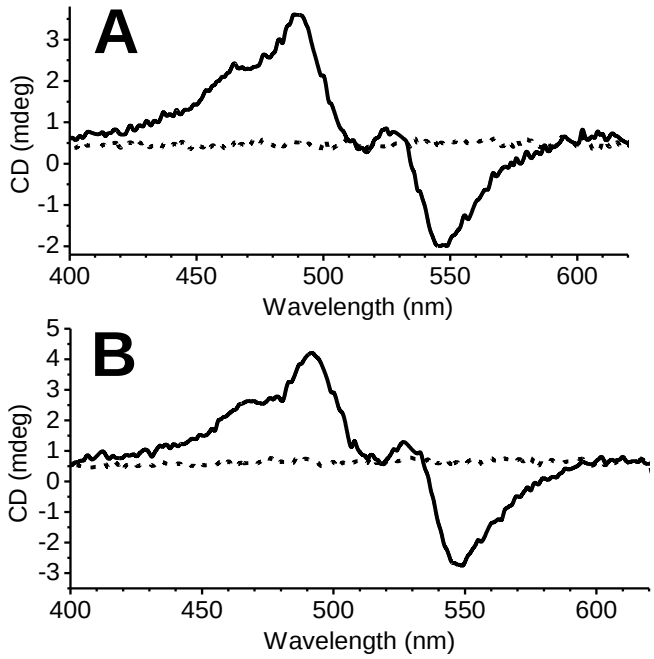

Figure 5.6. CD spectra of PL-Ala11 (solid line) and ML-Ala11 (dash line) (A); PL-Leu11 (solid line) and ML-Leu 11 (dash line) (B). All solutions are at a concentration of 5.9 μM in chloroform.

The ability of accepting electrons is among those important properties that make PDIs such useful materials. Electron accepting ability of monomers and polymers was evaluated using differential pulsed voltammetry with Fc/Fc^+ as the internal reference. As shown in **Figure 5.7**, all PDIs undergo two reduction processes in a potential window between -0.9V and -1.3 V with the peak potential values given in **Table 5.2**. It is obvious that all four PDI derivatives exhibited the similar reduction potentials. This is because the imide nitrogen atoms are at the node of both HOMO and LUMO wave functions of PDI, thus *N*-substitution has little effect of HOMO and LUMO levels. As the consequence, electrochemical property of PDIs is essentially independent on *N*-substitutions. The first reduction potential values (~-1.030V) of two PDI polymers

compare favorably with that of [6,6]-phenyl C_{61} butyric acid methyl ester (PCBM, a widely used electron acceptor in organic photovoltaics), which has a first reduction potential of -1.169 V vs. Fc/Fc^+ in 1, 2-dichlorobenzene solution.[67] This suggests that these two PDI polymers possess similar electron-accepting power as PCMB. This fact, in addition to the good film-forming ability of PL-Leu11, could make PL-Leu11 an attractive candidate as the electron acceptor in organic photovoltaic devices.

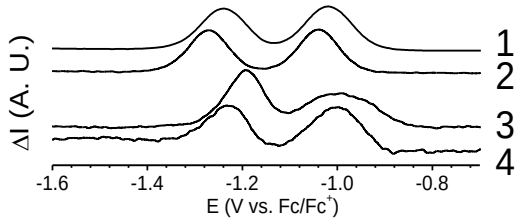

Figure 5.7. Differential pulse voltammetry traces of ML-Ala11 (1); ML-Leu11 (2); PL-Ala11 (3) and PL-Leu11 (4).

Table 5.2. Reduction Potentials of PDIs vs. Fc/Fc^+

Compound	E_1 (V)	E_2 (V)
ML-Ala11	-1.020	-1.240
ML-Leu11	-1.038	-1.272
PL-Ala11	-1.000	-1.193
PL-Leu11	-1.004	-1.231

5.3. Conclusions

The first two nonracemic chiral main chain PDI polymers were synthesized by ADMET polymerization. They exhibited appreciable solubility in chloroform due to the existence of π-stack tuning groups. Intra-molecular PDI π-stack formation was observed in dilute polymer chloroform solutions. Inside π-stacks, PDI chromophores organize in a left-handed helical fashion. Free-standing and flexible films can be cast

from PL-Leu11 chloroform solution. Good film-forming ability and strong electron affinity make PL-Leu11 a promising polymer for use in organic optoelectronic devices.

5.4. Experimental section

Instruments and Characterizations

All measurements were carried out at RT unless otherwise noted. ^{1}H NMR and ^{13}C NMR spectra were recorded on a Varian 300 MHz or 600 MHz NMR spectrometer with deuterated chloroform ($CDCl_3$) as the solvent at 25 ^{o}C. For ^{1}H NMR, the chemical shifts were reported using $CHCl_3$ residue (δ = 7.26 ppm) in deuterated chloroform as the internal standard. For ^{13}C NMR, the chemical shifts were reported using the $CDCl_3$ signal (δ = 77.16 ppm) as the reference. Elemental analysis was carried out by Atlantic Microlab, Inc. Mass measurement was carried out by CUNY-Hunter MS center. The IR spectra were acquired on a Nicolet Magna 550 FTIR spectrometer at a resolution of 2 cm^{-1}. UV-visible spectra were collected on a Varian UV-Vis spectrometer at a resolution of 1 nm. Size excluded chromatography analysis was carried out on an Alliance GPCV 2000 (Waters) instrument equipped with four Waters Styragel HR columns, i.e. HR-1, HR-3, HR-4, HR-5E. Measurements are relative to a calibration with polystyrene standards. HPLC grade THF was used as the eluent, at a flow rate of 1.0 mL/min at 30 $^{\circ}C$. An UV-visible detector was used with the detection wavelength set to 527 nm. Circular dichroism spectra were obtained on the AVIV Circular Dichroism model 410 spectrometer at 25 ℃ with a bandwidth of 1 nm. The wavelength step was 1 nm and three scans were averaged for every spectrum. Electrochemistry

measurements were performed with a three-electrode setup using a Princeton applied research M2273 potentiostat. Differential pulse voltammetry technique was employed. The pulse height and pulse width were 25 mV and 50 ms, respectively. The scan rate was 20 mV/s. A platinum wire and a silver wire electrode were employed as the counter electrode and the pseudo-reference electrode, respectively. The working electrode was a platinum disk with a diameter of 0.5 mm. Before each use, the working electrode was carefully polished using 0.3 μm aluminum oxide polishing compound and cleaned in an ultrasonic bath with acetone. Argon was bubbled through the solutions to remove oxygen, and a slight argon overpressure was maintained during each measurement. The solvent was o-dichlorobenzene, and the supporting electrolyte was tetrabutylammonium tetrafluoroborate. The potential values were reported versus the ferrocene/ferrocenium (Fc/Fc^+) couple, as recommended by IUPAC.[56]

Materials

All reagents and chemicals were purchased from Fisher scientific or VWR international and used as received unless otherwise noted. Grubbs II catalyst was purchased from Sigma-Aldrich. 1, 2-dichlorobenzene was distilled under a reduced pressure before use. Tetrabutylammonium tetrafluoroborate was dried overnight under vacuum at 80 ℃.

Synthesis of *N, N'*-di((*S*)-1-carboxyethyl)-3,4:9,10-perylenetetracarboxyldiimide (PDI-L-ala)

Into a 50 ml Schlenk flask were charged 1.87 g L-alanine (21 mmol),

3,4:9,10-perylenetetracarboxyldianhydride (PTCDA) 3.92 g (10 mmol), and imidazole (28 g). The mixture was purged with argon for 15 minutes before being heated at 120 ℃ until the reaction mixture was completely soluble in water. Subsequently, the reaction mixture was cooled to 90 ℃. Deionized water was added under the protection of argon. The dark-red solution was filtered to remove the trace amount of unreacted PTCDA. The solution was then acidified with 2 M HCl aqueous solution to a pH value of 3-4, the formed precipitate was collected by suction-filtration and thoroughly washed with deionized water until the filtrate was neutral; the red solid was collected and dried at 75 ℃ in vacuum oven until constant weight. 5.131 g (96 %) PDI-L-Ala was obtained as a dark-red solid.

Synthesis of *N, N'*-di((*S*)-1-carboxyl-3-methylbutyl)-3,4:9,10-perylenetetracarboxyl-diimide (PDI-L-Leu)

PDI-L-Leu was prepared using the same methodology as described for PDI-L-Ala, with L-leucine replacing L-alanine. 6.00 g (97 %) PDI-L-Leu was obtained as a dark-red solid.

Synthesis of *N, N'*-di((*S*)-2-(10-undecenoxyl)-1-methyl-2-oxoethyl)-3,4:9,10-perylenetetracarboxyldiimide (ML-Ala11)

Into a N_2-purged 20 mL vial were charged 1 mmol PDI-L-Ala (MW: 534 g/mol), 152 mg (1.1 mmol) K_2CO_3 and 5.8 g DMF solution containing 580 mg (2.2 mmol) 18-crown-6. The mixture was stirred for 30 minutes at RT, forming a deep purple solution. 583 mg (2.5 mmol) 11-bromo-1-undecene was then added to the solution.

The reaction mixture was stirred in dark at RT under an Argon atmosphere for 24 hours before being poured into 40 ml methanol. The orange crystalline precipitate was collected by centrifugation and dried at RT in a vacuum oven for 12 hours. The crude product is purified by column chromatography on silica gel using 20/1 (v/v) chloroform/acetone as the eluent. Yield 0.760 g (90.6 %) ML-Ala11 as a dark-red solid. ^{1}H NMR ($CDCl_3$, 300 MHz): δ (ppm) = 8.60 (d, J = 8.01 Hz, 4H, Ar), 8.45 (d, J = 8.1 Hz, 4H, Ar), 5.67 – 5.82 (m, 2H, NC**H**(COO)CH_3 and C**H**=CH_2), 4.87 – 4.97 (m, 4H, CH=C**H$_2$**), 4.2 (m, 4H, (COO)C**H$_2$)**, 1.91 – 1.98 (m, 4H, C**H$_2$**CH=CH_2), 1.76 (d, J = 7.03 Hz, 6H, NCH(COO)C**H$_3$**), 1.53 – 1.67 (m, 4H, (COO)CH_2C**H$_2$**), 1.16 – 1.3 (m, 24H, (COO)CH_2CH_2(C**H$_2$**)$_6$). ^{13}C NMR ($CDCl_3$, 75 MHz): δ (ppm) = 170.82 (ester C=O), 163.12 (imide C=O), 139.67 (H_2C=**C**H-), 135.13 (Ar), 132.16 (Ar), 129.90(Ar), 126.81 (Ar), 123.65 (Ar), 114.70 (H_2**C**=CH-), 66.24 ((COO)**C**H_2), 50.17(N**C**H(COO)CH_3), 34.33 (**C**H_2CH=CH_2), 30.00 (CH_2), 29.87 (CH_2), 29.70 (CH_2), 29.65 (CH_2), 29.40 (CH_2), 29.02 (CH_2), 26.45 (CH_2), 15.34 (NCH(COO)(**C**H_3)). FT-IR: 3077 (vinyl CH), 2925 (antisymmetric CH_2), 2854(symmetric CH_2), 1746 (ester C=O), 1700 (symmetric imide C=O symmetric), 1663 (antisymmetric imide C=O), 1594 (aromatic ring stretch). HRMS $(M+H)^+$: calcd for $C_{52}H_{59}N_2O_8$ 839.42714; found 839.42667.

Synthesis of *N, N'*-di((*S*)-2-(10-undecenoxyl)-1-(2-methylpropyl)-2-oxoethyl)-3,4:9,10-perylenetetracarboxyldiimide (ML-Leu11**)**

ML-Leu11 was prepared and purified using the same methodology as described for ML-Ala11, with PDI-Leu replacing PDI-Ala. Yield ML-Leu 0.838 g (90.8 %) as a

dark-red solid. ^{1}H NMR ($CDCl_3$, 600 MHz): δ (ppm) = 8.70 (d, J = 8.04 Hz, 4H, Ar), 8.63 (d, J = 8.1 Hz, 4H, Ar), 5.81 – 5.78 (m, 2H, NC**H** (COO)$CH_2CH(CH_3)_2$), 5.76 – 5.69 (m, 2H, C**H**=CH_2), 4.94 – 4.87 (m, 4H, CH=C**H$_2$**), 4.22 – 4.08 (m, 4H, (COO)C**H$_2$**), 2.29 – 2.12 (m, 4H, NCH(COO)C**H$_2$**$CH(CH_3)_2$), 1.91 – 1.95 (m, 4H, C**H$_2$**$CH=CH_2$), 1.64 – 1.57 (m, 6H, NCH(CH_2C**H**$(CH_3)_2$)(COO)CH_2C**H$_2$**$(CH_2)_7CH=CH_2$), 1.27 – 1.11 (m, 24H, (C**H$_2$**$)_6CH_2CH=CH_2$), 1.038 and 0.952 (d, d, J=6.6Hz, 12H, NCH(COO)CH_2CH(C**H$_3$**$)_2$). ^{13}C NMR ($CDCl_3$, 75 MHz): δ (ppm) = 170.88 (ester C=O), 163.68 (imide C=O), 139.66 (H_2C=**C**H-), 135.40 (Ar), 132.46 (Ar), 130.16 (Ar), 127.12 (Ar), 123.81 (Ar), 123.66 (Ar), 114.64 (H_2**C**=CH-), 66.18 (COO)**C**H_2CH_2), 52.98 (N**C**H(COO)$CH_2CH(CH_3)_2$), 38.64 (NCH(COO)**C**$H_2CH(CH_3)_2$), 34.29 (**C**$H_2CH=CH_2$), 29.98 (CH_2), 29.85 (CH_2), 29.67 (CH_2), 29.65 (CH_2), 29.40 (CH_2), 28.98 (CH_2), 26.44 (CH_2), 26.05 and 23.70 (NCH(COO)CH_2CH(**C**$H_3)_2$), 22.70 (NCH(COO)CH_2**C**$H(CH_3)_2$). FT-IR: 3077 (vinyl CH), 2927 (antisymmetric CH_2), 2855(symmetric CH_2), 1742 (ester C=O), 1702 (symmetric imide C=O symmetric), 1664 (antisymmetric imide C=O), 1594 (aromatic ring stretch). HRMS $(M+H)^+$: calcd for $C_{58}H_{71}N_2O_8$ 923.52104; found 923.52281.

Synthesis of PL-Ala11

100 mg ML-Ala11 and 1 mg Grubbs II catalyst were added into a tube containing 2 ml distilled 1, 2-dichlorobenzene. The mixture was stirred for 72 hours at 60 ^{o}C and continuously purged by N_2. 20 mL chloroform was then added to the reaction mixture. The solution and the solid residue were separated by centrifugation. The solid residue was extracted three times using 20 mL chloroform at 60 ℃. The chloroform solutions

were combined and the volume was reduced to 20 mL before 100 mL methanol was added to precipitate the product. The crude product PL-Ala11 was collected by centrifugation and dried in vacuum at 75 ℃. Grubbs II catalyst was removed by adding 1 ml CH_2Cl_2 solution containing 20 mg tris(hydroxymethyl)phosphine and 20 mg triethylamine into PL-Ala11 chloroform solution.[57] After stirring for 20 minutes, the solution was filtered through a short silica gel column. The solution volume was reduced to 20 ml by evaporation before 100 mL methanol was added. The precipitated polymer was collected and dried in vacuum oven at RT for 12 hours for further characterization. Yield PL-Ala11 64 mg (66 %) as a red solid. ^{1}H NMR (all peaks are broad) ($CDCl_3$, 300 MHz): δ (ppm) = 8.69 – 7.92 (8H, Ar), 5.76 (2H, NC**H**(COO)CH_3), 5.27 (2H, C**H**=C**H**), 4.24 (4H, (COO)C**H_2)**, 1.86 – 1.59 (14H, NCH(COO)(C**H_3**)CH_2C**H_2**$(CH_2)_6$C**H_2**CH=), 1.19 (24H, (COO)CH_2CH_2(C**H_2**$)_6$). FT-IR: 2926 (antisymmetric CH_2), 2853 (symmetric CH_2), 1745 (ester C=O), 1701 (symmetric imide C=O symmetric), 1663 (antisymmetric imide C=O), 1594 (aromatic ring stretch). Anal.: Calcd for $C_{50}H_{54}N_2O_8$: C, 74.05; H, 6.71; N, 3.45; O, 15.78. Found: C, 73.30; H, 6.61; N, 3.46.

Synthesis of PL-Leu11

ML-Leu11 and 1 mg Grubbs II catalyst were added into a tube containing 2 ml distilled 1, 2-dichlorobenzene. The mixture was stirred for 72 hours at 60 ^{o}C and continuously purged by N_2. After cooling the reaction mixture to RT, 10 mL chloroform was added to reaction mixture giving a homogenous solution. The crude product was

obtained by precipitating in excess methanol. The catalyst was removed by adding 1 ml CH_2Cl_2 solution containing 20 mg tris(hydroxymethyl)phosphine and 20 mg triethylamine into PL-Leu11 chloroform solution. After stirring for 20 minutes, the solution was filtered through a short silica gel column. The red solid product was recovered by precipitating in excess methanol. After drying in vacuum at RT for 12 hours, 46 mg (47 %) PL-Leu11 was obtained as a red solid. ^{1}H NMR ($CDCl_3$, 300 MHz): δ (ppm) = 8.47 – 8.27 (broad, 8H, Ar), 5.83-5.78 (2H, NC**H**(COO)$CH_2CH(CH_3)_2$), 5.26 (broad, 2H, C**H**=C**H**), 4.22 – 4.20 (m, 4H, (COO)C**H$_2$**), 2.32 – 2.10 (m, 4H, NCH(COO)C**H$_2$**$CH(CH_3)_2$), 1.85 (broad, 4H, C**H$_2$**$CH=CH_2$), 1.63 (broad, 6H, NCH(COO)(CH_2C**H**$(CH_3)_2$)CH_2C**H$_2$**$(CH_2)_7CH=$), 1.25 – 1.16 (broad, 24H, (C**H$_2$**)$_6CH_2CH=$), 1.041 and 0.966 (d, d, J = 6.6Hz, J = 6.3Hz, 12H, NCH(COO)CH_2CH(C**H$_3$**)$_2$). FT-IR: 2927 (antisymmetric CH_2), 2854 (symmetric CH_2), 1745 (ester C=O), 1701 (symmetric imide C=O symmetric), 1663 (antisymmetric imide C=O), 1594 (aromatic ring stretch). Anal.: Calcd for $C_{56}H_{66}N_2O_8$: C, 75.14; H, 7.43; N, 3.13; O, 14.30. Found: C, 74.30; H, 7.40; N, 3.07.

Fractionation of PL-Leu11

15 mL THF was added to a 3 ml $CHCl_3$ solution containing 16 mg PL-Leu11. The precipitate (PL-Leu11A, the high molecular weight part) was collected by suction filtration. The pink-red solution was evaporated to dryness affording PL-Leu11B (the low molecular weight part). Both components were dried in vacuum at RT for 12 hours. 12 mg PL-Leu11A and 4 mg PL-Leu11B were obtained.

CHAPTER 6. PERYLENE MONOANHYDRIDE DIESTER: A VERSATILE INTERMEDIATE FOR THE SYNTHESIS OF UNSYMMETRICALLY SUBSTITUTED PERYLENE TETRACARBOXYLIC DERIVATIVES

6.1. Introduction

Perylene tetracarboxylic acid-based dyes are under intense investigations due to their promising applications. In particular, *N*, *N'*-disubstituted perylene tetracarboxylic diimides (PDIs) have been widely used as lightfast colorants,[1] highly efficient fluorophores,[2] the electron acceptor in solar cells,[3] the active component in field effect transistors,[4] liquid crystalline materials[5] and versatile building block in self-assembly.[6] Structurally related tetraesters of perylene tetracarboxylic acid (PTEs) were also reported as liquid crystals,[7] fluorescent dyes,[2b] electron acceptor in light harvesting systems[8] and light emitting diodes.[9] Similar to PDIs, PTEs have appreciable electron-accepting power and are capable of forming perylene π-stacks in both solutions[10] and the solid state.[11] Recently, perylene tetracarboxylic diester monoimides (PEIs), where an imide and two ester groups connect to the same perylene core, have also attracted considerable attentions as more soluble alternative to PDIs.[12] Nevertheless, comparing to PDIs, the scope of applications of PTEs and PEIs are rather limited. Reports on PTEs are limited to symmetrically substituted tetraesters, whereas PEIs have been only explored in the form of simple alkyl derivatives very recently. In contrast, besides simple symmetrically substituted derivatives, PDIs have also been extensively incorporated into complex molecular and supramolecular architectures such as donor-acceptor dyads and

triads,[13] donor-bridge-acceptor molecules,[14] fluorescent sensors and light switches,[15] supramolecular assemblies[16] and PDI multichromophores,[17] as well as polymers as the side group.[18] This is probably because there are a number of methods by which unsymmetrically substituted PDIs can be readily accessed.[19] Contrarily, systematic synthetic strategies for PEIs have not been well-developed and there are no reports on unsymmetrically substituted PTEs. From materials science point of view, it is important to be able to integrate PTEs and PEIs into more structurally intricate systems as what has been realized with PDIs, especially those with light harvesting capabilities, considering the surging interest in organic photovoltaic materials. In order for a donor/acceptor organic photovoltaic system to achieve the optimal energy conversion efficiency, the electron affinity of the acceptor must be great enough to promote efficient exciton dissociation. On the other hand, an electron acceptor with an excessive electron affinity may lead to a deteriorated efficiency because of the reduced open-circuit voltage.[20] In other words, for a given electron donor, the best electron acceptor must have a matched electron affinity. PTEs are notably weaker electron-acceptors than PDIs, whereas the electron affinity of PEIs is between that of PDIs and PTEs. Thus, it is highly advantageous to have the ability to use PTEs or PEIs to replace the PDIs in those photovoltaic systems, as it provides a unique way to ***tune*** the electron accepting power the acceptor for the best possible conversion efficiency, in addition to the substantially improved solubility in common organic solvents. This calls for the capacity to access unsymmetrically substituted PTEs and PEIs. Here we report the design and synthesis of

perylene tetracarboxylic monoanhydride diester **1**. It can serve as a versatile intermediate for the synthesis of unsymmetric PTEs and PEIs, as well as PDIs.

6.2. Results and discussion

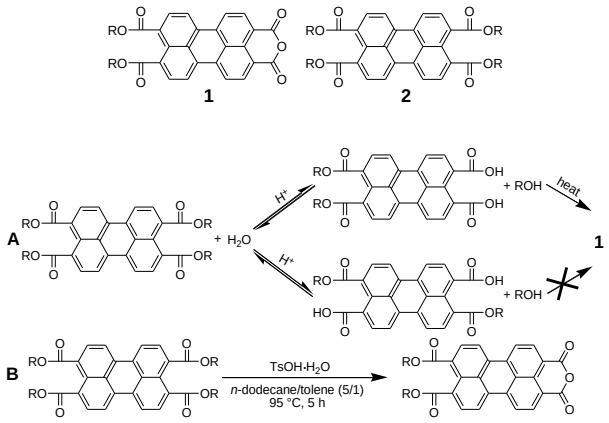

R = decyl

Scheme 6.1

1 is intrinsically unsymmetric. The reactivity difference between the anhydride and the ester group is great enough for a nucleophile to selectively attack the anhydride group. Two flexible decyl groups provide the necessary solubility in organic solvents, which facilitate purification and characterization.

It was envisioned that **1** could be prepared from a symmetrically tetrasubstituted PTE **2** via either basic or acidic hydrolysis. The acid-catalyzed route is chosen because of its potential high yield as depicted in **Scheme 6.1A**. First, an acid-catalyzed hydrolysis reaction is a reversible reaction. Therefore even the initial ester bond cleavages did not occur at "right" positions, they could be "corrected" through the esterification-hydrolysis equilibrium. Second, at a relative high temperature (typically > 90 ℃), once two carboxyl groups formed from a **2** molecule are at "correct" positions, a unimolecular cyclization reaction occurs rapidly forming a six-membered cyclic anhydride. This

removes the product out of the esterification-hydrolysis equilibrium and contributes to a high yield. To obtain the highest possible yield, the further hydrolysis of the ester groups in **1** must be avoided. One approach is to use a solvent that dissolves **2** very well but hardly dissolves **1** at the reaction temperature. In this way, **1** may tend to precipitate from the solution upon its formation, which slows down the further cleavage of the ester groups in **1**. It has been found that a mixture of *n*-dodecane and toluene (5/1 v/v) is well suitable for this purpose. Finally, reaction time must also be controlled to maximize the yield of **1**. The optimized reaction condition is given in **Scheme 6.1B**. A high concentration (~0.62 M) of **2** and 1 equivalent of p-toluenesulfonic acid monohydrate (TsOH H_2O, serving as the acid catalyst and the water source) react at 95 ℃ for 5 h gave **1** in a satisfactory (74%) isolated yield. **2** was prepared in an excellent yield (97%) according to a slightly modified literature procedure.[21]

The identity of **1** has been confirmed by ^{1}H NMR, FT-IR, HRMS and UV.[22] **1** dissolves in various common organic solvents such as chloroform, dichloromethane, toluene, acetone, THF and pyridine. Although its RT solubility in most solvents (except chloroform) is low (~ 10^{-4} M), the solubility increases substantially in warm or hot solvents. In molten imidazole, a widely used solvent for imidization reactions of perylene anhydrides, **1** dissolves considerably at 100 ℃ affording a bright red solution at about 10^{-2} M concentration. This implies that the condensation of **1** with primary amines will be smoother than that of perylene tetracarboxylic dianhydride which is insoluble in any organic solvents.

To demonstrate the applicability of **1** for the synthesis of unsymmetric PEIs, it

was condensed with four amines as shown in **Table 6.1**.[23] The desired PEIs were obtained at good to excellent yields, which confirms the suitability of **1** as a precursor of unsymmetric PEIs. It is worth mentioning that a large excess of amine is not necessary to achieve a high yield. This is practically important especially when the primary amine must be prepared by a multi-step synthesis. When a less reactive amine (entry 3) is used, the reaction can be significantly accelerated by adding 4-dimethyl-aminopyridine (DMAP) (Supplementary Material). The use of DMAP as the general acylation catalyst is well-documented. However, to the best of our knowledge, it has not been applied to the reactions involving perylene anhydrides. Probably this is because the low solubility of perylene tetracarboxylic dianhydride **Table 6.1** Condensation of **1** with amines

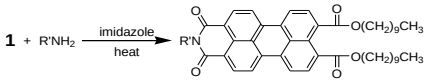

Table 6.1 R = decyl

Entry	R'NH_2	Reaction condition	Product (%Yield)
1	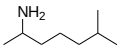	120 ℃ 3 h	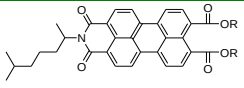 (**3a**, 99%)
2	Ammonium decanoate	120 ℃ 1 h	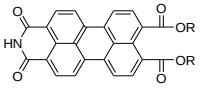 (**3b**, 88%)
3	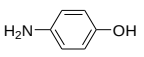	130 ℃ 3 h DMAP	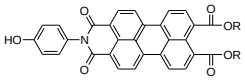 (**3c**, 85%)
4	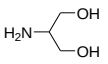	130 ℃ 1.5 h	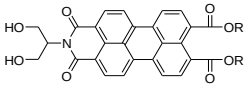 (**3d**, 79%)

was the major limiting factor for most of such reactions. For **1**, such a solubility limitation is lifted so that the nucleophilic attack to carbonyl may become the rate-limiting step which can be catalyzed by DMAP.

Another unique application of **1** is as the precursor of unsymmetric PTEs. The availability of **1** made it possible to synthesize the first unsymmetrically substituted PTE **4**,[24] as outlined in **Scheme 6.2**. The good overall yield (80%) signifies the effectivenessof **1** as the precursor of unsymmetric PTEs.

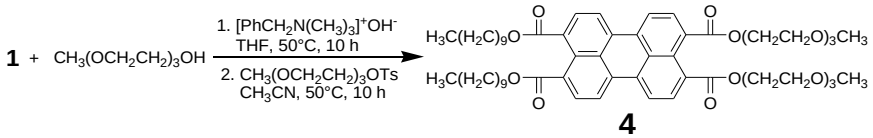

4

Scheme 6.2

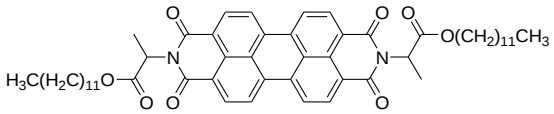

5

Finally, electron-accepting powers of different perylene tetracarboxylic acid derivatives were examined electrochemically. Their first reduction potential values were listed in **Table 6.2**. For the purpose of comparison, the first reduction potential of PDI **5**[5d] with the structure shown above was also measured. As the anhydride group is more electron withdrawing than the imide group, the electron affinity of **1** is greater than that of PEIs. The PTEs **2** and **4** are the least electron deficient materials due to four least electron withdrawing ester groups. As expected, six PEIs exhibit intermediate electron affinity between the PTEs and PDI **5**. It is quite interesting to observe that the

difference in first reduction potential values among PEIs is as great as 0.119 V. Evidently, the availability of unsymmetric PEIs and PTEs as PDI alternatives will allow one to tune the acceptor electron affinity of to a considerable degree, which may help minimize the energy loss during the electron transfer from the donor to the acceptor.

In conclusion, we have designed and successfully synthesized a soluble perylene tetracarboxylic monoanhydride diester. This compound can serve as the versatile intermediate for the synthesis of novel unsymmetrically substituted PTEs and PEIs which could be further converted to unsymmetric PDIs. The ability to access unsymmetric PEIs, PTEs and PDIs would enable molecular engineering of complex organic functional systems having the electron acceptor with tuneable electron affinity, which may lead to the optimum optoelectronic performance.

Table 6.2 The first reduction potentials of perylene tetracarboxylic derivatives vs. Fc/Fc^+

Compound	E_1 (V)	Compound	E_1 (V)
1	-1.162	**3a**	-1.311
2	-1.589	**3b**	-1.256
4	-1.568	**3c**	-1.255
5	-1.044	**3d**	-1.214
		3e	-1.333
		3f	-1.284

6.3. Experimental section

Synthesis of 1

In a Shrenk flask, 1.647 g (1.67 mmol) **2** was added to 0.45 ml toluene and 2.25 ml *n*-dodecane and heated to 95 ^oC. After the yellow powder **2** all dissolved, 316 mg

(1.67 mmol) TsOH H_2O was added to the solution. The reaction took 5 hours to form **1** at 95 ^oC before cooled down and dissolved in $CHCl_3$. The eluent in the column chromatography was 20/1 (v/v) $CHCl_3$/acetone. The yield of **1** was 0.852 g (74 %).

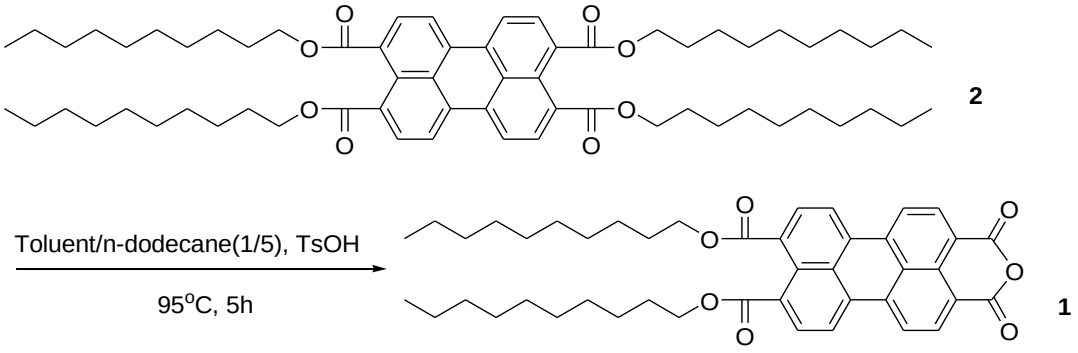

Synthesis of 3a

0.218 g (0.315 mmol) **1** and 60 mg (0.464 mmol) 1, 5-dimethylhexelamine was mixed with 1 g imidizole in a Shrenk flask. After N_2 was purged, the stirring began and the flask was heated to 120 ^oC and maintained for 3 hours. After the reaction, the mixture was cooled to 90 ^oC and water was poured to the flask to disperse the solid. The solid was collected by centrifuge and purified by column chromatography. The eluent was 25/1(v/v) $CHCl_3$/acetone. The yield of **3a** was 802 mg (99 %).

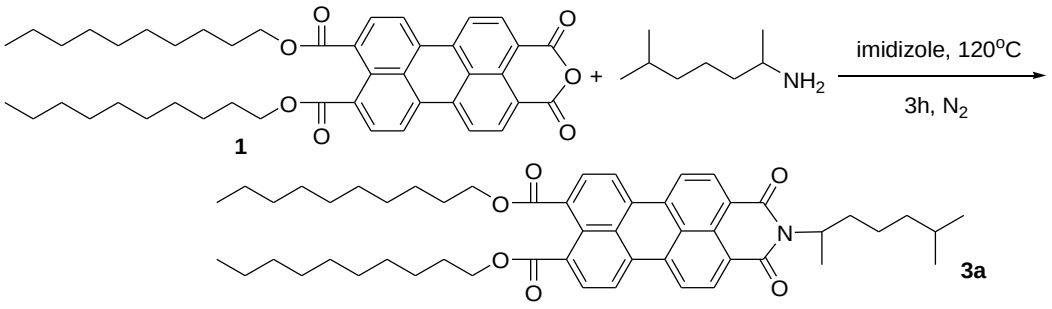

Synthesis of 3b

1.72 g decanoic acid and 1.46 g ammonium hydroxide was mixed in a 20 ml vial.

The vial was sealed and the mixture was shaken well until it became a transparent gel. The gel was dried upon vacuum at room temperature. 972 mg (1.41 mmol) **1** and 607 mg (3.24 mmol) *n*-decanoate amonium was added to a 20 ml vial with 8 g imidizole. The vial was sealed and heated to 120 ^{o}C for 1 hour. The solution was cooled to 90 ^{o}C and 15 ml deionized water was poured to the vial. The precipitate was collected by centrifuge and dried in vacuum at 75 ^{o}C over night. The eluent to purify the product **3b** in column chromatography was 50/3(v/v) $CHCl_3$/acetone $CHCl_3$. Yield was 0.859 g (88 %).

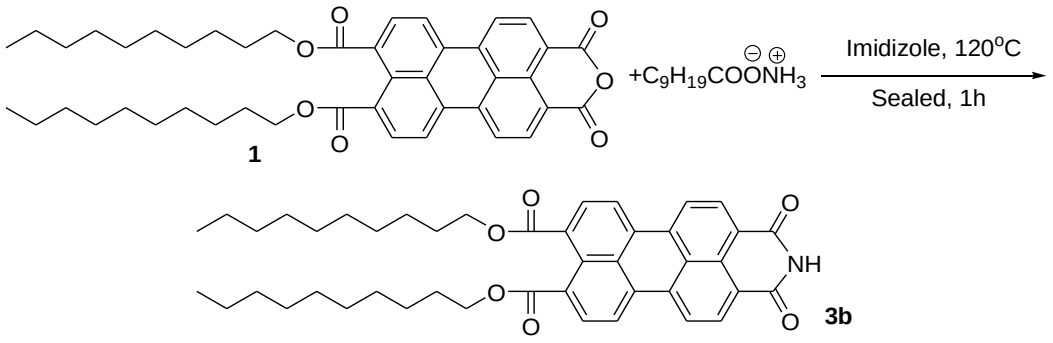

Synthesis of 3c

In a Shrenk flask, 264 mg (0.382 mmol) **1**, 54 mg (0.5 mmol) 4-aminophenol, 47 mg(0.382 mmol) DMAP and 2 g imidizole was mixed together and heated to 130 ^{o}C for 3 hours while on stirring. After the reaction, the mixture was cooled to 90 ^{o}C and water was poured to the flask to disperse the solid. The solid **3c** was collected by centrifuge and purified by column chromatography. The eluent was 50/1(v/v) $CHCl_3$/methanol. Yield was 253 mg (85 %).

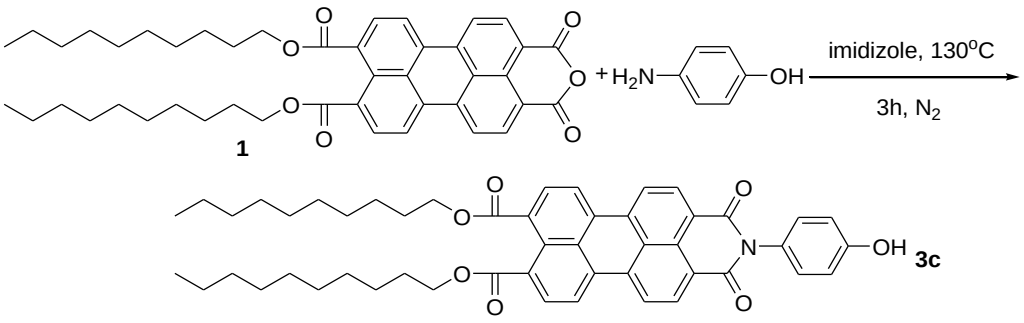

Synthesis of 3d

52 mg (0.57 mmol) 2-amino-1,3-propanediol and 303 mg (0.44 mmol) **1** was mixed well with 2 g imidizole in to a Shrenk flask before stirring and being heated to 130 ^{o}C. After the mixture was heated to solution, 16 mg (0.13 mmol) DMAP was introduced into the flask. The reaction lasted for 1.5 hours. Water was poured to the mixture after the reaction at 90 ^{o}C. The product **3d** was collected by centrifuging. The **3d** was purified by column chromatography, the eluent was 50/1 (v/v) $CHCl_3$/methanol. Yield & was 0.265 mg (79 %).

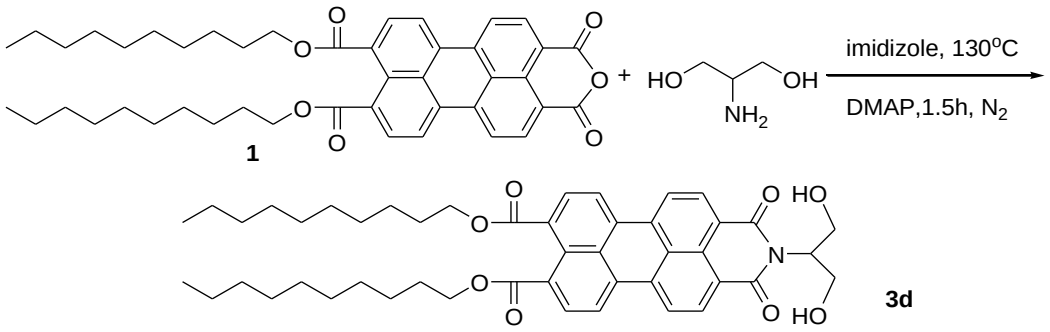

Synthesis of 4

The benzyltrimethylammonium hydroxide, 40 wt. % solution was dried before use. 50.4 mg (0.3 mmol) benzyltrimethylammonium hydroxide was mixed with 123 mg (0.75 mmol) triethylene glycol monomethyl ether in 5 ml THF, the solution was stirred for 10 minutes. 173 mg (0.25 mmol) **1** and was added to the solution and 123 mg (0.75 mmol)

triethylene glycol monomethyl ether was added afterwards. The solution was stirred for 20 hours at 50 ^{o}C. After the reaction, the mixture was dried by rotate evaporating and the product **4** was purified by column chromatography. The eluent was 100/1 (v/v) $CHCl_3$/methanol. Yield was 200 mg (80 %).

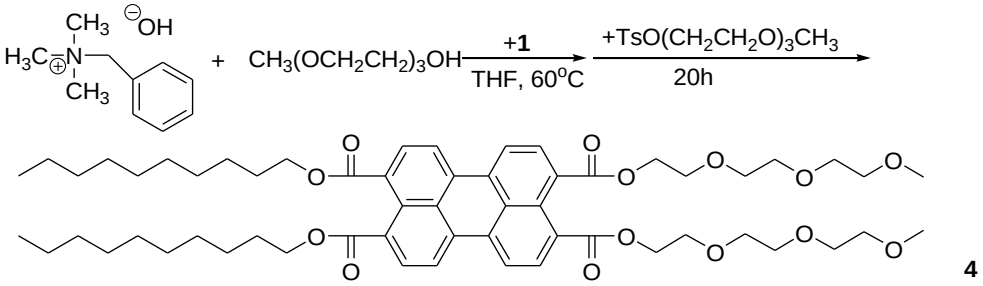

4

BIBLIOGRAPHY

CHAPTER 1

[1] Y. Shirota, H. Kageyama, *Chem. Rev.* **2007,** 107,953.

[2] Y. Shirota, *J. Mater. Chem.*, **2000**, 10, 1.

[3] Y. Shirota, *J. Mater. Chem.*, **2005**, 15, 75.

[4] (a) L. Schmidtmende, *Science* **2001**,293, 1119; (b) C. Im, W. Tian, H. Bassler, A. Fechtenkotter, M. Watson, K. Müllen, *Synth. Met.* **2003**, 139 (3), 683; (c) B. A. Gregg, *J. Phys. Chem.*, **1996**, 100 (2), 852. (d) B. A. Gregg , *J. Phys. Chem. B,* **2003**,107, 5688.

[5] (a) G. Horowitz, F. Kouki, P. Spearman, D. Fichou, C. Nogues, X. Pan, F. Garnier, *Adv. Mater.* **1996**, 8 (3), 242; (b) B. Jones, M. Ahrens, M. Yoon, A. Facchetti, T. Marks, M. Wasielewski, *Ang. Chem., Int. Ed.* **2004**, 43 (46), 6363; (c) R. J. Chesterfield, *J. Phys. Chem.B,* **2004**, 108, 19281.

[6] (a) R. Chesterfield, J. McKeen, C. Newman, P. Ewbank, D. da Silva, J. Bredas, L. Miller, K. Mann, C. Frisbie, *J. Phys. Chem. B* **2004**.108 (50), 19281; (b) C. R. Newman, *Chem. Mater.*,**2004**, 16, 4436; (c)B. Q. XU, *J. Am. Chem. Soc.*, **2005**, 127, 2386.

[7] (a) P. Ranke, *Appl. Phys. Lett.*,**1997**, 71, 1332. (b) T. Zukawa, *J. Appl. Phys.*, **2002**, 91, 1171.

[8] U. Rohr, *Ang. Chem., Int. Ed.* **1998**, 37, 1434.

[9] (a)H. Zollinger, *Color Chemistry*, 3rd edn., VCH, Weinheim, **2003**. (b) W. Herbst, K. Hunger, *Industrial Organic Pigments: Production,Properties, Applications*, 2nd edn., WILEY-VCH, Weinheim, **1997**.

[10] (a) M. P. O'Neil, M. P. Niemczyk, W. A. Svec, D. Gosztda, G. L. Gaines III, M. R. Wasielewski, *Science*, 1992, **257**, 63; (b) S. Prathapan, S. I. Yang, J. Seth, M. A. Miller, D. F. Bocian, D. Holten, J. S. Lindsey, *J. Phys. Chem. B.*, 2001, **105**, 8237; (c) J. M. Serin, D. W. Brousmiche and J. M. J. Frechet, *Chem. Commun.*, **2002**, 2605.

[11] (a)M. Sadrai, G. R. Bird, *Opt. Commun.*, 1984, **51**, 62; (b) H.-G. Löhmannsröben, H. Langhals, *Appl. Phys. B*, 1989, **48**, 449; (c) R. Reisfeld, G. Seybold, *Chimia*, 1990, **44**, 295; (d) W. E. Ford, P. V. Kamat, *J. Phys. Chem.*, 1987, **91**, 6373–6380; (e) G. Seybold, G. Wagenblast, *Dyes Pigm.*, 1989, **11**, 303; (f) G. Seybold, A. Stange (BASF AG), *Ger. Pat.*, DE 35 45 004, 1987 (*Chem. Abstr.*, 1988, **108**, 77134c); (g) R. Gvishi, R. Reisfeld, Z. Burshtein, *Chem. Phys. Lett.*, 1993, **213**, 338.

[12] S. Mais, J. Tittel, T. Basché, C. Bräuchle, W. Göhde, H. Fuchs, G. Müller, K. Müllen, *J. Phys. Chem. A*, 1997, **101**, 8435; H.Langhals, H. Jaschke, U. Ring and P. von Unold, *Angew. Chem., Int. Ed.*, **1999**, 38, 201.

[13] L. Zang, R. Liu, M. W. Holman, K. T. Nguyen, D. M. Adams, *J. Am.Chem. Soc.*, **2002**, 124, 10640.

[14] F. Würthner, *Chem. Commun.*, **2004**, 1564.

[15] X. Zhang, Z. Chen, F. Würthner, *J. Am. Chem. Soc.* **2007**, 129, 4886.

[16] F. Würthner, A. Sautter, D. Schmid, P. J. A. Weber, *Chem. Eur. J.*, **2001**, 7, 894; F. Würthner, A. Sautter, *Org. Biomol. Chem.*, **2003**, 1, 240; C.-C. You, F. Würthner, *J. Am. Chem. Soc.*, **2003**, 125, 9716.

[17] (a)G. Klebe, F. Graser, E. Hadicke, J. Berndt, *Acta Cryst.* **1989**. B45, 69-77; (b) E.

Hadicke, F. Graser, *Acta Cryst.* **1986**. C42, 189-195; (c) E. Hadicke, F. Graser, *Acta Cryst.* **1986**. C42, 195-198;(d) V. Marcon, W. Pisula, J. Dahl, D. W. Breiby, J. Kirkpatrick, S. Patwardhan, F. Grozema, D. Andrienko, *J. Am. Chem. Soc.* **2009**, 131,11426

[18] H. Langhals, *Heterocycles*, **1995**, 40, 477.

[19] (a) U. Rohr, P. Schlichting, A. Bohm, M. Gross, K. Meerholz, C. Brauchle, K. Mullen, *Angew. Chem., Int. Ed.* **1998**, 37, 1434; (b) H. Langhals, S. Demmig, H. Huber, *Spectrochim. Acta*, **1988**, 44A, 1189.

[20] G. Seybold, G. Wagenblast, *Dyes Pigm.*, **1989**, 11, 303; G. Seybold, A. Stange (BASF AG), *Ger. Pat.*, DE3545004, 1987 (*Chem. Abstr.*, **1988**, 108, 77134c).

[21] A. Stange, G. Wagenblast, G. Seybold, *BMFT-Bericht T 86*, Fachinformationszentrum Karlsruhe, Germany, **1986**.

[22] R. Iden, G. Seybold (BASF AG), *Ger. Pat. Appl.*, DE 3434059 A1, 1985 (*Chem. Abstr.*, **1985**, 103, 38696q).

[23] M. Sandrai, L. Hadel, R. R. Sauers, S. Husain, K. Krogh-Jespersen, J. D. Westbrook, G. R. Bird, *J. Phys. Chem.*, **1992**, 96, 7988.

[24] A. Böhm, H. Arms, G. Henning and P. Blaschka, (BASF AG), *Ger. Pat. Appl.*, DE 19547209 A1, 1997 (*Chem. Abstr.*, **1997**, 127, 96569g).

[25] M. J. Ahrens, M. J. Fuller, M. R. Wasielewski, *Chem. Mater.*, **2003**, 15, 2684.

[26] Y. Zhao, M. R. Wasielewski, *Tetrahedron Lett.*, **1999**, 40,7047; A. S. Lukas, Y. Zhao, S. E. Miller, M. R. Wasielewski, *J. Phys. Chem. B*, **2002**, 106, 1299.

[27] Hoechst AG (inv. E. Spietschka and M. Urban), ***D.O.S.*** 3208192 (March 6, 1982) (Chem. Abstr., **1983**, 99, 214170y).

[28] I. Lukic, H. Langhals, *Chem. Ber.*, **1983**, 116, 3524.

[29] BASF AG (Inv. F. Graser) ***D.O.S.*** 2139688 (Febr. 15, 1973), ***D.O.S.*** 2210170 (Sept. 6, **1973**) (Chem. Abstr., **1973**, 78**,** 137962v, Chem. Abstr., **1974**, 80**,** 49261h).

[30] A. Rademacher, S. Marklev, H. Langhals, *Chem. Ber.*, **1982**, 115, 2927.

[31] H. Langhals, *Chem.Ber.*, **1985**, 118, 4641.

[32] H. Langhals, ***D.O.S.*** 3703513 (Febr. 5, 1987) (*Chem. Abstr.*, **1988**, 109**,** P212376w).

[33] Y. Nagao, Y. Tanabe, T. Misono, N. Kaishi, **1979**, 528 (*Chem. Absrr.*, **1979**, 91, 38468a).

[34] H. Troster, Dyes Pigm., **1983**, 4, 171 (*Chem. Abstr.*, **1983**, 99, 39794f).

[35] (a) M. Sadrai, G. R. Bird, *Opt. Commun.*, **1984**, 51**,** 62; (b) H.-G. Ldmannsroben. H. Langhals, *Appl. Phys.*, **1989**, B48.449; (c) M. Sadrai, L. Hadel, R. R. Sauers, S. Husain, K. Krogh-Jespersen, J. D. Westbrook, G. R. Bird, *J. Phys. Chem.*, **1992**, 96, 7988.

[36] (a)H. Langhals, S. Demmig and H. Huber, *Spectrochim. Acta*, **1988**, 44A, 1189–1193; (b) S. Icli, H. Icil, *Spectrosc.* Lett. **1996**, 29, 1253; **1994**, 27, 323; (c) F. Graser, E. Hädicke, *Liebigs Ann. Chem.* **1980**, 1994; (d) M. Sadrai, G. R. Bird, *Opt. Commun*. **1984**, 51, 62; (e) A. Rademacher, S. Märkle, H. Langhals, *Chem. Ber.*

1982, 115, 2927; (f) B. A. Gregg, J. Sprague, M. W. Peterson, *J. Phys. Chem. B,* **1997**, 101, 5362.

[37] H. Langhals, S. Demmig and T. Potrawa, *J. Prakt. Chem.*, **1991**, 333, 733.

[38] G. Seybold, G. Wagenblast, *Dyes Pigm.*, **1989**, 11, 303; G. Seybold, A. Stange (BASF AG), *Ger. Pat.*, DE 3545004, 1987 (*Chem. Abstr.*, **1988**, 108, 77134c).

[39] H. Langhals, J. Karolin, L. B.-A. Johansson, *J. Chem. Soc., Faraday Trans.*, **1998**, 94, 2919.

[40] M. P. O'Neil, M. P. Niemczyk, W. A. Svec, D. Gosztda, G. L. Gaines III, M. R. Wasielewski, *Science*, **1992**, 257, 63.

[41] S. Prathapan, S. I. Yang, J. Seth, M. A. Miller, D. F. Bocian, D. Holten, J. S. Lindsey, *J. Phys. Chem. B.*, **2001**, 105, 8237.

[42] F. Graser, E. Hädicke, *Liebigs Ann. Chem.*, **1980**, 1994; F. Graser and E. Hädicke, *Liebigs Ann. Chem.*, **1984**, 483; E. Hädicke, F. Graser, *Acta Crystallogr., Sect. C*, **1986**, 42, 189; E. Hädicke, F. Graser, *Acta Crystallogr., Sect. C*, **1986**, 42, 195; G. Klebe, F. Graser, E. Hädicke, J. Berndt, *Acta Crystallogr., Sect. B*, **1989**, 45, 69.

[43] P. Zugenmaier, J. Duff, T. L. Bluhm, *Cryst. Res. Technol.*, **2000**, 35, 1095.

[44] Z. Chen, M. G. Debije, T. Debaerdemaeker, P. Osswald, F. Würthner, *ChemPhysChem*, **2004**, 5, 137.

[45] F. Würthner, A. Sautter, J. Schilling, *J. Org. Chem.*, **2002**, 67, 3037.

[46] G. Seybold, G. Wagenblast, *Dyes Pigm.*, **1989**, 11, 303; G. Seybold, A. Stange (BASF AG), *Ger. Pat.*, DE 3545004, 1987 (*Chem. Abstr.*, **1988**, 108, 77134c).

[47] C. W. Struijk, A. B. Sieval, J. E. J. Dakhorst, M. van Dijk, P. Kimkes, R. B. M. Koehorst, H. Donker, T. J. Schaafsma, S. J. Picken, A. M. van de Craats, J. M. Warman, H. Zuilhof, E. J. R. Sudhölter, *J. Am. Chem. Soc.* **2000**, 122, 11057.

[48] P. M. Kazmaier, R. Hoffmann, *J. Am. Chem. Soc.*, 1994, **116**, 9684.

[49] H.-M. Zhao, J. Pfister, V. Settels, M. Renz, M. Kaupp, V. C. Dehm, F. Würthner, R. F. Fink, B. Engels, *J. Am. Chem. Soc*. **2009**, 131, 15660.

[50] (a) J. Mizuguchi, *J. Appl. Phys*. **1998**, 84, 4479; (b) T. E. Kaiser, H. Wang, V. Stepanenko, F. Würthner, *Angew. Chem.* **2007**, 119, 5637; (c) T. E. Kaiser, H. Wang, V. Stepanenko, F. Würthner, *Angew. Chem. Int. Ed.* **2007**, 46, 5541; (d) S. Yagai, T. Seki, T. Karatsu, A. Kitamura, F. Würthner, *Angew. Chem. Int. Ed*. **2008**, 47, 3367. [51] F. Würthner, C. Thalacker, S. Diele, C. Tschierske, *Chem. Eur. J.*, **2001**, **7**, 2245; F. Würthner, C. Thalacker (BASF AG), *Ger. Pat. Appl.*, DE 10039232 A1, 2000 (*Chem. Abstr.*, **2002**, 136, 185323).

[52] W. Wang, L.-S. Li, G. Helms, H.-H. Zhou, A. D. Q. Li, *J. Am. Chem. Soc.*, **2003**, 125, 1120; A. D. Q. Li, W. Wang, L.-Q. Wang, *Chem. Eur. J.*, **2003**, 9, 4594.

[53] R. A. Cormier, B. A. Gregg, *J. Phys. Chem. B*, **1997**, 101, 11004; R. A. Cormier, B. A. Gregg, *Chem. Mater.*, **1998**, 10, 1309.

[54] U. Rohr, P. Schlichting, A. Böhm, M. Groß, K. Meerholz, C. Bräuchle, K. Müllen, *Angew. Chem., Int. Ed.*, **1998**, 37, 1434; U. Rohr, C. Kohl, K. Müllen, A. van de Craats, J. Warman, *J. Mater. Chem.*, **2001**, 11, 1789.

[55] T. Hassheider, S. A. Benning, H.-S. Kitzerow, M.-F. Achard, H. Bock, *Angew.*

Chem., Int. Ed., **2001**, 40, 2060.

[56] S. Benning, H.-S. Kitzerow, H. Bock, M.-F. Achard, *Liq. Cryst.*, **2000**, 27, 901.

[57] S. Alibert-Fouet, S. Dardel, H. Bock, M. Oukachmih, S. Archambeau, I. Seguy, P. Jolinat, P. Destruel, *ChemPhysChem*, **2003**, 4, 983.

[58] F. Würthner, C. Thalacker, S. Diele, C. Tschierske, *Chem. Eur. J.*, **2001**, 7, 2245; F. Würthner, C. Thalacker (BASF AG), *Ger. Pat. Appl.*, DE 10039232 A1, 2000 (*Chem. Abstr.*, **2002**, 136, 185323).

[59] S. Alibert-Fouet, S. Dardel, H. Bock, M. Oukachmih, S. Archambeau, I. Seguy, P. Jolinat, P. Destruel, *ChemPhysChem*, **2003**, 4, 983.

[60] B. A. Gregg, J. Sprague, M. W. Peterson, *J. Phys. Chem. B*, 1997, **101**, 5362.

[61] P. Ehrenfest, *Proc. Acad. Sci., Amsterdam*, 1933; 36,153; Suppl. 75b, Mitt. Kammerlingh Onnes Inst. Leiden.

[62] Friedel, G. *Ann. Physique* **1922**, *18*,273.

[63] P. Mariani, F. Rustichelli, G. Torquati, *In physics of Liquid Crystalline Materials*; Khoo, I.C., Simoni, F., Eds.; Gordon and Breach Science: Philadelphia, **1988.**

[64] P. S. Pershan, *Structure of Liquid Crystal Phase*; Wold Scientific: Singapore, **1988.**

[65] G. S. Smith, E. B. Sirota, C. R. Safinya, R. J. Plano, N. A. Clark, *J. Chem. Phys.* **1990**, 92, 4519.

CHAPTER 2

[1] (a) S. Yoshikawa, Y. Kotani, Y. Shirota, *69th Annual Meeting of the Chemical Society of Japan, Kyoto*, **1995**, prepr. no.2, p. 641; (b)Y. Shirota, K. Moriwaki, S.

Yoshikawa, T. Ujike, H. Nakano, *J. Mater. Chem*., **1998**, 8, 2579.

[2] P. Rochon, E. Batalla, A. Natansohn, *Appl. Phys. Lett.*, **1995**, 66, 136.

[3] D. Y. Kim, S. K. Tripathy, L. Li, J. Kumar, *Appl. Phys. Lett.*, **1995**, 66, 1166.

[4]C. J. Barrett, A. L. Natansohn, P. L. Rochon, *J. Phys. Chem.*, **1996**, 100, 8836.

[5] J. Kumar, L. Li, X. Jiang, D.Y. Kim, T. S. Lee, S. Tripathy, *Appl. Phys. Lett.*, **1998**, 72, 2096.

[6] N. K. Viswanathan, D. Y. Kim, S. Bian, J. Williams, W. Liu, L. Li, L. Samuelson, J. Kumar, S. K. Tripathy, *J. Mater. Chem.*, **1999**, 9, 1941.

[7] L. Andruzzi, A. Altomare, F. Ciardelli, R. Solaro, S. Hvilsted, P. S. Ramanujam, *Macromolecules*, **1999**, 32, 448.

[8] P. Lefin, C. Fiorini, J.M. Nunzi, *Pure Appl. Opt.*, **1998**, 7, 71.

[9] C. Fiorini, N. Prudhomme, G. de Veyrac, I. Maurin, P. Raimond, J.M. Nunzi, *Synth. Met.*, **2000**, 115, 121.

[10] T. Ubukata, T. Seki, K. Ichimura, *Adv. Mater.*, **2000**, 12, 1675.

[11] H. Utsumi, D. Nagahama, H. Nakano, Y. Shirota, *J. Mater. Chem.*, **2002**, 12, 2612.

[12] T. Tsujioka, Y. Hamada, K. Shibata, A. Taniguchi, T. Fuyuki, *Appl. Phys. Lett.*, **2001**, 78, 2282.

[13] T. Tsujioka, H. Kondo, *Appl. Phys. Lett.*, **2003**, 83, 937.

[14] M. Yoshiiwa, H. Kageyama, Y. Shirota, F. Wakaya, K. Gamo, M. Takai, *Appl. Phys. Lett*., **1996**, 69, 2605.

[15] T. Kadota, H. Kageyama, F. Wakaya, K. Gomo, Y. Shirota, *J. Photopolym. Sci.*

Technol., **1999**, 12, 375.

[16] T. Kadota, H. Kageyama, F. Wakaya, K. Gamo, Y. Shirota, *J. Photopolym. Sci. Technol.*, **2000**, 13, 203.

[17] T. Kadota, M. Yoshiiwa, H. Kageyama, F. Wakaya, K. Gamo, Y. Shirota, *Proc. SPIE-Int. Soc. Opt. Eng.*, **2001**, 4345, 891.

[18] T. Kadota, H. Kageyama, F. Wakaya, K. Gamo, Y. Shirota, *Mater. Sci. Eng. C*, **2001**, 16, 91.

[19] T. Kadota, H. Kageyama, F. Wakaya, K. Gamo, Y. Shirota, *Chem. Lett.*, **2004**, 33, 706.

[20]C. W. Tang, S. A. VanSlyke, *Appl. Phys. Lett.*, **1987**, 51, 913.

[21] J. H. Burroughes, D. D. C. Bradley, A. R. Brown, R. N. Marks, K. Mackay, R. H. Friend, P. L. Burns, A. B. Holmes, *Nature*, **1990**, 347, 539.

[22] A. Kraft, A. C. Grimsdale, A. B. Holmes, *Angew. Chem., Int. Ed.*, **1998**, 37, 402.

[23] R. H. Friend, R. W. Gymer, A. B. Holmes, J. H. Burroughes, R. N. Marks, C. Taliani, D. D. C. Bradley, D. A. Dos Santos, J. L. Bredas, M. Logdlund, W. R. Salaneck, *Nature*, **1999**, 397, 121.

[24] U. Mitshke and P. Bäuerle, *J. Mater. Chem.*, **2000**, 10, 1471.

[25] P. Peumans, V. Bulovic, S. R. Forrest, *Appl. Phys. Lett.*, **2000**, 76, 2650.

[26] M. K. Nazeeruddin, A. Kay, I. Rodicio, R. Humphry-Baker, E. Muller, P. Liska, N. Vlachopoulos, M. Grätzel, *J. Am. Chem. Soc.*, **1993**, 115, 6382.

[27] J. Hagen, W. Schaffrath, P. Otschik, R. Fink, A. Bacher, H.W. Schmidt, D. Haarer,

Synth. Met., **1997**, 89, 215.

[28] U. Bach, D. Lupo, P. Comte, J. E. Moser, F. Ewissortel, J. Salbeck, H. Spreitzer, M. Grätzel, *Nature*, **1998**, 395, 583.

[29] P. M. Lundquist, R. Wortmann, C. Geletneky, R. J. Twieg, M. Jurich, V. Y. Lee, C. R. Moylan, D. M. Burland, *Science*, **1996**, 274, 1182.

[30] L. Wang, Y. Zhang, T. Wada, H. Sasabe, *Appl. Phys. Lett.*, **1996**, 69, 728.

[31] C. Hohle, U. Hofmann, S. Schloter, M. Thelakkat, P. Strohriegl, D. Haarer, S. J. Zilker, *J. Mater. Chem.*, **1999**, 9, 2205.

[32] F. Würthner, R. Wortmann, K. Meerholz, *ChemPhysChem*, **2002**, 3, 17.

[33] Yasuhiko Shirota, *J. Mater. Chem.*, **2005**, 15, 75.

[34] H. Zollinger, *Color Chemistry*, 3rd edn., VCH, Weinheim, **2003**.

[35] W. Herbst, K. Hunger, *Industrial Organic Pigments: Production, Properties, Applications*, 2nd edn., WILEY-VCH, Weinheim, **1997**.

[36] L. Schmidt-mende, *Science* **2001,** 293, 1119.

[37] C. Im, W. Tian, H. Bassler, A. Fechtenkotter, M. Watson, K. Müllen, *Synth. Met.* **2003**, 139(3), 683.

[38] B. A. Gregg, *J. Phys. Chem.*, **1996,**100, 852.

[39] B. A. Gregg, *J. Phys. Chem.B,* **2003,**107, 5688.

[40]Horowitz, G.; Kouki, F.; Spearman, P.; Fichou, D.; Nogues, C.; Pan, X.; Garnier, F. *Adv. Mater.* **1996**, 8(3), 242.

[41] Jones, B.; Ahrens, M.; Yoon, M.; Facchetti, A.; Marks, T.; Wasielewski, M. *Ang.*

Chem., Int. Ed. **2004**, 43 (46), 6363.

[42] R. J. Chesterfield, *J. Phys. Chem.B,* **2004**, 108, 19281.

[43] R. J. Chesterfield, J. C. McKeen, C. R. Newman, P. C. Ewbank, D. Filho, J. L. Bredas, L. L. Miller, K. R. Mann, C. D. Frisbie, *J. Phys. Chem. B,* **2004**, 108, 19281.

[44] *C. R. Newman,* C. D. Frisbie, J. L. Bedras, P. C. Ewbank, K. R. Mann, *Chem. Mater.*, **2004**, 16, 4436.

[45] B. Q. Xu, X. Y. Xiao, X. M. Yang, L. Zang, N. J. Tao, *J. Am. Chem. Soc,* **2005**, 127, 2386.

[46] P. Ranke, I. Bleyl, J. Simmerer, D. Haarer, A. Bacher, H. W. Schmidt, *Appl. Phys. Lett.* **1997, 71**, 1332.

[47] T. Zukawa, S. Naka, H. Okada, H. Onnagawa, *J. Appl. Phys*., **2002**, **91**, 1171.

[48] F. Würthner, C. Thalacker, S. Diele, C. Tschierske, *Chem. Eur. J.*, **2001**, 7, 2245.

[49] Z. An, J. Yu, S. C. Jones, S. Barlow, S. Yoo, B. Domercq, P. Prins, L. D. A. Siebbeles, B. Kippelen, S. R. Marder, *Adv. Mater.*, **2005**, 17, 2580, and its Supporting Information.

[50] Y. Zakrevskyy, C. F. J. Faul, Y. Guan, J. Stumpe, *Adv. Funct. Mater*. **2004**, 14, 835.

[51] F. Würthner, Z. Chen, V. Dehm, V. Stephanenko, *Chem. Commun.* **2006**, 1188.

[52] J. van Herrikhuyzen, A. Syamakumari, A. P. H. H. Schenning, E. W. Meijer, *J. Am. Chem. Soc.*, **2004**, 126, 10021.

[53] R. A. Cormier, B.A. Gregg, *J. Phys. Chem. B*, **1997**, 101, 11004.

[54] R. A. Cormier, B.A. Gregg, *Chem. Mater.* **1998**, 10, 1309.

[55] C. W. Struijk, A. B. Sieval, J. E. J. Dakhorst, M. van Dijk, P. Kimkes, R. B. M. Koehorst, H. Donker, T. J. Schaafsma, S. J. Picken, A. M. van de Craats, J. M. Warman, H. Zuilhof, E. J. R. Sudhölter, *J. Am.Chem. Soc.* **2000**, *122*, 11057. see the Supporting Information.

[56] An, Z.; Yu, J.; Jones, S. C.; Barlow, S.; Yoo, S.; Domercq, B.; Prins,P.; Siebbeles, L. D. A.; Kippelen, B.; Marder, S. R. *Adv. Mater.* **2005**, 17, 2580.

[57] A. Wicklein, A. Lang, M. Muth, M. Thelakkat, *J. Am. Chem. Soc.* **2009**, 131, 14442.

[58] J. Mizuguchi, *J. Appl. Phys.***1998**, 84, 4479.

[59] D. Volpati, A. E. Job, R. F. Aroca,C. J. Constantino, *J. Phys. Chem. B*, **2008**, 112, 3894.

[60] S. Vajiravelu, L. Ramunas, G. J. Vidas, G. Valentas, J. Vygintas, S. Valiyaveettil, *J. Mater. Chem.*, **2009**, **19**, 4268.

[61] H. Graaf, W. Michaelis, G. Schnurpfeil, N. Jaeger, D. Schlettwein, *Organic Electronics*, **2004**, 5, 237.

[62] J. F. Pan, W. H. Zhu, S. F. Li, J. Xu, H. Tian, *J. Org. Chem.*, **2006**, 986.

[63] V.Sivalmurugan, K.Kazlauskas, S.Jursenas, A.Gruodis, J.Simokaitiene, Grazulevicius, J. V. Valiyaveettil, S. *J. Phys. Chem. B*, **2010,** *114*, 1782.

[64] D. Liu, H. C. Ren, J. Y. Li, Q. Tao, Z. X. Gao, *Chem. Phys. Lett.* **2009**, 482, 72.

[65] P. Posch, M. Thelakkat, H. W. Schmidt, *Synthetic Metals*, **1999**, 1110.

[66] G. Klebe, F. Graser, E. Hädicke, J. Berndt, *Acta Cryst*. **1989**. B45, 69.

[67] E. Hädicke, F. Graser, *Acta Cryst*. **1986**. C42, 189.

[68] E. Hädicke, F. Graser, *Acta Cryst*. **1986**. C42, 195.

[69] V. Marcon, W. Pisula, J. Dahl, D. W. Breiby, J. Kirkpatrick, S. Patwardhan, F. Grozema, D. Andrienko, *J. Am. Chem. Soc*. **2009**, 131,11426.

[70] Y. Xu, S. Leng, C. Xue, R. Sun, J. Pan, J. Ford, S. Jin, *Ang. Chem., Int. Ed.*, **2007**,46, 3896.

[71] F. Würthner, *Chem. Commun.*, **2004**, 1564 and its references.

[72] A. D. Q. Li, W. Wang, L. Q. Wang, *Chem. Eur. J*. **2003**, 9, 4594.

[73] Refer to Chapter 4

[74] F. Graser, E. Hädicke, *Liebigs Ann. Chem.* **1980**, 1994.

CHAPTER 3

[1] (a) L. Schmidtmende, *Science* **2001**,293, 1119; (b) C. Im, W. Tian, H. Bassler, A. Fechtenkotter, M. Watson, K. Müllen, *Synth. Met.* **2003**, 139 (3), 683; (c) B. A. Gregg, *J. Phys. Chem.*, **1996**, 100 (2), 852. (d) B. A. Gregg , *J. Phys. Chem. B,* **2003**,107, 5688.

[2] (a) G. Horowitz, F. Kouki, P. Spearman, D. Fichou, C. Nogues, X. Pan, F. Garnier, *Adv. Mater*. **1996**, 8 (3), 242; (b) B. Jones, M. Ahrens, M. Yoon, A. Facchetti, T. Marks, M. Wasielewski, *Ang. Chem., Int. Ed.* **2004**, 43 (46), 6363; (c) R. J. Chesterfield, *J. Phys. Chem.B,* **2004**, 108, 19281.

[3] (a) R. Chesterfield, J. McKeen, C. Newman, P. Ewbank, D. da Silva, J. Bredas, L.

Miller, K. Mann, C. Frisbie, *J. Phys. Chem. B* **2004**.108 (50), 19281; (b) C. R. Newman, *Chem. Mater.*,**2004**, 16, 4436; (c)B. Q. XU, *J. Am. Chem. Soc.*, **2005**, 127, 2386.

[4] (a) P. Ranke, *Appl. Phys. Lett.*,**1997**, 71, 1332. (b) T. Zukawa, *J. Appl. Phys.*, **2002**, 91, 1171.

[5] U. Rohr, *Ang. Chem., Int. Ed.* **1998**, 37, 1434.

[6] F. Würthner, *Chem. Commun.* **2004**, 1564.

[7] (a)A. S. Lukas, Y. Zhao, S. E. Miller, M. R. Wasielewski, *J. Phys. Chem. B* **2002**, *106*, 1299; (b)M. J. Ahrens, M. J. Fuller, M. R. Wasielewski *Chem. Mater.* **2003,** *15*, 2684.

[8] X. Zhang, Z. Chen,; F. Würthner, *J. Am. Chem. Soc.* **2007**, *129*, 4886.

[9] F. Würthner, A. Sautter, D. Schmid, P. J. A. Weber, *Chem. Eur. J.*, **2001**, 7, 894; F. Würthner, A. Sautter, *Org. Biomol. Chem.*, **2003**, 1, 240; C.-C. You, F. Würthner, *J. Am. Chem. Soc.*, **2003**, 125, 9716.

[10] (a)G. Klebe, F. Graser, E. Hadicke, J. Berndt, *Acta Cryst.* **1989**. B45, 69-77; (b) E. Hadicke, F. Graser, *Acta Cryst.* **1986**. C42, 189-195; (c) E. Hadicke, F. Graser, *Acta Cryst.* **1986**. C42, 195-198;(d) V. Marcon, W. Pisula, J. Dahl, D. W. Breiby, J. Kirkpatrick, S. Patwardhan, F. Grozema, D. Andrienko, *J. Am. Chem. Soc.* **2009**, 131,11426

[11] F. Würthner, V. Stepanenko, Z. Chen, C. R. Saha-Möller, N. Kocher, D. Stalke, *J. Org. Chem.* **2004**, *69*, 7933-7939; F. Wurthner, P. Osswald, R. Schmidt, T. E.

Kaiser, H. Mansikkamaki, M. Kolnemann, *Org. Lett.*, **2006**, 8, 3765.

[12] R. A. Cormier, B. A. Gregg, *J. Phys. Chem. B* **1997**, *101*, 11004.

B. Jancy, S. K. Asha *J. Phys. Chem. B* **2006**, *110*, 20937; A. Wicklein, A. Lang, M. Muth, M. Thelakkat, *J. Am. Chem. Soc*. **2009**, *131*, 14442.

[13] F. Würthner, Z. Chen, F. J. M. Hoeben, P. Osswald, C.-C. You, P. Jonkheijm, J. v. Herrikhuyzen, A. P Schenning, P. A. M. van der Schoot, E. W. Meijer, E. H. A. Beckers, S. C. J. Meskers, R. A. J. Janssen *J. Am. Chem. Soc*. **2004**, 126, 10611; M. R. ASIELEWSKI , Accounts of Chemical Research, **2009**, 42, 1910.

[14] a) F. Würthner, C. Thalacker, S. Diele, C. Tschierske, *Chem. Eur. J.* **2001**, 7, 2245; b) Z. An, J. Yu, S. C. Jones, S. Barlow, S. Yoo, B. Domercq, P. Prins, L. D. A. Siebbeles, B. Kippelen, S. R. Marder, *Adv. Mater.* **2005**, 17, 2580, and its Supporting Information; c) Y. Zakrevskyy, C. F. J. Faul, Y. Guan, J. Stumpe, *Adv. Funct. Mater.* **2004**, 14, 835; d) F. Würthner, Z. Chen, V. Dehm, V. Stephanenko, *Chem. Commun.* **2006**, 1188; e) J. van Herrikhuyzen, A. Syamakumari, A. P. H. H. Schenning, E. W. Meijer, *J. Am. Chem. Soc.* **2004**, 126, 10021.

[15] a) R. A. Cormier, B.A. Gregg, *J. Phys. Chem. B* **1997**, 101, 11004; b) R. A. Cormier, B.A. Gregg, *Chem. Mater.* **1998**, 10, 1309.

[16] C.W. Struijk, et al., *J. Am. Chem. Soc.* **2000**, 122, 11057; see the Supporting Information.

[17] Z. An, J. Yu, S. C. Jones, S. Barlow, S. Yoo, B. Domercq, P. Prins, L. D. A. Siebbeles, B. Kippelen, S. R. Marder, *Adv. Mater.* **2005**, 17, 2580; A. Wicklein, A.

Lang, M. Muth, M. Thelakkat *J. Am. Chem. Soc.* **2009**, *131*, 14442.

[18] A. M. van de Craats, J. M. Warman, A. FechtenkRtter, J. D. Brand, M. A. Harbison, K. MPllen, *Adv. Mater*. **1999**, 11, 1469.

[19] P.G. de Gennes, J. Prost, "The Physics of Liquid Crystals." Oxford University Press, Oxford, **1995**.

[20] E. Fontes, P. A. Heiney, W. H. de Jeu, *Phys. Rev. Lett.* **1988**, 61, 1202.a

[21] A. Mori, M. Yokoo, M. Hashimoto, S. Ujiie, S. Diele, U. Baumeister, C. Tschierske, *J. Am. Chem. Soc.* **2003**, 125, 6620.

[22] Y. Xu, S. Leng, C. Xue, R. Sun, J. Pan, J. Ford, S. Jin, **2007**, 46, 3896.

[23] N.V. Venkataraman, S. Vasudevan, *J.Phys.Chem.B* **2001**,105, 1805, and references therein.

[24] S. P. Srivastava, T. Butz, H. -J. Oschmann, I. Rahimian, *PETROLEUM SCIENCE AND TECHNOLOGY*, **2000**, 18(5&6),493.

CHAPTER 4

[1] H. Zollinger, *Color Chemistry*, 3rd edn., VCH, Weinheim, 2003.

[2] W. Herbst and K. Hunger, *Industrial Organic Pigments: Production, Properties, Applications*, 2nd edn., WILEY-VCH, Weinheim, 1997.

[3]F. Graser, E. Hädicke, *Liebigs Ann. Chem.*, **1980**, 1994.

[4] F. Graser and E. Hädicke, *Liebigs Ann. Chem.*, **1984**, 483.

[5] E. Hädicke, F. Graser, *Acta Crystallogr., Sect. C*, **1986**, 42, 189.

[6]E. Hädicke, F. Graser, *Acta Crystallogr., Sect. C*, **1986**, 42, 195.

[7] G. Klebe, F. Graser, E. Hädicke, J. Berndt, *Acta Crystallogr., Sect. B*, **1989**, 45, 69.

[8] F. Würthner, *Chem. Commun.,* **2004**, 1564 and the references there in.

[9] P. M. Kazmaier, R. Hoffmann, *J. Am. Chem. Soc.*, 1994, **116**, 9684.

[10] J. Vura-Weis, M. A. Ratner, M. R. Wasielewski, *J. Am. Chem. Soc.* **2010**, *132*, 1738.

[11] P. M. Kazmaier, R. Hoffmann, *J. Am. Chem. Soc.*, 1994, **116**, 9684.

[12] B. A. Gregg, J. Sprague, M. W. Peterson, *J. Phys. Chem. B*, 1997, **101**, 5362.

[13] H.-M. Zhao, J. Pfister, V. Settels, M. Renz, M. Kaupp, V. C. Dehm, F. Würthner, R. F. Fink, B. Engels, *J. Am. Chem. Soc*. **2009**, 131, 15660..

CHAPTER 5

[1]H. Langhals, *Heterocycles* **1995**, 40(1), 477.

[2]H. Langhals, W. Jona, F. Einsiedl, S. Wohnlich, *Adv Mater* **1998**, 10(13),1022.

[3]R. Samudrala, X. Zhang, R. M. Wadkins, D. L. Mattern. *Biorg Med Chem*, **2007**, 15(1), 186.

[4]H. Langhals, R. Ismael, O. Yuruk, *Tetrahedron* **2000**, 56(30), 5435.

[5]H. Langhals, J. Karolin, L. B. Johansson, *J. Chem. Soc., Faraday Trans* **1998**, 94(19), 2919.

[6]A. Rademacher, S. Maerkle, H. Langhals H. *Chem Ber* **1982**, 115(8), 2927.

[7]C. W. Struijk, A. B. Sieval, J. E. J. Dakhorst, M. van Dijk, P. Kimkes, R. B. M. Koehorst, H. Donker, T. J. Schaafsma, S. J. Picken, A. M. van de Craats, J. M. Warman, H. Zuilhof, E. J. R. Sudholter. *J Am Chem Soc* **2000**, 122(45), 11057.

[8]Z.S. An, J. S. Yu, S. C. Jones, S. Barlow, S. Yoo, B. Domercq, P. Prins, L. D. A. Siebbeles, B. Kippelen, S. R. Marder. *Adv Mater* **2005**, 17(21), 2580.

[9]V. Dehm, Z. J. Chen, U. Baumeister, P. Prins, L. D. A. Siebbeles, F. Wurthner, *Org Lett* **2007**, 9(6), 1085.

[10]F. Wurthner, *Chem Commun* **2004**, (14), 1564.

[11] F. J. M. Hoeben, P. Jonkheijm, E. W. Meijer, A. P. H. J. Schenning, *Chem Rev* **2005**, 105(4), 1491.

[12] R. F. Kelley, W. S. Shin, B. Rybtchinski, L .E. Sinks, M. R. Wasielewski. *J Am Chem Soc* **2007**, 129(11), 3173.

[13] S. Yagai, Y. Monma, N. Kawauchi, T. Karatsu, A. Kitamura, *Org Lett* **2007**, 9(6), 1137.

[14] X.-Q. Li, V. Stepanenko, Z. Chen, P. Prins, L. D. A. Siebbeles, F. Würthner, *Chem Commun*, **2006,** (37), 3871.

[15] G. Karayannidis, D. Stamelos, D. Bikiaris, *Makromol Chem* **1993**, 194(10), 2789.

[16] D. Dotcheva, M. Klapper, K. Müllen, *Macromol Chem Phys* **1994**, 195(6), 1905.

[17] H. Ghassemi, A. S. Hay, *Macromolecules* **1994**, 27(15), 4410.

[18] H. Quante, P. Schlichting, U. Rohr, Y. Geerts, K. Müellen, *Macromol Chem Phys* **1996**, 197(12), 4029.

[19] H. Icil, S. Icli, *J Polym Sci, Part A: Polym Chem* **1997**, 35(11), 2137.

[20] Z. Y. Wang, Y. Qi, J. P. Gao, G. G. Sacripante, P. R. Sundararajan, J. D. Duff, *Macromolecules* **1998**, 31(7), 2075.

[21] S. M. Mackinnon, Z. Y. Wang, *Journal of Polymer Science, Part A: Polymer Chemistry* **2000**, 38(19), 3467.

[22] E. E. Neuteboom, R. A. J. Janssen, E. W. Meijer, *Synth Met* **2001**, 121(1-3), 1283.

[23] M. Thelakkat, P. Poesch, H.-W. Schmidt, *Macromolecules* **2001**, 34(21), 7441.

[24] W. Huang, D. Yan, Q. Lu, Y. Huang, *Eur Polym J* **2003**, 39(6), 1099.

[25] A. D. Q. Li, W. Wang, L.-Q. Wang, *Chem Eur J* **2003**, 9(19), 4594.

[26] D. Yao, P. R. Sundararajan, *Eur Polym J* **2006**, 42(2), 302.

[27] K. Yuney, H. Icil, *Eur Polym J* **2007**, 43(6), 2308.

[28] C. B. Nielsen, D. Veldman, R. Martin-Rapun, R. A. J. Janssen, *Macromolecules* **2008**, 41(4), 1094.

[29] H. Langhals, S. Demmig, T. Potrawa, *J Prakt Chem* **1991**, 333(5), 733.

[30] V. J. Sapagovas, V. Gaidelis, V. Kovalevskij, A. Undzenas, *Dyes Pigments* **2006**, 71(3), 178.

[31] K. Balakrishnan, A. Datar, T. Naddo, J. Huang, R. Oitker, M. Yen, J. Zhao, L. Zang, *J Am Chem Soc* **2006**, 128(22), 7390.

[32] G. Seybold, G. Wagenblast, *Dyes Pigments* **1989**, 11(4), 303.

[33] A. Böhm, H. Arms, G. Henning, P. Blaschka (BASF AG), *Ger. Pat. Appl., DE* 19547209 A1, **1997**.

[34] Y. Zhao, M. R. Wasielewski, *Tetrahedron Lett* **1999**, 40(39), 7047.

[35] A. S. Lukas, Y. Zhao, S. E. Miller, M. R. Wasielewski, *J Phys Chem B* **2002**, 106(6), 1299.

[36] S. Demmig, H. Langhals, *Chem Ber* **1988**, 121(2), 225.

[37] F. Würthner, C. Thalacker, S. Diele, C. Tschierske, *Chem Eur J* **2001**, 7(10), 2245.

[38] S. K. Lee, Y. Zu, A. Herrmann, Y. Geerts, K. Müllen, A. J. Bard, *J Am Chem Soc* **1999**, 121(14), 3513.

[39] R. Gomez, J. L. Segura, N. Martin, *Org Lett* **2005**, 7(4), 717.

[40] S. Fukuzumi, K. Ohkubo, J. Ortiz, A. M. Gutierrez, F. Fernandez-Lazaro, A. Sastre-Santos, *Chem Commun* **2005**, (30), 3814.

[41] E. E. Neuteboom, S. C. J. Meskers, E. H. A. Beckers, S. Chopin, R. A. J. Janssen, *J. Phys. Chem. A* **2006**, 110(45), 12363.

[42] L. D. Wescott, D. L. Mattern, *J Org Chem* **2003**, 68(26), 10058.

[43] G. J. Mohr, U. E. Spichiger, W. Jona, H. Langhals, *Anal Chem* **2000**, 72(5), 1084.

[44] L. Zang, R. Liu, M. W. Holman, K. T. Nguyen, D. M. Adams, *J Am Chem Soc* **2002**, 124(36), 10640.

[45] T. Fukaminato, M. Irie, *Adv Mater* **2006**, 18(24), 3225.

[46] E. E. Neuteboom, E. H. A. Beckers, S. C. J. Meskers, E. W. Meijer, R. A. J. Janssen, *Org Biomol Chem* **2003**, 1(1), 198.

[47] A. Marcos Ramos, S. C. J. Meskers, E. H. A. Beckers, R. B. Prince, L. Brunsveld, R. A. J. Janssen, *J Am Chem Soc* **2004**, 126(31), 9630.

[48] H. Langhals, W. Jona, *Angew Chem Int Ed* **1998**, 37(7), 952.

[49] M. J. Tauber, R. F. Kelley, J. M. Giaimo, B. Rybtchinski, M. R. Wasielewski, *J Am Chem Soc* **2006**, 128(6), 1782.

[50] M. W. Holman, R. Liu, L. Zang, P. Yan, S. A. DiBenedetto, R. D. Bowers, D. M. Adams, *J Am Chem Soc* **2004**, 126(49), 16126.

[51] E. E. Neuteboom, P. A. van Hal, R. A. J. Janssen, *Chem Eur J* **2004,** 10(16), 3907.

[52] S. M. Lindner, M. Thelakkat, *Macromolecules* **2004**, 37(24), 8832.

[53] J. Hernando, P. A. J. de Witte, E. M. H. van Dijk, J. Korterik, R. J. M. Nolte, A. E. Rowan, M. F. Garcia-Parajo, N. F. van Hulst, *Angew Chem Int Ed* **2004**, 43(31), 4045.

[54] Y. J. Xu, S. W. Leng, C. M. Xue, R. K. Sun, J. Pan, J. Ford, S. Jin, *Angew Chem Int Ed* **2007**, 46(21), 3896.

[55] R. K. Sun, C. M. Xue, M. Owak, R. M. Peetz, S. Jin, *Tetrahedron Lett* **2007**, 48(38), 6696.

[56] G. Gritzner, J. Kuta, *Pure and Applied Chemistry* **1984**, 56(4), 461.

[57] H. D. Maynard, R. H. Grubbs, *Tetrahedron Lett* **1999**, 40(22), 4137.

[58] K. B. Wagener, J. M. Boncella, J. G. Nel, *Macromolecules* **1991**, 24(10), 2649.

[59] T. W. Baughman, K. B. Wagener, *Adv Polym Sci* **2005**, 176(Metathesis Polymerization), 1.

[60] W. E. Ford, *J Photochem* **1987**, 37(1), 189.

[61] W. Wang, J. J. Han, L. Q. Wang, L. S. Li, W. J. Shaw, A. D. Q. Li, *Nano Lett* **2003**, 3(4), 455.

[62] W. Wang, L.-S. Li, G. Helms, H.-H. Zhou, A. D. Q. Li, *J Am Chem Soc* **2003**, 125(5), 1120.

[63] A. D. Q. Li, W. Wang, L.-Q Wang, *Chem Eur J* **2003**, 9(19), 4594.

[64] G. Klebe, F. Graser, E. Haedicke, J. Berndt, *Acta Crystallographica*, *Section B: Structural Science* **1989**, B45(1), 69.

[65] Z. Chen, V. Stepanenko, V. Dehm, P. Prins, D. A. Siebbeles Laurens, J. Seibt, P. Marquetand, V. Engel, F. Würthner, *Chem Eur J* **2007**, 13(2), 436.

[66] N. Harada, K. Nakanishi, *Circular Dichroism Spectroscopy*; Oxford: Oxford University Press, **1983**.

[67] J. C. Hummelen, B. W. Knight, F. LePeq, F. Wudl, J. Yao, C. L. Wilkins, *J Org Chem* **1995**, 60(3), 532.

CHAPTER 6

[1](a) H. Langhals, *Heterocycles* **1995**, 40, 477 and references therein; (b) H. Langhals, W. Jona, F. Einsiedl, S. Wohnlich, *Adv. Mater*. **1998**, 10, 1022.

[2](a) H. Langhals, R. Ismael, O. Yürük, *Tetrahedron* **2000**, 56, 5435; (b) H. Langhals, J. Karolin, L. B. Johansson, *J. Chem. Soc., Faraday Trans.* **1998**, 94, 2919; (c) A. Rademacher, S. Märkle, H. Langhals, *Chem. Ber.* **1982**, 115, 2927.

[3](a) P. Peumans, S. Uchida, S. R. Forrest, *Nature* **2003**, 158; (b) H. Hansel, H. Zettl, G. Krausch, R. Kisselev, M. Thelakkat, H. W. Schmidt, *Adv. Mater.* **2003**, 15, 2056; (c) S. M. Lindner, S. Huettner, A. Chiche, M. Thelakkat, G. Krausch, *Angew. Chem. Int. Ed*. **2006**, 45, 3364.

[4](a) G. Horowitz, F. Kouki, P. Spearman, D. Fichou, C. Nogues, X. Pan, F. Garnier, *Adv. Mater.* **1996,** 8, 242; (b) P. R. L. Malenfant, C. D. Dimitrakopoulos, J. D.

Gelorme, L. L. Kosbar, T. O. Graham, A. Curioni, W. Andreoni, *Appl. Phys. Lett.* **2002**, 80, 2517; (c) S. Huttner, M. Sommer, M. Thelakkat, *Appl. Phys. Lett.* **2008**, 92, 093302/1-093302/3.

[5](a) R. A. Cormier, B. A. Gregg, *J. Phys. Chem. B* **1997**, 101, 11004; (b) C. W. Struijk, A, B. Sieval, J. E. J. Dakhorst, M. van Dijk, P. Kimkes, R. B. M. Koehorst, H. Donker, T. J. Schaafsma, S. J. Picken, A. M. van de Craats, J. M. Warman, H. Zuilhof, E. J. R. Sudholter, *J. Am. Chem. Soc.* **2000**, 122, 11057; (c) F. Würthner, C. Thalacker, S. Diele, C. Tschierske, *Chem. Eur. J.* **2001**, 7, 2245; (d) Y. J. Xu, S. W. Leng, C. M. Xue, R. K. Sun, J. Pan, J. Ford, S. Jin, *Angew. Chem. Int. Ed.* **2007**, 46, 3896.

[6](a) F. Würthner, *Chem. Comm.* **2004**, 1564 and references therein; (b) F. J. M. Hoeben, P. Jonkheijm, E. W. Meijer, A. P. H. J. Schenning, *Chem. Rev.* **2005**, 105, 1491; (c) S. Yagai, Y. Monma, N. Kawauchi, T. Karatsu, A. Kitamura, *Org. Lett.* **2007**, 9, 1137; (d) X. Q. Li, V. Stepanenko, Z. J. Chen, P. Prins, L. D. A. Siebbeles, F. Würthner, *Chem. Comm.* **2006**, 3871.

[7] S. Benning, H. S. Kitzerow, H. Bock, M. F. Achard, *Liq. Cryst.* **2000**, 27, 901.

[8] (a) M. J. Yang, S. L. Lu, Y. Li, *J. Mater. Sci. Lett.* **2003**, 22, 813; (b) T. Hassheider, S. A. Benning, M. W. Lauhof, H. S. Kitzerow, H. Bock, M. D. Watson, K. Müellen, *Mol. Cryst. Liq. Cryst.* **2004**, 413, 2597.

[9] T. Hassheider, S. A. Benning, H.-S. Kitzerow, M.-F. Achard,; H. Bock, *Angew. Chem. Int. Ed.* **2001**, 40, 2060.

[10] A. Arnaud, J. Belleney, F. Boue, L. Bouteiller, G. Carrot, V. Wintgens, *Angew. Chem. Int. Ed.* **2004**, 43, 1718.

[11] I. Seguy, P. Jolinat, P. Destruel, R. Mamy, H. Allouchi, C. Courseille, M. Cotrait, H. Bock, *Chemphyschem* **2001**, 2, 448.

[12] (a) L. Yang, M. Shi, M. Wang, H. Chen, *Tetrahedron* **2008**, 64, 5404; (b) X. B. Zhang, Y. F. Wu, J. Z. Li, F. Li, M. Li, *Dyes Pigments* **2008**, 76, 810.

[13] (a) R. Gómez, J. L. Segura, N. Martin, *Org. Lett.* **2005**, 7, 717; (b) S. Fukuzumi, K. Ohkubo, J. Ortiz, A. M. Gutierrez, F. Fernandez-Lazaro, A. Sastre-Santos, *Chem. Comm.* **2005**, 3814; (c) E. E. Neuteboom, S. C. J. Meskers, E. H. A. Beckers, S. Chopin, R. A. J. Janssen, *J. Phys. Chem. A* **2006**, 110, 12363.

[14] Wescott, L. D.; Mattern, D. L. *J. Org. Chem.* **2003**, 68, 10058.

[15] (a) G. J. Mohr, U. E. Spichiger, W. Jona, H. Langhals, *Anal. Chem.* **2000**, 72, 1084; (b) L. Zang, R. Liu, M. W. Holman, K. T. Nguyen, D. M. Adams, *J. Am. Chem. Soc.* **2002**, 124, 10640; (c) T. Fukaminato, M. Irie, *Adv. Mater.* **2006**, 18, 3225.

[16] (a) E. E. Neuteboom, E. H. A. Beckers, S. C. J. Meskers, E. W. Meijer, R. A. J. Janssen, *Org. Biomol. Chem.* **2003**, 1, 198; (b) A. M. Ramos, S. C. J. Meskers, E. H. A. Beckers, R. B. Prince, L. Brunsveld, R. A. J. Janssen, *J. Am. Chem. Soc.* **2004**, 126, 9630.

[17] (a) H. Langhals, W. Jona, *Angew. Chem. Int. Ed.* **1998**, 37, 952; (b) M. J. Tauber, R. F. Kelley, J. M. Giaimo, B. Rybtchinski, M. R. Wasielewski, *J. Am. Chem. Soc.*

2006, 128, 1782; (c) P. Yan, A. Chowdhury, M. W. Holman, D. M. Adams, *J. Phys. Chem. B* **2005**, 109, 724.

[18] (a) E. E. Neuteboom, P. A. van Hal, R. A. J. Janssen, *Chem. Eur. J.* **2004**, 10, 3907; (b) S. M. Lindner, M. Thelakkat, *Macromolecules* **2004**, 37, 8832; (c) J. Hernando, P. A. J. de Witte, E. M. H. van Dijk, J. Korterik, R. J. M. Nolte, A. E. Rowan, M. F. García-Parajó, N. F. van Hulst, *Angew. Chem. Int. Ed.* **2004**, 43, 4045.

[19] (a) Y. Nagao, T. Misono, *Bull. Chem. Soc. Jpn.* **1981**, 54, 1269; (b) Y. Nagao, T. Misono, *Bull. Chem. Soc. Jpn.* **1981**, 54, 1191; (c) H. Tröster, *Dyes Pigments* **1983**, 4, 171; (d) H. Kaiser, J. Lindner, H. Langhals, *Chem. Ber.* **1991**, 124, 529; (e) R. K. Sun, C. M. Xue, M. Owak, R. M. Peetz, S. Jin, *Tetrahedron Lett.* **2007**, 48, 6696.

[20] M. Lenes, G.-J. A. H. Wetzelaer, F. B. Kooistra, S. C. Veenstra, J. C. Hummelen, P. W. M. Blom, *Adv. Mater.* **2008**, 20, 2116.

[21] X. Mo, H.-Z. Chen, M.-M. Shi, M. Wang, *Chem. Phys. Lett.* **2006**, 417, 457. See supplementary data for the modification.

[22]*Spectroscopic data for **1***:

^{1}H NMR ($CDCl_3$, 600 MHz): δ (ppm) = 8.66 (d, J = 8.07 Hz, 2H, Ar), 8.55 (d, J = 8.16 Hz, 2H, Ar), 8.53 (d, J = 7.97 Hz, 2H, Ar), 8.15 (d, J = 7.92 Hz, 2H, Ar), 4.34 (t, J = 6.99 Hz, 4H, (COO)C**H$_2$**), 1.83 – 1.78 (m, 4H, (COO)CH_2C**H$_2$**), 1.47 – 1.27 (m, 28H, (COO)CH_2CH_2(C**H$_2$**)$_7$), 0.88 (t, J = 7.02 Hz, 6H, CH_2C**H$_3$**). FT-IR (cm^{-1}): 2920 (antisymmetric CH_2), 2854 (symmetric CH_2), 1770 (anhydride C=O), 1723 (ester C=O), 1595 (aromatic ring stretch). HRMS $(M+e)^-$: calcd for $C_{44}H_{50}O_7$

690.35565; found 690.35515. UV-vis (in $CHCl_3$): 480 and 507 nm (λ_{max}).

[23]*Spectroscopic data for **3a***:

^{1}H NMR ($CDCl_3$, 600 MHz): δ (ppm) = 8.62 (d, J = 8.07 Hz, 2H, Ar), 8.50 (d, J = 8.07 Hz, 2H, Ar), 8.48 (d, J = 7.92 Hz, 2H, Ar), 8.12 (d, J = 7.93 Hz, 2H, Ar), 5.33 – 5.27 (m, 1H, NC**H**(CH_3)CH_2), 4.33 (t, J = 6.90 Hz, 4H, $CO_2C\mathbf{H_2}$), 2.23 – 2.16 and 1.94 – 1.88 (m, 1H, C**H**(CH_3)$_2$), 1.82 – 1.77 (m, 4H, $CO_2CH_2C\mathbf{H_2}$), 1.60 (d, J = 6.90 Hz, 3H, NCH(C**H$_3$**)CH_2), 1.52 – 1.19 (m, 34H, $CO_2CH_2CH_2(C\mathbf{H_2})_7$ and NCH(CH_3)C**H$_2$**C**H$_2$**C**H$_2$**CH(CH_3)$_2$), 0.87 (t, J = 7.05 Hz, 6H, NCH(CH_3)$CH_2CH_2CH_2$CH(C**H$_3$**)$_2$), 0.83 – 0.81 (m, 6H, CH(C**H$_3$**)$_2$). ^{13}C NMR ($CDCl_3$, 75 MHz): δ (ppm) = 168.20 (ester C=O), 163.68 (imide C=O), 134.24 (Ar), 131.57 (Ar), 131.44 (Ar), 130.68 (Ar), 129.98 (Ar), 128.82 (Ar), 128.48 (Ar), 128.46 (Ar), 125.02 (Ar), 122.14 (Ar), 121.98 (Ar), 121.26 (Ar), 65.99 ((COO)**C**H_2), 49.83 (N**C**H(CH_3)), 38.85 (**C**H_2CH(CH_3)$_2$), 33.86 (**C**H(CH_3)$_2$), 32.04 (**C**H_2), 29.74 (**C**H_2), 29.55 (**C**H_2), 29.48 (**C**H_2), 28.75 (**C**H_2), 27.98 (**C**H_2), 26.18 (**C**H_2), 25.09 (**C**H_2), 22.81 (CH(**C**H_3)$_2$), 22.79 (**C**H_2), 22.68 (**C**H_2), 18.33 (NCH(**C**H_3)), 14.25 ($CO_2CH_2(CH_2)_7CH_2$**C**H_3). FT-IR: 2955 (antisymmetric CH_3), 2923 (antisymmetric CH_2), 2871 (symmetric CH_3), 2854 (symmetric CH_2), 1718 (ester C=O), 1697 (symmetric imide C=O), 1654 (antisymmetric imide C=O), 1595 (aromatic ring stretch). HRMS $(M+H)^+$: calcd for $C_{52}H_{68}NO_6$ 802.50466; found 802.50449. UV-vis (in $CHCl_3$): 475 and 506 nm (λ_{max}).

*Spectroscopic data for **3b***:

^{1}H NMR ($CDCl_3$, 300 MHz): δ (ppm) = 8.59 (d, J = 8.13 Hz, 2H, Ar), 8.49 (s, 1H, N**H**), 8.46 (d, J = 8.13 Hz, 2H, Ar), 8.44 (d, J = 8.02 Hz, 2H, Ar), 4.34 (t, J = 6.93 Hz, 4H, $CO_2C\mathbf{H_2}$), 1.86 – 1.76 (m, 4H, $CO_2CH_2C\mathbf{H_2}$), 1.50 – 1.27 (m, 28H, $CO_2CH_2CH_2(C\mathbf{H_2})_7$), 0.87 (t, J = 6.6 Hz, 6H, $C\mathbf{H_3}$). ^{13}C NMR ($CDCl_3$, 75 MHz): δ (ppm) = 168.32 (ester C=O), 163.35 (imide C=O), 136.18 (Ar), 132.30 (Ar), 131.93 (Ar), 131.27 (Ar), 130.59 (Ar), 130.45 (Ar), 129.26 (Ar), 129.02 (Ar), 126.40 (Ar), 122.99 (Ar), 121.92 (Ar), 121.87 (Ar), 66.11 ($O\mathbf{C}H_2CH_2$), 32.06 ($\mathbf{C}H_2$), 29.74 ($\mathbf{C}H_2$), 29.48 ($\mathbf{C}H_2$), 28.75 ($\mathbf{C}H_2$), 26.18 ($\mathbf{C}H_2$), 22.84 ($\mathbf{C}H_2$), 14.27 ($\mathbf{C}H_3$). FT-IR (cm^{-1}): 2924 (antisymmetric CH_2), 2854 (symmetric CH_2), 1720 (ester C=O), 1701 (symmetric imide C=O), 1648 (antisymmetric imide C=O), 1593 (aromatic ring stretch). HRMS $(M+Na)^+$: calcd for $C_{44}H_{51}NNaO_6$ 712.36141; found 712.36110. UV-vis (in $CHCl_3$): 478 and 508 nm (λ_{max}).

*Spectroscopic data for **3c***:

^{1}H NMR ($CDCl_3$, 600 MHz): δ (ppm) = 8.45 (d, J = 7.78, 2H, perylene Ar), 8.10 – 8.08 (m, 4H, perylene Ar), 8.00 (d, J = 7.79, 2H, perylene Ar), 7.23 (d, J = 8.51, 2H, phenol Ar), 6.84 (d, J = 8.36, 2H, phenol Ar), 6.68 (broad, 1H, O**H)**, 4.38 (t, J = 7.0 Hz, 4H, $CO_2C\mathbf{H_2}$), 1.88 – 1.83 (m, 4H, $CO_2CH_2C\mathbf{H_2}$), 1.52 – 1.27 (m, 28H, $CO_2CH_2CH_2(C\mathbf{H_2})_7$), 0.88 (t, J = 7.08 Hz, 6H, $C\mathbf{H_3}$). ^{13}C NMR ($CDCl_3$, 75 MHz): δ (ppm) = 168.17 (ester C=O), 164.01 (imide C=O), 157.38 (ArOH), 134.98 (Ar), 131.98 (Ar), 131.11 (Ar), 130.34 (Ar), 129.69 (Ar), 128.72 (Ar), 128.22 (Ar), 126.58 (Ar), 125.07 (Ar), 122.56 (Ar), 121.63 (Ar), 121.44 (Ar), 117.01 (Ar), 66.12

(O**C**H_2CH_2), 32.09 (**C**H_2), 29.83 (**C**H_2), 29.81 (**C**H_2), 29.63 (**C**H_2), 29.53 (**C**H_2), 28.82 (**C**H_2), 26.24 (**C**H_2), 22.85 (**C**H_2), 14.27 (**C**H_3). FT-IR (cm^{-1}): 3392 (OH), 2924 (antisymmetric CH_2), 2854 (symmetric CH_2), 1722 (ester C=O), 1709 (symmetric imide C=O symmetric), 1645 (antisymmetric imide C=O), 1593 (aromatic ring stretch). HRMS $(M+H)^+$: calcd for $C_{50}H_{56}NO_7$ 782.40568; found 782.40641. UV-vis (in $CHCl_3$): 478 and 508 nm (λ_{max}).

*Spectroscopic data for **3d***:

^{1}H NMR ($CDCl_3$, 600 MHz): δ (ppm) = 8.60 (d, J = 7.92 Hz, 2H, Ar), 8.41 (d, J = 8.21 Hz, 2H, Ar), 8.40 (d, J = 8.07 Hz, 2H, Ar), 8.09 (d, J = 7.93 Hz, 2H, Ar), 5.58 – 5.54 (m, 1H, NC**H**$(CH_2OH)_2$), 4.34 (t, J = 6.99 Hz, 4H, CO_2C**H_2**), 4.25 – 4.16 (m, 4H, NCH(C**H_2**$OH)_2$), 3.18 – 3.16 (m, 2H, NCH(CH_2O**H**$)_2$), 1.83 – 1.78 (m, 4H, CO_2CH_2C**H_2**), 1.48 – 1.27 (m, 28H, $CO_2CH_2CH_2(C$**H_2**$)_7$), 0.88 (t, J = 7.05 Hz, 6H, $O(CH_2)_9C$**H_3**). FT-IR (cm^{-1}): 3491 (OH), 2924 (antisymmetric CH_2), 2854 (symmetric CH_2), 1713 (ester C=O), 1697 (symmetric imide C=O), 1658 (antisymmetric imide C=O), 1592 (aromatic ring stretch). HRMS $(M+Na)^+$: calcd for $C_{47}H_{57}NNaO_8$ 786.39819; found 786.39743. UV-vis (in $CHCl_3$): 481 and 512 nm (λ_{max}).

[24]*Spectroscopic data for **4***:

^{1}H NMR ($CDCl_3$, 300 MHz): δ (ppm) = 7.99 (d, J = 8.24 Hz, 2H, Ar), 7.97 (d, J = 8.13 Hz, 2H, Ar), 7.88 (d, J = 7.80 Hz, 2H, Ar), 7.87 (d, J = 7.91Hz, 2H, Ar), 4.51 (t, J = 5.28 Hz, 4H, CO_2C**H_2**CH_2O), 4.35 (t, J = 6.98 Hz, 4H, CO_2C**H_2**CH_2CH_2**)**, 3.91 –

3.57 (m, 20H, $CO_2CH_2C\mathbf{H_2}OC\mathbf{H_2}C\mathbf{H_2}OC\mathbf{H_2}C\mathbf{H_2}OCH_3$), 3.32 (s, 6H, $OC\mathbf{H_3}$), 1.88 – 1.78 (m, 4H, $OCH_2C\mathbf{H_2}(CH_2)_7CH_3$), 1.50 – 1.19 (m, 28H, $OCH_2CH_2(C\mathbf{H_2})_7CH_3$, 0.87 (t, J = 7.03 Hz, 6H, $OCH_2CH_2(CH_2)_7C\mathbf{H_3}$). ^{13}C NMR ($CDCl_3$, 75 MHz): δ (ppm) = 168.62 (ester C=O), 168.48 (ester C=O), 132.94 (Ar), 132.64 (Ar), 130.71 (Ar), 130.43 (Ar), 130.35 (Ar), 129.72 (Ar), 128.78 (Ar), 128.60 (Ar), 128.52 (Ar), 121.48 (Ar), 121.31 (Ar), 71.98 ($O\mathbf{C}H_2\mathbf{C}H_2O$), 70.78 ($O\mathbf{C}H_2\mathbf{C}H_2O$), 70.71 ($O\mathbf{C}H_2\mathbf{C}H_2O$), 70.64 ($O\mathbf{C}H_2\mathbf{C}H_2O$), 69.09 ($O\mathbf{C}H_2\mathbf{C}H_2O$), 65.73 ($O\mathbf{C}H_2\mathbf{C}H_2O$), 64.53 ($O\mathbf{C}H_2\mathbf{C}H_2O$), 59.08 ($O\mathbf{C}H_3$), 32.00 ($\mathbf{C}H_2$), 29.69 ($\mathbf{C}H_2$), 29.49 ($\mathbf{C}H_2$), 29.43 ($\mathbf{C}H_2$), 28.76 ($\mathbf{C}H_2$), 26.16 ($\mathbf{C}H_2$), 22.78 ($\mathbf{C}H_2$), 14.21 ($CH_2CH_2\mathbf{C}H_3$). FT-IR ($cm^{-1}$): 2920 (antisymmetric CH_2), 2850 (symmetric CH_2), 1724 (ester C=O), 1591 (aromatic ring stretch). HRMS $(M+NH_4)^+$: calcd for $C_{58}H_{84}NO_{14}$ 1018.58918; found 1018.59059. UV-vis (in $CHCl_3$): 444 and 473 nm (λ_{max}).